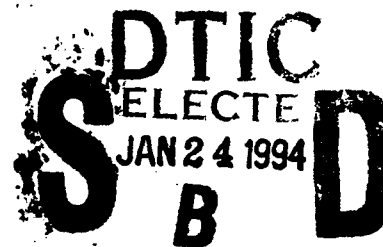


AD-A274 788



2

NAVAL POSTGRADUATE SCHOOL Monterey, California



DISSERTATION

TOPICS IN
LONGSHORE CURRENTS

by

John Casey Church

September, 1993

Thesis Advisor:

E.B. Thornton

Approved for public release; distribution is unlimited.

1308 94-01971



94 1 21 142

REPORT DOCUMENTATION PAGE			Form Approved OMB No. 0704-0188	
Public reporting burden for this collection of information is estimated to average 1 hour per response, including the time for reviewing instruction, searching existing data sources, gathering and maintaining the data needed, and completing and reviewing the collection of information. Send comments regarding this burden estimate or any other aspect of this collection of information, including suggestions for reducing this burden, to Washington headquarters Services, Directorate for Information Operations and Reports, 1215 Jefferson Davis Highway, Suite 1204, Arlington, VA 22202-4302, and to the Office of Management and Budget, Paperwork Reduction Project (0704-0188) Washington DC 20503.				
1. AGENCY USE ONLY (Leave blank)		2. REPORT DATE 23 Sep 93		3. REPORT TYPE AND DATES COVERED Doctoral Dissertation
4. TITLE AND SUBTITLE TOPICS IN LONGSHORE CURRENTS UNCLASSIFIED			5. FUNDING NUMBERS	
6. AUTHOR(S) Church, John Casey				
7. PERFORMING ORGANIZATION NAME(S) AND ADDRESS(ES) Naval Postgraduate School Monterey CA 93943-5000			8. PERFORMING ORGANIZATION REPORT NUMBER	
9. SPONSORING/MONITORING AGENCY NAME(S) AND ADDRESS(ES)			10. SPONSORING/MONITORING AGENCY REPORT NUMBER	
11. SUPPLEMENTARY NOTES The views expressed in this thesis are those of the author and do not reflect the official policy or position of the Department of Defense or the U.S. Government.				
12a. DISTRIBUTION/AVAILABILITY STATEMENT Approved for public release; distribution is unlimited.			12b. DISTRIBUTION CODE A	
13. ABSTRACT (maximum 200 words) The momentum equation governing mean longshore currents on straight beaches is a balance of forcing from the momentum transfer of the oscillatory wave motion, turbulent momentum transfer (mixing), and bottom stress. Of these, the wave's contribution is well understood, but the remaining two are not, principally due to the complicated hydrodynamics of the surf-zone. Addressing the bottom stress term, a longshore current model is developed which includes a modification of the bottom stress due to the effects of breaking-wave induced turbulence. A one-dimensional turbulent kinetic energy equation is used to model this breaking-wave induced turbulence, producing a spatially varying bottom friction coefficient. The modeled longshore current cross-shore profiles show improved agreement with field observations. In a second bottom stress study, vertical profiles of mean longshore currents are examined using field data obtained with vertically stacked electromagnetic current meters with the goal of measuring the bottom stress and its associated drag coefficient. The profiles are observed to become vertically uniform whenever the ratio of wave height to depth exceeds 0.3, indicating that nearly all of the waves passing a given location are breaking. Finally, horizontal turbulent momentum transfer (mixing) is examined for the case of shear instabilities of the longshore current. These instabilities are linked to the potential vorticity pattern produced by the horizontal shear of the longshore current. The model generated stream function amplitudes are calibrated via observed energy density spectra. For the barred beach studied, the predicted mixing is in qualitative agreement with that required for modeled longshore current profiles to agree with observed profiles.				
14. SUBJECT TERMS longshore current, nearshore, bottom stress, surf-zone, radiation stress, breaking waves			15. NUMBER OF PAGES 131	
			16. PRICE CODE	
17. SECURITY CLASSIFICATION OF REPORT Unclassified	18. SECURITY CLASSIFICATION OF THIS PAGE Unclassified	19. SECURITY CLASSIFICATION OF ABSTRACT Unclassified	20. LIMITATION OF ABSTRACT UL	

Approved for public release; distribution is unlimited.

Topics in Longshore Currents

by

John Casey Church
Lieutenant Commander, United States Navy
B.S., University of Michigan

Submitted in partial fulfillment
of the requirements for the degree of

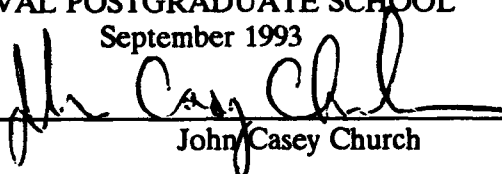
DOCTOR OF PHILOSOPHY IN PHYSICAL OCEANOGRAPHY

from the


NAVAL POSTGRADUATE SCHOOL

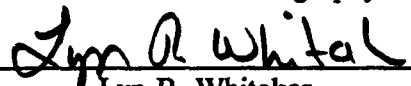
September 1993


Author:



John Casey Church

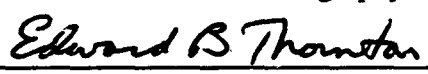
Approved by:


Peter C. Chu
Professor of Oceanography


Lyn R. Whitaker
Professor of Operations Research


Philip A. Durkee
Professor of Meteorology


Thomas C. Lippmann
Professor of Oceanography


Edward B. Thornton
Professor of Oceanography
Dissertation Supervisor

Approved by:


Curtis A. Collins, Chairman, Department of Oceanography

Approved by:


Richard E. Elster, Dean of Instruction

ABSTRACT

The momentum equation governing mean longshore currents on straight beaches is a balance of forcing from the momentum transfer of the oscillatory wave motion, turbulent momentum transfer (mixing), and bottom stress. Of these, the wave's contribution is well understood, but the remaining two are not, principally due to the complicated hydrodynamics of the surf-zone. Addressing the bottom stress term, a longshore current model is developed which includes a modification of the bottom stress due to the effects of breaking-wave induced turbulence. A one-dimensional turbulent kinetic energy equation is used to model this breaking-wave induced turbulence, producing a spatially varying bottom friction coefficient. The modeled longshore current cross-shore profiles show improved agreement with field observations. In a second bottom stress study, vertical profiles of mean longshore currents are examined using field data obtained with vertically stacked electromagnetic current meters with the goal of measuring the bottom stress and its associated drag coefficient. The profiles are observed to become vertically uniform whenever the ratio of wave height to depth exceeds 0.3, indicating that nearly all of the waves passing a given location are breaking. Finally, horizontal turbulent momentum transfer (mixing) is examined for the case of shear instabilities of the longshore current. These instabilities are linked to the potential vorticity pattern produced by the horizontal shear of the longshore current. The model generated stream function amplitudes are calibrated via observed energy density spectra. For the barred beach studied, the predicted mixing is in qualitative agreement with that required for modeled longshore current profiles to agree with observed profiles.

DTIC QUALITY INSPECTED 5

iii

Accession For	
NTIS GRA&I	<input checked="checked" type="checkbox"/>
DTIC TAB	<input type="checkbox"/>
Unannounced	<input type="checkbox"/>
Justification	
By	
Distribution/	
Availability Codes	
Dist	Avail and/or Special
A-1	

TABLE OF CONTENTS

I. INTRODUCTION	1
II. EFFECTS OF BREAKING WAVE INDUCED TURBULENCE WITHIN A LONGSHORE CURRENT MODEL	6
III. VERTICAL PROFILES OF LONGSHORE CURRENTS: FIELD OBSERVATIONS	35
IV. MIXING BY SHEAR INSTABILITIES OF THE LONGSHORE CURRENT	69
V. SUMMARY AND CONCLUSIONS	119
VI. INITIAL DISTRIBUTION LIST	123

ACKNOWLEDGMENTS

I wish to express my deep appreciation to Prof. Edward Thornton who guided me through this work. His efforts to ensure that I developed the proper sense of scientific reason, while not forgetting the reasons why I wanted to become a scientist, have made the past two years enjoyable. He is responsible for introducing me to the wonderful misery of laying awake nights, unable to shake some exciting new idea that could not wait until morning.

I would also like to thank Prof. R.T. Guza, of the Scripps Institution of Oceanography, for both his interest in my ideas and his contribution to my maturation as a scientist.

Additionally, my thanks to Prof. Tim Stanton, Mary Bristow, and Rob Wyland, all of the Naval Postgraduate School for acquiring and pre-processing the data which I used from the SUPERDUCK and DELILAH experiments, to Dr. Tom Lippmann and Dr. Joan Oltman-Shay for their encouraging support and stimulating discussions, and to the Office of Naval Research who made my doctoral work possible through their fellowship.

Most importantly, I thank my wife, Jenny, and sons, Tom (who explained to me that turbulence is like the way he dances) and Conor (who fears no wave, whether real or modeled), for their support, encouragement, and never ending interest in things that I found captivating.

I. INTRODUCTION

Longshore currents within the surf-zone may reach speeds of over 1.5 m/s and are of interest not only because of the challenges they pose to amphibious landing craft and special forces operations, but also because of the sediment transport they produce. Assuming steady state, the alongshore momentum equation governing mean longshore currents on straight beaches is a balance between forcing by the momentum flux of obliquely incident waves, \tilde{S}_{yx} , (generally termed the radiation stress), with turbulent momentum flux, S'_{yx} , (mixing), bottom stress, and wind stress (e.g. Phillips, 1966):

$$\frac{\partial \tilde{S}_{yx}}{\partial x} + \frac{\partial S'_{yx}}{\partial x} = -\overline{\tau_y^b} + \overline{\tau_y^\eta} \quad (1)$$

where (x,y) are the (cross-shore, alongshore) co-ordinates and

$$\tilde{S}_{yx} = \int_{-h}^0 \rho \bar{u}\bar{v} dz \quad S'_{yx} = \int_{-h}^0 \rho \overline{u'v'} dz \quad (2)$$

where ρ is density and h the depth of water. The wind stress contribution is generally small and will be subsequently neglected. The \tilde{S}_{yx} is conserved outside the surf zone prior to breaking. When the waves break, there is a change in the radiation stress, and it is the gradient of the radiation stress that is the primary forcing of longshore currents.

Early radiation stress models of longshore current generation (Bowen 1969, Longuet-Higgins 1970a & b, Thornton 1970), describing waves as monochromatic, produced reasonable cross-shore current distributions over planar beaches, but relied heavily on mixing through parameterization of the turbulent excess momentum flux for smoothing of the velocity profile. Such mixing is required since \tilde{S}_{yx} is conserved outside the surf zone, but an infinite gradient in radiation stress is predicted at the singular location of breaking predicted for monochromatic waves. Horizontal mixing terms, found throughout the literature, vary significantly in both form and physics. This mixing was initially considered to be the result of horizontal eddy viscosity with a variety of mixing lengths and

characteristic velocities. Subsequently Battjes (1975, 1983) linked breaking-wave produced turbulence to horizontal momentum mixing, which provides a more physically appealing approach in the surf-zone. It is interesting to note that as pointed out in a summary paper by McDougal and Hudspeth (1986), all of the mixing forms (in the case of planar beaches) do a reasonably good job of producing smoothed profiles in keeping with the observations, despite their differing physics.

Waves observed in nature are seldom monochromatic and more recent models of wave transformation describe wave heights as random. This randomness is described through use of a representative statistic, such as H_{rms} , obtained via either a probabilistic (eg. Thornton and Guza (1983)) or a deterministic (eg. Dally *et al.* (1985)) approach. In the latter, a Monte Carlo scheme is used in which some large number of waves of differing heights are individually transformed across the surf zone. A random sample of these individual waves is then taken and combined into a representative wave height. In the probability distribution approach, *a priori* probability density functions are used to describe the variability of broken and unbroken waves. The distribution is then transformed via an energy balance across the surf zone in an ensemble manner producing the transformation of H_{rms} directly. This work employs such a probabilistic method, patterned here after the observationally based approach of Thornton and Guza (1983), which has been found to give good estimates of H_{rms} transformation across the surf zone.

\tilde{S}_{yx} forcing is directly a function of H_{rms} . Thornton and Guza (1986) found that for the near-planar beach at Santa Barbara, the distribution of breaker locations produced through such randomness results in a smooth \tilde{S}_{yx} cross-shore distribution and a satisfactory velocity profile without the inclusion of a horizontal mixing term. This simple model is not, however, able to explain longshore currents on barred beaches. Conceptually, as waves approach a bar they shoal, and if sufficiently large, break, producing a region of high radiation stress gradient over the bar. The waves then pass into the deeper trough region where the waves cease breaking resulting in a radiation stress minimum, i.e. no forcing of the longshore current in the trough. The waves then break again on the beach face where a second maximum in the radiation stress gradient is formed. The same radiation

stress approach which performs well on a planar beach now predicts two maxima in forcing and, if mixing is omitted, two maxima in longshore current velocity. This prediction is in conflict with observations from the DELILAH experiment, (an acronym for *Duck Experiment on Low-frequency and Incident-band Longshore and Across-shore Hydrodynamics*), conducted at Duck, North Carolina, which generally show a single maximum in longshore current over the trough, where the model predicted radiation stress gradient is near zero. Standard mixing length approaches to horizontal excess momentum flux cannot reasonably be expected to rectify this situation, as the production of a new maxima between the locations of two previous maxima requires hydrodynamically unfeasible up-gradient transfer of momentum. The deficiencies of the present models to properly describe the longshore current in the trough of a barred beach, and in particular the bottom shear stress and turbulent mixing terms, are the motivation of this study.

The bottom friction term on the right side of Eq. 1 typically contains a bottom friction coefficient (c_f), used to relate the bottom stress to the free stream velocity. Considerable range in the value of this coefficient is found in the literature. Using field data from Torrey Pines, California, Guza and Thornton (1978) and Thornton and Guza (1981) solved the momentum balance for local c_f values based on measured velocity covariance calculations of radiation stress. In both instances, spatially variable c_f 's tended to decrease shoreward, but current meter alignment difficulties in their calculations of \tilde{S}_{yx} prevented the results from being conclusive. Whitford and Thornton (1993) used a mobile sled to more precisely measure the alongshore momentum balance at various cross-shore locations during SUPERDUCK (also located at Duck, North Carolina) and then solved for local c_f values. Their data indicated significant cross-shore variation in c_f but possible physical explanations of bottom roughness and decreasing wave current interaction could not be confirmed. In general, while theories exist relating c_f to physical parameters such as bottom roughness and wave steepness, data suitable to test these theories are extremely sparse.

In Chapter II a non-linear bottom stress formulation will be presented in which c_f is likewise used to relate the free stream velocity to the bottom stress (i.e. the law of the wall), but incorporates

the effects of breaking-wave produced turbulence, in that $c_f = c_{fl} + c_{fr}$, where l and r denote local (bottom boundary layer) and remote (breaking-wave) turbulence effects. In regions of breaking waves, the remotely generated turbulence is hypothesized to be a significant source of vertical mixing of the mean longshore flow and is thus essential to relating the free stream velocity to the bottom stress. Whereas the locally generated (boundary layer) turbulence is limited in magnitude by the restriction of equilibrium between the mixing it induces and the shear which produces it, the mixing potential of the remotely generated turbulence is essentially limitless. The result of this breaking-wave induced mixing is that for a given bottom stress, the free stream velocity is decreased. The cross-shore distribution of turbulent kinetic energy (modeled by a simple vertically integrated balance between breaking-wave production and dissipation), combined with a penetration parameter, is proposed to describe the intensity of near bottom breaking-wave induced turbulence, and thereby the modification of the relationship between bottom stress and free stream velocity. In an effort to measure such proposed effects of breaking wave induced turbulence upon the vertical profile of the mean longshore currents, data from two experiments in which current was measured over the vertical will be examined in Chapter III.

The hypothesis that shear instabilities of the longshore current produce $\overline{u'v'}$ values which describe the turbulent mixing in Eq. 1 is investigated in Chapter IV. During the 1986 nearshore experiment SUPERDUCK, Oltman-Shay *et al.* (1989) observed low frequency oscillations (<0.01 Hz), with wavelengths less than 300m. The uniqueness of these oscillations lies in the fact that the wavelengths measured were an order of magnitude shorter than the shortest infragravity wave under applicable conditions (a function of frequency and beach slope). These oscillations were considered to be kinematically distinct based upon their frequency / wavenumber range and were linked to the potential vorticity pattern produced by the longshore currents' horizontal shear. Previous linear models of these shear instabilities of the longshore current (Bowen and Holman 1989, Dodd *et al.* 1992 and Putrevu and Svendsen 1992) do not predict the magnitude of $\overline{u'v'}$ profiles due to the non-dimensional amplitudes of the stream-functions utilized. The magnitude of this turbulent covariance

will be determined by scaling the model results with observed kinetic energy distributions over the appropriate frequency range and across the surf zone. The scaled mixing term is found to be in qualitative agreement with the mixing required to explain the observed longshore current distributions.

A summary and suggested directions for future research are contained in Chapter V.

II. EFFECTS OF BREAKING WAVE INDUCED TURBULENCE WITHIN A LONGSHORE CURRENT MODEL

(This chapter consists of a journal article published by
Coastal Engineering, 20, pp 1-28, July 1993.)

Effects of breaking wave induced turbulence within a longshore current model

John Casey Church¹ and Edward B. Thornton

Naval Postgraduate School, Department of Oceanography, 833 Dyer Rd., Rm 331, Monterey,
CA 93943-5000, USA

(Received 27 May 1992; accepted after revision 6 April 1993)

ABSTRACT

A longshore current model which includes a modification of the bottom stress term due to the effects of breaking-wave induced turbulence is developed and applied to field data from both barred and planar beaches. This turbulence is postulated as producing a vertical mixing which alters the near-bottom vertical profile of the longshore current. As a result, the bottom friction coefficient, c_b , used to relate the free stream current velocity to the bottom stress is modeled as consisting of two components, c_b , a spatially constant value which is assumed to be related to bottom characteristics and c_{bt} , which is dependent upon breaking-wave induced near-bottom turbulence levels. Employing a one-dimensional turbulent kinetic energy equation to model this breaking-wave induced turbulence, a spatially varying bottom friction coefficient is obtained. The spatially constant c_b is estimated based on data taken seaward of the surf zone, where the wind stress is assumed to be balanced by the bottom stress. The concept is demonstrated without the inclusion of horizontal mixing in the longshore current model formulation. The model predicted cross-shore profiles of longshore current show improved agreement with observations compared with treatments using constant c_b values.

INTRODUCTION

Early radiation stress models of longshore current generation (Bowen, 1969; Longuet-Higgins, 1970a,b; Thornton, 1970), describing waves as monochromatic, produced reasonable cross-shore current distributions over planar beaches, but relied heavily on horizontal mixing for smoothing of the velocity profile. Such mixing is required because the radiation stress associated with the alongshore component of the wave-induced momentum flux, S_{xx} , is conserved outside the surf zone, but an infinite gradient in radiation stress is predicted at the singular location of breaking predicted for monochromatic waves. Horizontal mixing terms, found throughout the literature, vary significantly in both form and physics. This mixing was initially considered to be the result of horizontal eddy viscosity with a variety of mixing lengths and

¹Present address: Naval Research Laboratory, Marine Geoscience Division, Code 7400, Building 105, Stennis Space Center, MS 39529-5000, USA.

characteristic velocities. Subsequently Battjes (1975, 1983) linked breaking-wave produced turbulence to horizontal momentum mixing, which provides a more physically appealing approach in the surf-zone. It is interesting to note that as pointed out in a summary paper by McDougal and Hudspeth (1986), all of the mixing forms (in the case of planar beaches) do a reasonably good job of producing smoothed profiles in keeping with the observations, despite their differing physics.

Waves observed in nature are seldom monochromatic and more recent models of wave transformation describe wave heights as random. This randomness is described through use of a representative statistic, such as H_{rms} , obtained via either a probabilistic (e.g. Thornton and Guza, 1983) or a deterministic (e.g. Dally et al., 1985) approach. In the latter, a Monte Carlo scheme is used in which some large number of waves of differing heights are individually transformed across the surf zone. A random sample of these individual waves is then taken and combined into a representative wave height. In the probability distribution approach, a priori probability density functions are used to describe the variability of broken and unbroken waves. The distribution is then transformed via an energy balance across the surf zone in an ensemble manner producing the transformation of H_{rms} directly. This work employs such a probabilistic method, patterned here after the observationally based approach of Thornton and Guza (1983).

Thornton and Guza (1986) found that for the near-planar beach at Santa Barbara, the distribution of breaker locations produced through such randomness results in a smooth S_{yx} cross-shore distribution and a satisfactory velocity profile without the inclusion of a horizontal mixing term. The random wave height model is not, however, able to explain longshore currents on barred beaches. Conceptually, as waves approach a bar they shoal, and if sufficiently large, break, producing a region of high radiation stress gradient. The wave energy next passes over the trough region, where the wave height-to-depth ratio is below the breaking criteria and so no decrease in the wave's radiation stress is expected. The wave shoals once more prior to breaking on the beach face where a second maximum in the radiation stress gradient is formed. The same radiation stress approach which performs well on a planar beach now predicts two maxima in forcing and, if mixing is omitted, two maxima in longshore current velocity. This is in conflict with observations from the DELILAH experiment (an acronym for *Duck Experiment on Low-frequency and Incident-band Longshore and Across-shore Hydrodynamics*), conducted at Duck, North Carolina, which generally show a single maximum in longshore current over the trough, where the model predicted radiation stress gradient is near zero. Standard mixing length approaches to horizontal momentum transfer cannot reasonably be expected to rectify this situation, as the production of a new maximum between the locations of two previous maxima requires hydrodynamically unfeasible up-gradient transfer of mo-

mentum. New horizontal mixing mechanisms which have been suggested, such as shear instabilities of the longshore current (Dodd and Thornton, 1990), and undertow (Putrevu and Svendsen, 1991), appear relevant, but may not completely answer the question.

Most longshore current models assume a spatially constant bottom friction coefficient (c_f) which is used to relate the bottom stress to the free stream velocity. Considerable range in the values is found in the literature. Using field data from Torrey Pines, California, Guza and Thornton (1978) and Thornton and Guza (1981) solved the momentum balance for local c_f values based on measured velocity covariance calculations of radiation stress. In both instances, spatially variable c_f 's tended to decrease shoreward, but current meter alignment difficulties in their calculations of S_{rx} prevented the results from being conclusive. Whitford and Thornton (1993) used a mobile sled to more precisely measure the alongshore momentum balance at various cross-shore locations during SUPERDUCK (also located at Duck, North Carolina) and then solved for local c_f values. Their data indicated significant cross-shore variation in c_f , but possible physical explanations of bottom roughness and decreasing wave current interaction could not be confirmed. Thornton (1970) utilized a friction coefficient which was dependent upon near-bottom water particle excursion amplitude (weakly varying in the cross-shore) and bottom roughness (held constant), following Jonsson (1967). In general, while theories exist relating c_f to physical parameters such as bottom roughness and wave steepness, data suitable to test these theories are extremely sparse.

The present study utilizes a non-linear bottom stress formulation in which c_f is likewise used to relate the free stream velocity to the bottom stress (i.e. the law of the wall), but incorporates the effects of breaking-wave produced turbulence, in that $c_f = c_b + c_r$, where b and r denote local (bottom boundary layer) and remote (breaking-wave) turbulence effects. In regions of breaking waves, the remotely generated turbulence is hypothesized to be a significant source of vertical mixing of the mean longshore flow and is thus essential to relating the free stream velocity to the bottom stress. Whereas the locally generated (boundary layer) turbulence is limited in magnitude by the restriction of equilibrium between the mixing it induces and the shear which produces it, the mixing potential of the remotely generated turbulence is essentially limitless. The result of this breaking-wave induced mixing is that for a given bottom stress, free stream velocity is decreased (Fig. 1). This modification of the longshore current/bottom stress coupling by the breaking-wave induced turbulence is the essence of the present study. The cross-shore distribution of turbulent kinetic energy (modeled by a simple vertically integrated balance between breaking-wave production and dissipation), combined with a penetration parameter, is proposed to describe the intensity of near bottom

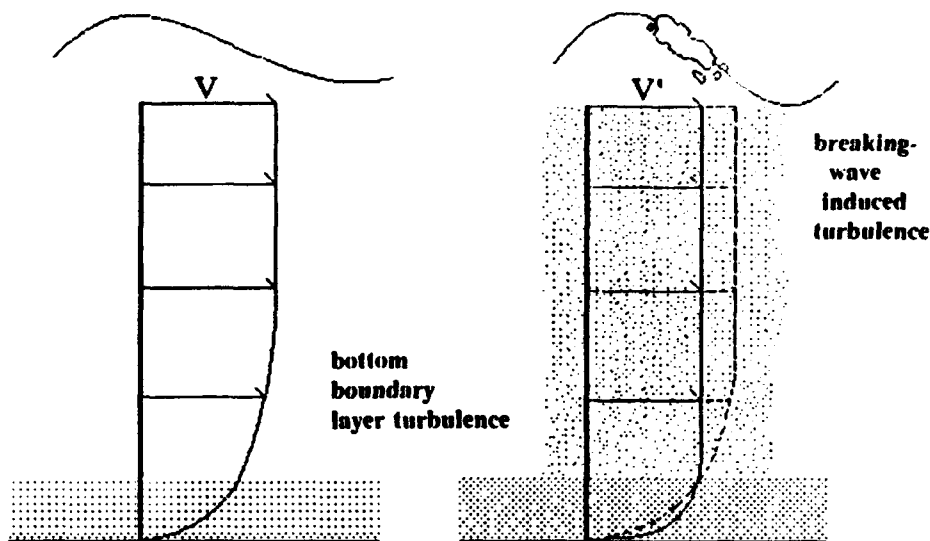


Fig. 1. Conceptualizations of the modification of the vertical profile of the mean longshore current due to addition of breaking waves as a source of turbulence.

breaking-wave induced turbulence, and thereby the modification of the relationship between bottom stress and free stream velocity.

Comparison with data from a barred beach (the DELILAH experiment at Duck, North Carolina) and data from a near planar beach (NSTS data from Leadbetter Beach, Santa Barbara, California) yields improved agreement. Observations of winds and current taken well seaward of the surf zone during DELILAH will be used to estimate values of c_n . A description of the Duck, North Carolina DELILAH experiment is included in the present work. Thornton and Guza (1986) provides a description of the NSTS Santa Barbara experiment.

LONGSHORE CURRENT FORMULATION

Assumptions

Linear wave theory is utilized, with x -axis perpendicular to the assumed straight and parallel contours, but arbitrary cross-shore profile. Mean currents are assumed steady state and vertically uniform. All quantities are assumed homogeneous in the alongshore direction. Current shear is assumed sufficiently small that refractive interaction may be neglected. Narrowbandness is assumed for both direction and frequency of the incident wave field.

Equations

The time averaged, depth integrated momentum equation in the along-

shore direction produces a simple balance between the gradient of the radiation stress and the bottom and wind stresses, e.g. Phillips (1966):

$$\frac{\partial S_{yx}}{\partial x} = \frac{\partial \bar{S}_{yx}}{\partial x} + \frac{S'_{yx}}{\partial x} = -\bar{\tau}_y^b + \bar{\tau}_y^w \quad (1)$$

The radiation stress has been separated into two terms, one associated with the wave motion (\sim) and the other due to turbulence ($'$) and it is assumed the wave motion and turbulence are statistically independent of each other. The turbulent radiation stress, which is equivalent to the Reynold's stress integrated over depth, is typically either parameterized as a horizontal mixing term or, as in the present case, neglected. Although it is recognized that mixing is a real element of natural hydrodynamics, the incomplete understanding of the physics could obscure the purpose of this study which is to examine the effects of breaking wave induced turbulence upon the bottom stress. All subsequent references to "radiation stress" will pertain to wave associated radiation stress and the turbulence will be omitted.

Radiation stress forcing

After applying Snell's law for wave refraction based on the assumption of straight and parallel contours, the gradient of the alongshore momentum flux may be written as:

$$\frac{\partial S_{yx}}{\partial x} = \frac{\sin \alpha_0}{C_0} \frac{\partial}{\partial x} (EC_g \cos \alpha) \quad (2)$$

where the term on the rhs in parentheses is the onshore directed energy flux in which energy, through linear wave theory, is given by $E = (1/8)\rho g H^2$, with H denoting wave height. C_g is group velocity, C is phase speed, and α is incident wave angle. The subscript 0 indicates values at some initial point well seaward of breaking.

A wave height transformation model following Thornton and Guza (1983) is applied, wherein randomness in wave height is modeled through a probabilistic treatment. Based on field data analysis from Torrey Pines and Fort Ord, California beaches, the Rayleigh distribution, combined with a weighting function, is considered a reasonable description of the wave height distribution for both broken and unbroken waves within the surf zone. Other authors, e.g. Battjes and Janssen (1978), Dally et al. (1985), and Goda (1975) have suggested modified Rayleigh distributions but comparison of results show that the H_{rms} transformation is not sensitive to the assumed distribution. Visual observations of breaking wave percentages obtained during SUPER-DUCK were incorporated in the weighting function by Thornton and Whitford (1993) such that dissipation by the breaking waves is related to H_{rms} through periodic linear bore theory, via

$$\langle \epsilon_b \rangle = \frac{3}{16} \sqrt{\pi \rho g} B^3 \frac{H_{rms}^3}{h} M \left[1 - \frac{1}{[1 + (H_{rms}/\gamma h)^2]^{5/2}} \right] \quad (3)$$

with M given by:

$$M = \left\{ 1 + \tanh \left[8 \left(\frac{H_{rms}}{\gamma h} - 1.0 \right) \right] \right\} \quad (4)$$

Thornton and Guza (1983) have shown that dissipation of wave energy by bottom friction may be neglected and so the gradient of onshore directed energy flux contained in Eq. (2) is taken as:

$$\frac{\partial}{\partial x} (EC_s \cos \alpha) = \langle \epsilon_b \rangle \quad (5)$$

Two parameters are included in the model; the first γ , describes the saturation conditions given by $\gamma = H_{rms}/h$, at which all waves are consider to be breaking. The second, B , is a measure of the intensity of breaking.

Bottom stress

The exact nature of the bottom boundary layer flow is complicated due to the combination of the oscillating wave induced motion and the steady (time averaged) longshore current. A number of authors including Grant and Madsen (1979), Christoffersen and Jonsson (1985), Sleath (1990, 1991), and Trowbridge and Madsen (1984) have proposed both theory and experiment based models, but none specifically address breaking-wave regimes. Although treatment of the bottom stress term is critical (all longshore current models employing radiation stress solve for the mean current velocity through its role in the bottom friction term), simplifications concerning linearization in velocity and/or restriction of incidence angles are commonly made.

The general form of the component of the bottom stress in the alongshore direction is given by:

$$\overline{\tau_y^b} = c_f \rho \overline{|U|} (\overline{V} + \overline{v}) \quad (6)$$

where the overbar denotes averaging over time and V is the mean longshore current velocity. The magnitude of U , which represents the vector sum of the steady and unsteady flow is obtained from

$$|U| = (\tilde{u}^2 + 2\tilde{u}V\sin\alpha + V^2)^{1/2} \quad (7)$$

where the depth integrated cross-shore mean velocity, \tilde{u} , is assumed equal to zero locally through conservation of mass. The result is then:

$$\overline{\tau_y^b} = \frac{1}{T} \int_T \rho c_f (\tilde{u}^2 + 2\tilde{u}V\sin\alpha + V^2)^{1/2} (V + \tilde{u}\sin\alpha) dt \quad (8)$$

The two primary simplifications frequently found in the literature involve the ratio of magnitudes of the oscillatory and current velocities and restrictions to the angle of wave incidence to the beach. Assuming the incident wave field approaches with a small angle of incidence ($\sin \alpha \ll 1$), yields

$$\overline{\tau}_y^b \cong c_f \rho (\bar{u}^2 + V^2)^{1/2} \bar{V} \quad (9)$$

Further assuming the magnitude of the current is small compared with the orbital velocity and averaging over one period results in:

$$\overline{\tau}_y^b = \frac{2}{\pi} c_f \rho U_0 V \quad (10)$$

where U_0 is the amplitude of the orbital velocity (note that when using ensemble averaging, as in the case of this study, the integration produces a value $\pi/2$ times greater, or simply $c_f \rho U_0 V$). This simple equation for the bottom friction stress, with linear dependence upon V , was used in early longshore current studies by a number of authors. Larson and Kraus (1991) compared this linearized form with the general nonlinear form for three selected angles of incidence and found significant underprediction of the bottom friction throughout much of the range of values (Fig. 2). For strong currents, it is seen that the linear bottom stress is nearly half that calculated using the nonlinear term. Although the model put forward in the present work utilizes the general non-linear bottom stress form, results using the above linearization will be shown for comparison.

In considering the non-linear form of the bottom stress for the case of ran-

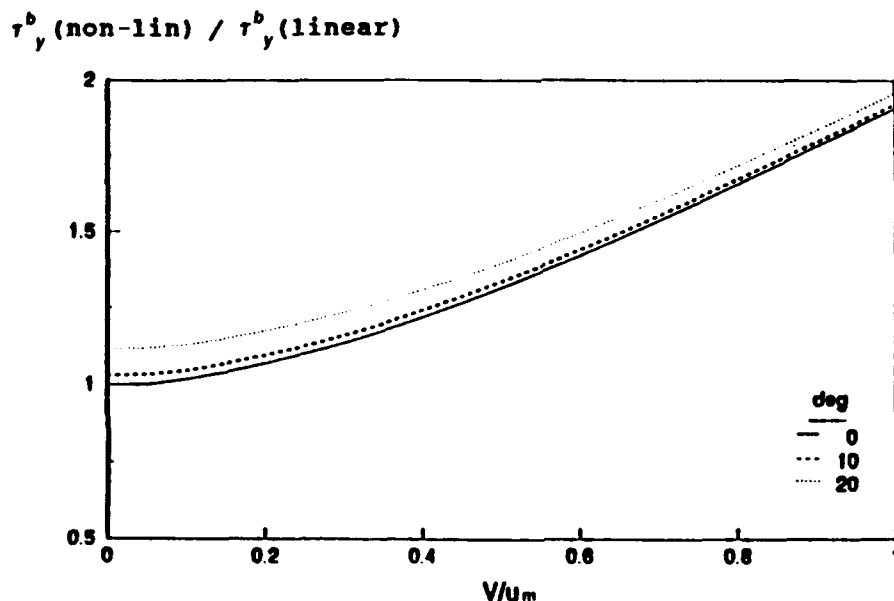


Fig. 2. Ratio of non-linear to linear bottom friction terms as a function of current to orbital wave velocity ratio and incidence angle. (Following Larson and Kraus, 1991.)

dom wave heights, ensemble averaging is required. Specifically, \bar{u} cannot be solved for based directly on H_{rms} , but instead the bottom stress for each wave height within the distribution is calculated and then ensemble averaged as given by:

$$\langle \bar{\tau}_y^b \rangle = \int_0^{\infty} \bar{\tau}_y^b(H) p(H) dH \quad (11)$$

An iterative method described in Thornton and Guza (1986) is used to calculate the longshore current velocity.

Bottom stress and free stream velocity

In general, a friction coefficient c_f , has been used to relate the bottom stress to the free stream velocity. The exact profile of the longshore current within the boundary layer is not required, but it is inherently assumed, in accordance with Prandtl's mixing length hypothesis, that a state of equilibrium exists between the vertical mixing effect of the mechanically generated turbulence and the shear generated through the no-slip condition. In this manner, the friction coefficient, c_f , not only relates the free stream velocity, V , to the bottom stress, τ_y^b , but also to the characteristic turbulence/friction velocity, u_* , through:

$$\bar{\tau}_y^b = \rho u_*^2 = c_f \rho |\bar{U}| (\bar{V} + \bar{v}) \quad (12)$$

In most instances, for homogeneous fluids, the only source of turbulence (as represented by u_*) is local mechanical generation linked to the near-bottom current shear. Within the surf-zone, where breaking-wave generated turbulence is present, there are clearly two distinct sources. The intensity of the remotely generated turbulence is not limited by the equilibrium condition and so must be solved for separately. In regions where sufficient remotely produced turbulence is present, its vertical mixing effect may significantly alter the vertical profile of the longshore current. This modification to the relationship between bottom stress and free stream velocity is included in the proposed model through inclusion of a separate c_f , namely, c_{fr} . Considering the two sources separately, the bottom stress may be written as:

$$\bar{\tau}_y^b = (c_n + c_{fr}) \rho |\bar{U}| (\bar{V} + \bar{v}) \quad (13)$$

Conceptually, for the same free stream longshore velocity, enhanced vertical mixing would increase the velocity near the bed and increase the bottom stress, or conversely, the same bottom stress would be associated with a reduced free stream velocity (see again Fig. 1).

In regions of high breaking-wave induced turbulence penetration, c_{fr} is expected to dominate, while away from breaking-wave induced turbulence, bottom stress is again governed by the local generation through c_n . In the present work c_n is obtained through observation of wind forced currents seaward of

the surf zone. c_{tr} is formulated based upon a proposed model of horizontal and vertical distributions of turbulent kinetic energy (tke); a turbulence penetration parameter, χ , and a fitting coefficient, A .

Horizontal distribution of turbulent kinetic energy

A one-dimensional turbulent kinetic energy equation (tke- ϵ) (see for example Launder and Spalding (1972)) is used to solve for the temporally and vertically averaged breaking-wave induced tke, based on local balance of dissipation and production. Turbulent kinetic energy is assumed to be a sink for the decaying wave energy, which is estimated herein based upon surface elevation and the assumed equal partitioning of potential and kinetic wave energy given by linear theory. Horizontal (cross-shore) advection of the turbulence has been neglected, as in Deigaard et al. (1986), based on the small cross-shore net particle velocities considered over the column. (Comments regarding tke as it relates to longshore current forcing may be found in the discussion section). Vertical distribution is assumed to be through turbulent vortices injected from the surface, as concluded by Svendsen (1987) in his analysis of experimental data. More elaborate models of turbulence under breaking waves exist and include roller effects, multi-interface generation, and bi-directional advection (shoreward above trough and seaward below) (see for example Deigaard et al., 1991), and so these stated assumptions represent perhaps the simplest of views. However, the broad range of findings obtained thus far from laboratory data, and the general lack of field data, seems not to warrant more than a basic formulation.

The resulting equation is then:

$$\frac{\partial(Ec_{tx})}{\partial x} = \rho \int_{-h}^0 c_d \left\langle \frac{tke^{3/2}}{l_v} \right\rangle dz \quad (14)$$

where the left hand side represents production of tke, and the right hand side, dissipation. Here c_d is a coefficient taken as 0.08 following Launder and Spalding (1972), and l_v is the length scale of the vortices estimated as $0.07h$, with h representing depth, following Deigaard et al. (1986). Assuming vertically uniform tke and the combining of c_d and l_v into a single coefficient, $c_d/l_v \approx 1.0/h$, as done by Roelvink and Stive (1989), integration of Eq. (14) yields:

$$tke = \left[\frac{1}{\rho} \frac{\partial Ec_{tx}}{\partial x} \right]^{2/3} \quad (15)$$

Vertical distribution of turbulent kinetic energy

The vertical distribution of breaking-wave induced turbulence is quite likely

non-uniform, but at present is unresolved. Deigaard et al. (1986, 1991) present a theoretical model with significant vertical variation, while Svendsen (1987), summarizing a number of field and laboratory studies, found the turbulence to be surprisingly uniform. Different assumptions regarding advection and diffusion have been made and the subject appears far from resolved.

The present work reflects the uncertainty in predicting the magnitude of near-bottom breaking-wave induced turbulence through the use of a fitting coefficient, A , and a penetration parameter, χ , which scales the vertically averaged, wave induced turbulent kinetic energy contribution. This rather crude approach seeks the computational advantage of the assumption of vertically uniform tke, while recognizing that physically there must be some decay in tke close to the bed, ultimately reaching zero. Intuitively, one might expect the turbulent penetration to be related to breaker type, with increasing penetration going from spilling, to plunging, to collapsing breakers. Thus the new parameter,

$$\chi = \frac{\tan\beta(x)}{gH_{rms0}} \quad (16)$$

(with H_{rms0} denoting initial wave height and $\tan\beta(x)$, the local bottom slope) is employed. This parameter is similar to the surf parameter

$$\xi = \frac{\tan\beta(x)}{\sqrt{2\pi \frac{H_{rms0}}{gT^2}}} \quad (17)$$

but satisfies the dimensional requirements such that the product of χ and the vertically averaged tke is non-dimensional.

The wave height transformation model (Thornton and Guza, 1983), which stresses an ensemble view of wave breaking, assumes the wave heights are described by the Rayleigh distribution. Waves may break at any location throughout the surf zone with the likelihood at any given point also being based upon the Rayleigh distribution. Thus, some small percent of the waves might break on the shore side of the bar, a region in which the bottom slope, $\tan\beta$, is negative, producing a negative value of χ ; use of this parameter in predicting the turbulence penetration would yield non-physical negative values over the shoreward side of the bar. To eliminate this problem with the least disturbance to the relative nature of the parameter χ , $(\tan\beta + 0.03)$ was universally inserted in place of $\tan\beta$. In all of the cases studied, this was sufficient to ensure positive values throughout the surf zone, (i.e. the shoreward sloping faces do not exceed -0.03). In the planar beach case presented, this is of course unnecessary, but for comparison of the fitting parameter, results with and without this adjustment have been included. Although this modifi-

cation is rather cumbersome, it should be emphasized that χ , as used, is merely a relative measure and so it is cross-shore variation, and not magnitude, which is important.

An important point regarding the calculation of either χ or ξ over barred topography is that near the beach face, where the newly reformed wave rises up to break again, no history of the original wave height is maintained, and so the utility of the original H_{rms0} in such a parameter as ξ or χ is limited. Instead, it is suggested that a new value of H_{rms1} (i.e. that found over the trough), is used when considering breaking at the beach face. This implies

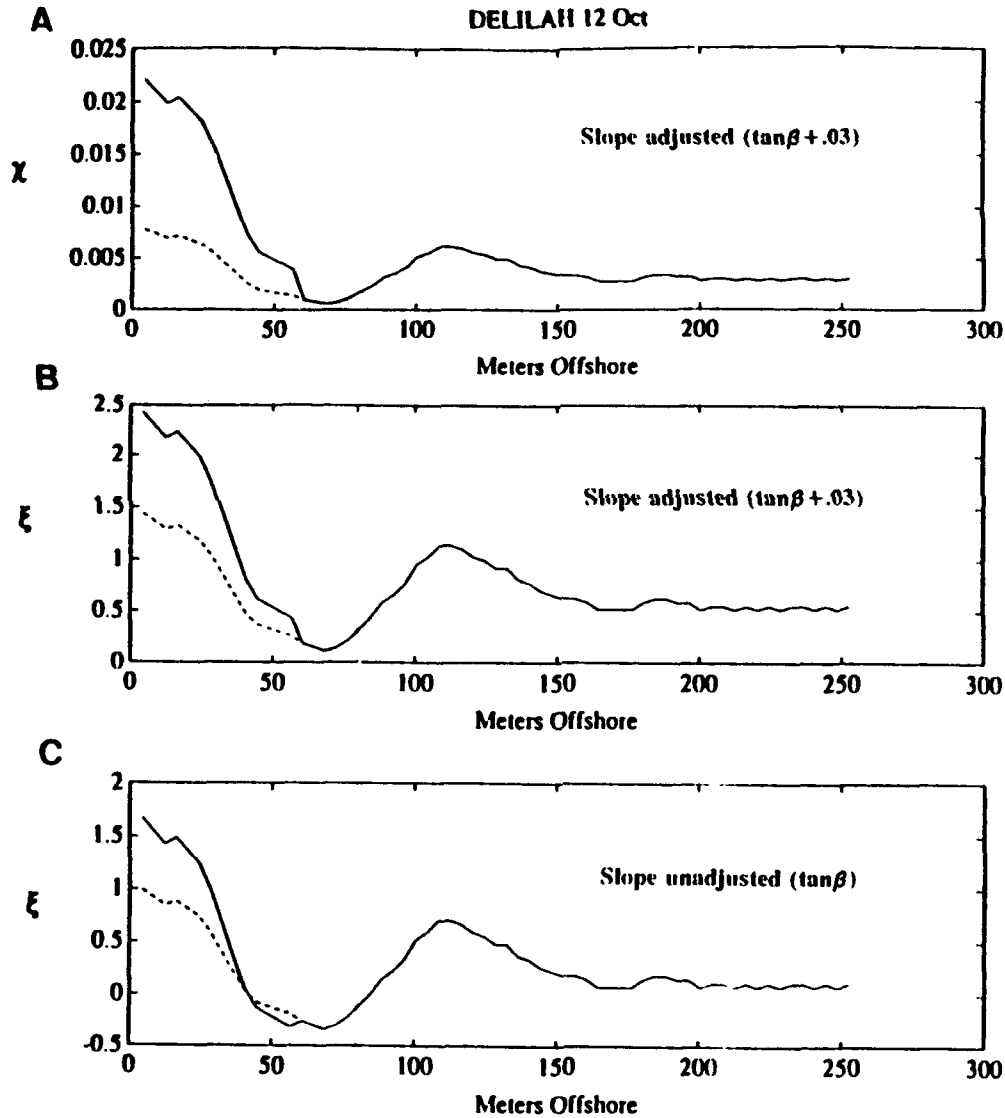


Fig. 3. Cross-shore profiles of (a) proposed penetration parameter χ , (b) surf characteristic parameter ξ (both containing the adjusted bottom slope of $\tan\beta + 0.03$), and (c) ξ without the bottom slope adjustment. Dashed lines indicate the values using only a single initial H_{rms0} .

(assumes) that surf characteristics are locally determined and should not be represented by characteristics measured seaward of some previous breaking region. Calculated values of $\chi(x)$ and $\xi(x)$, including the adjustment of $\tan\beta + 0.03$, for 12 Oct are shown in Fig. 3a and b. Values of $\xi(x)$ without the adjustment to $\tan\beta$ are shown in Fig. 3c. In each case, the values obtained through use of only the original H_{rms0} , measured seaward of the bar, have been plotted as dashed lines. Values produced through the proposed modification to include H_{rms1} (measured over the trough), are indicated as solid lines. The general behavior of the two parameters (comparing Figs. 3a and 3b) is quite similar. For both $\chi(x)$ and $\xi(x)$, values at the beach face are significantly increased through inclusion of the trough defined H_{rms1} (175% for χ and 67% for ξ). ξ is typically used as a parameter to determine breaker type and here comparisons to standard scales can most readily be done using Fig. 3c, which does not contain the $\tan\beta$ modification. In this case, re-initializing H_{rms0} to H_{rms1} increases the beach face value of ξ from 1.0 to 1.5, better corresponding with the visual observations that breakers at the beach face tended to be plunging. Recognition of the relevance of the trough region's H_{rms1} to beach-face breaking is not only significant in the present penetration parameterization, but likewise in any application of a surf parameter on a barred beach.

The proposed modification of bottom stress due to the near bottom mixing effect of the breaking-wave produced turbulence is now completed by including a fitting coefficient A , such that:

$$c_{fr} = A\chi(x)tke(x) \quad (18)$$

Wind stress and calculation of c_n

Since c_n is intended to relate bottom stress to free stream velocities without the influence of breaking wave induced turbulence, data from outside the surf zone are used to estimate its value. It is assumed that at some point sufficiently seaward of the surf zone observed currents are the result of wind forcing and not due to radiation stress decay. With this assumption, the y -momentum equation (Eq. 1) reduces to $\bar{R}_y = 0$ or $-\bar{\tau}_y^b + \bar{\tau}_y^\eta = 0$ where η refers to the surface. Wind data were measured by an anemometer mounted on the seaward end of the FRF pier, 550 meters offshore at an elevation of 19 m. Assuming a logarithmic profile, wind velocity, W , were translated to values at the standard 10 m elevation. The wind friction coefficient used, $c_{wd} = 1.2875 \times 10^{-3}$, is taken from the WAMDI Group (1988) results for light wind situations. Current data were from a current meter located just shoreward of the 8 m depth contour, roughly 800 m offshore. The assumed along-shore balance of bottom and surface stresses can now be written:

$$c_n \rho |\bar{U}| (\bar{V} + \bar{v}) = c_{wd} \rho_a |\bar{W}| \bar{W}_y \quad (19)$$

where ρ_a is the density of air. The general (non-linear) form of the bottom stress cannot be solved analytically due to the non-linear wave-current interaction, and so c_n is obtained through the iterative method previously discussed. Although the wind friction coefficient may be altered by conditions within the surf zone (cf. Whitford and Thornton, 1993), the wind stress is included in the longshore current model using the WAMDI Group value as a conservative estimate.

Solution method

The model equations are then:

$$\frac{\partial}{\partial x}(EC_s \cos \alpha) = \langle \epsilon_b \rangle \quad (5)$$

$$\frac{\partial S_{yx}}{\partial x} = \frac{\sin \alpha_0}{C_0} \frac{\partial}{\partial x}(EC_s \cos \alpha) \quad (2)$$

$$\frac{\partial S_{yx}}{\partial x} = -\bar{\tau}_y^b + \bar{\tau}_y^\eta \quad (1)$$

$$\bar{\tau}_y^b = (c_n + c_{fr})\rho \overline{|U|(V + \tilde{v})} \quad (13)$$

$$tke = \left[\frac{1}{\rho} \frac{\partial EC_{gx}}{\partial x} \right]^{2/3} \quad (15)$$

$$c_{fr} = A\chi(x)tke(x) \quad (18)$$

$$c_n \rho \overline{|U|(V + \tilde{v})} = c_{wd} \rho_a \overline{|W|W_y} \quad (19)$$

The Thornton and Guza (1983) wave height transformation model using bore dissipation theory (Eq. 5) is used to predict the gradient of cross-shore wave energy flux, used in Eq. (2) to calculate the radiation stress gradient (which serves as the forcing term in equation Eq. 1). The penetration parameter (used in Eq. 18) is similarly given by the wave transformation model. The cross-shore distribution of tke is solved for through Eq. (15) and is then used in Eq. (18) to estimate the vertical mixing effect of the breaking-wave induced turbulence. The modification of the bottom stress due to the breaking-wave induced turbulence is then modeled through Eq. (13). The locally generated bottom friction, c_n , is obtained through the assumed stress balance well outside the surf zone, given by Eq. (19). Balancing the radiation stress gradient with the bottom stress in Eq. (1) allows solution for the longshore current velocity.

DELILAH EXPERIMENT DESCRIPTION

The DELILAH experiment was conducted between October 1 and 21, 1990 at the US Army Corps of Engineers' Field Research Facility (FRF) at Duck, North Carolina, a barred beach which was the site of the previous experiments DUCK 85 and SUPERDUCK. Site selection was based upon the presence of the FRF and its infrastructure, including the permanent directional wave array which the FRF maintains in 8 meters of water, and the relative isolation of the beach. Three principle arrays (co-located current meters and pressure sensors), shown in Fig. 4, were used to acquire data near-continuously throughout the experiment with a sampling rate of 8 Hz. The cross-shore array consisted of 9 current meter/pressure gage stations deployed from the beach face to just beyond the 4 meter contour. The two alongshore arrays, one of 6 current meters and the second of 5, were located in approximately

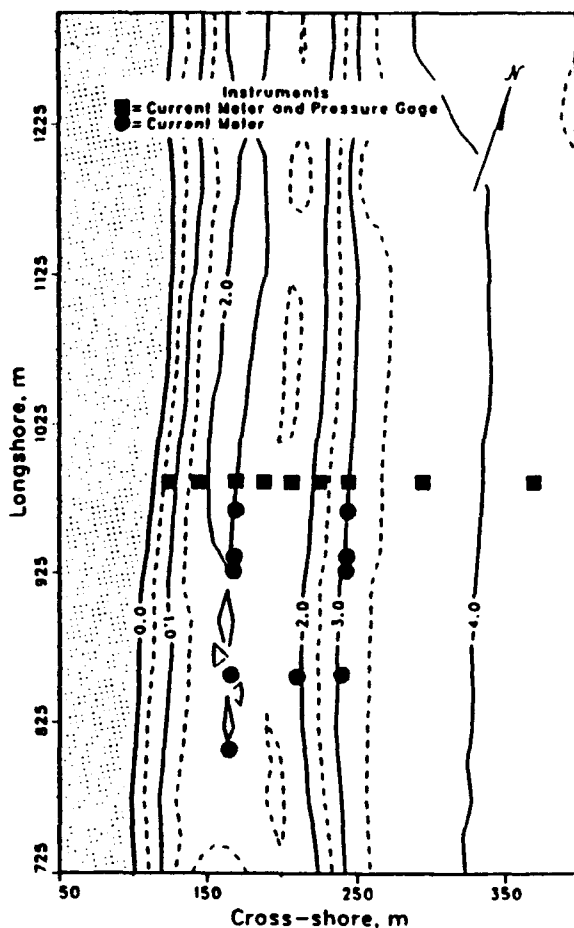


Fig. 4. Current meter and pressure sensor placement during the DELILAH experiment (bathymetry shown is for 12 Oct 90).

1.5 and 3 meters of water. An autonomous Coastal Research Amphibious Buggy (CRAB), which was designed to provide a relatively stable platform for operations within the surf zone, was used for daily bathymetric measurements, instrument installation/removal, and towing of an instrumented sled.

A variety of wave conditions occurred during the experiment, including mild swell waves from the south between 2 and 9 October; a "southeaster" starting on the 11th, causing waves to reach nearly 2 meters in height; and an interval of long period, windless swell reaching approximately 2.5 meters in height, initiated remotely by hurricane Lili, arriving on the 13th. Strong long-shore currents were observed frequently. Reversals in the direction of the mean longshore current were observed to correspond with the shifting of the direction of the principal incident wave component. Four experiment days are chosen for model comparisons (Oct 10, 11, 12, and 13) when waves were narrowbanded, varying in rms wave height from 0.77 to 1.43 m and arriving at relatively large angle (14.0 – 16.8°), see Table 1. Reasonable narrowbandedness in both frequency and direction can be seen in the two-dimensional energy density spectra for the four DELILAH data sets (Fig. 5).

The assumption of uniformity in the alongshore direction is related to the

TABLE 1

Wave/wind/current conditions and parameters

Location	DELILAH				Santa Barbara
Date Time	10 Oct 0500	11 Oct 0100	12 Oct 2100	13 Oct 0300	4 Feb
H_{rms0} (m)	0.77	1.43	1.14	1.30	0.56
H_{rmst}^a (m)	0.27	0.70	0.45	0.70	
α ($^\circ$)	16.7	16.6	14.0	16.8	9.0
f_{peak} (Hz)	0.094	0.110	0.075	0.078	0.070
B	1.3	1.1	1.3	1.3	1.3
γ	0.38	0.46	0.40	0.42	0.41
Wind speed (m/s)	2.3	11.7	6.8	4.7	
U_{8m}^b (m/s)	0.06	0.32	0.19	0.11	
c_n	0.0010	0.0014	0.0010	0.0008	0.001 ^c
c_r	2.0	3.0	1.2	2.2	4.0 (7.5 ^d)
Mean c_r^e	0.0025	0.0042	0.0020	0.0030	

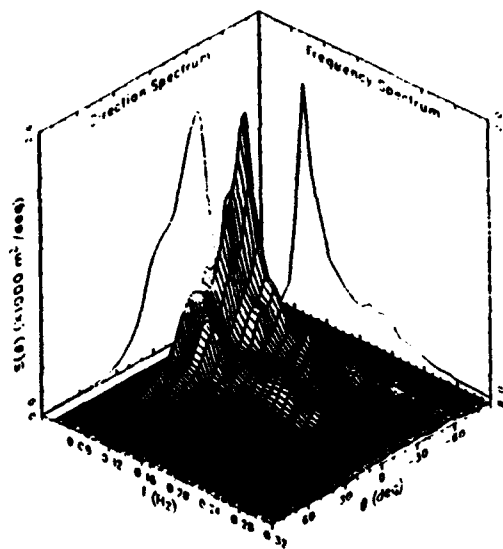
^a H_{rmst} measured over trough.

^bMeasured at 8 m FRF array, approx. 800 m offshore.

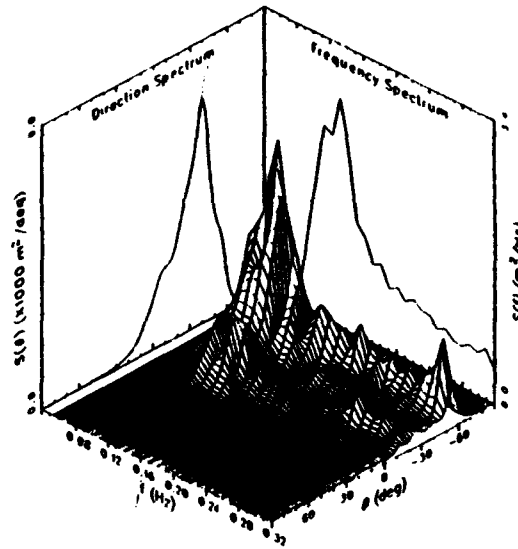
^cAssumed value.

^dValue without $\tan\beta$ adjustment.

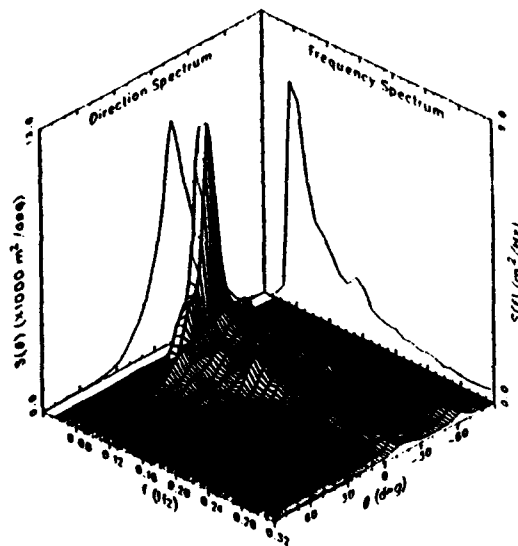
^eCross-shore mean of $c_n + c_r$.



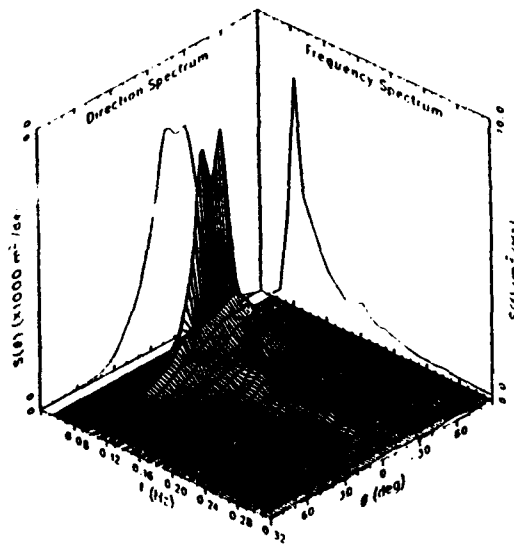
DELILAH 10 October, 1990



DELILAH 11 October, 1990



DELILAH 12 October, 1990



DELILAH 13 October, 1990

Fig. 5. Frequency and direction two-dimensional energy density spectra for the four DELILAH data sets, Oct 10–13.

two-dimensionality of the bathymetry. The beach tends to form 3-D rhythmic crescentic bars during times of (normal) moderate waves, shifting toward a 2-D linear bar when the waves are large. Commencing on the 9th, long period swell arrived at relatively large incident angles from the south, produced a near-linear bar throughout the remainder of the experiment. Oct 12 is a rep-

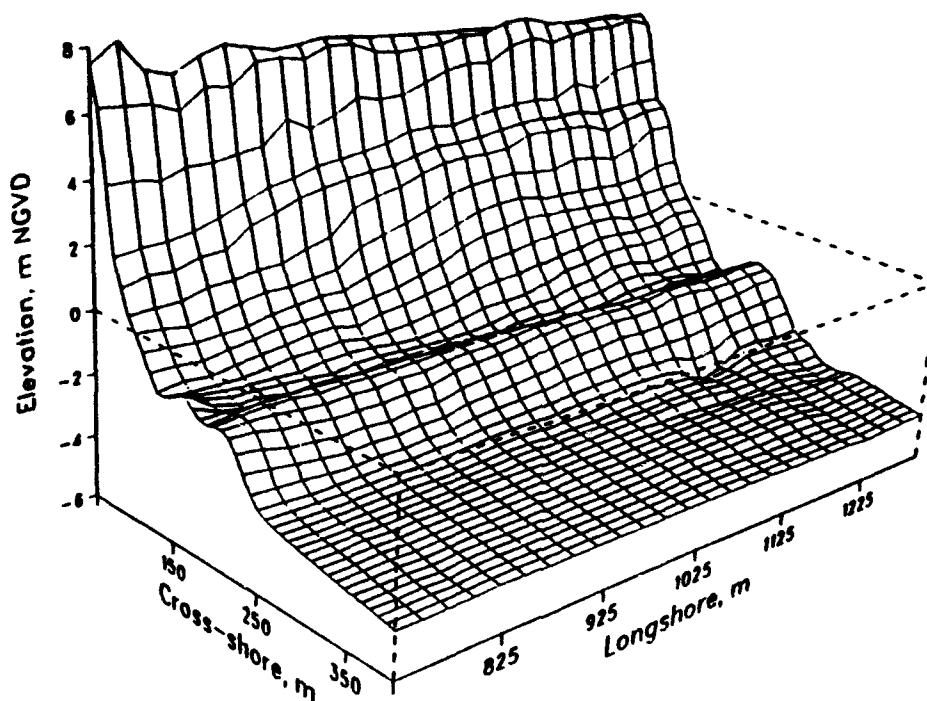


Fig. 6. Bathymetry acquired by CRAB for 12 Oct.

representative day and the measured bathymetry is shown in Fig. 6. Wave activity on Oct 13 prevented bottom profiling, and so an average profile calculated based on the 12th and 14th has been used within the model. Bathymetry for Santa Barbara on 4 Feb is described in Thornton and Guza (1983) and is near planar with a slope of 0.038.

COMPARISON WITH DATA

Model results are presented in Figs. 7–11 for Feb 4 Santa Barbara NSTS data and the four data sets from the DELILAH experiment (Oct 10, 11, 12, and 13). Each wave height plot contains measured and predicted rms-wave heights together with bathymetry and predicted tide distributions. Each longshore current plot contains bathymetry and 3 longshore current profiles (one for a linear bottom stress term, one for a non-linear term, and one for the proposed term which is also non-linear, but includes the effects of breaking-wave induced turbulence).

H_{rms} modeling results

Agreement between observed and predicted H_{rms} is generally good. Values for the two coefficients contained in the wave height transformation model, γ

Santa Barbara 4 FEB

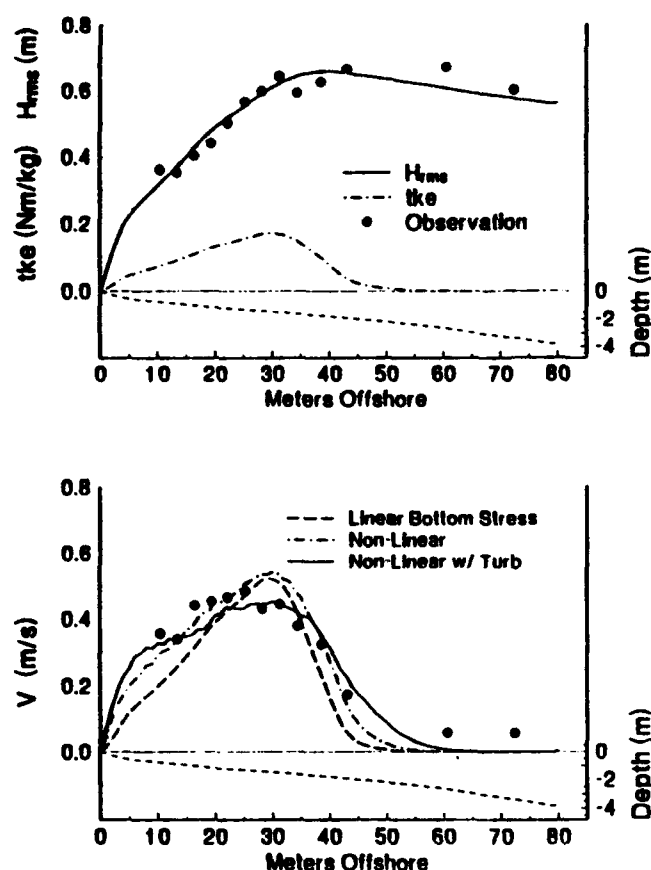


Fig. 7. Model predictions and observations for Santa Barbara 4 Feb. Upper panel shows predicted H_{rms} and tke profiles with measured H_{rms} and bathymetry. Lower panel shows longshore current profiles for the three bottom stress forms: linear ($C_f=0.008$), non-linear ($C_f=0.006$), and non-linear with addition of breaking wave induced turbulence ($\lambda=7.5$, $C_n=0.001$).

and B , obtained by fitting the model to the data in a least-square-sense, are included in Table 1. Results for the near planar beach at Santa Barbara (Fig. 7), show a broad cross-shore distribution of tke produced by wave breaking, which occurs throughout the surf zone. The DELILAH predictions contain two breaker regions; the first of which, just seaward of the bar, is somewhat broad; the second, at the beach face, is rather abrupt.

The narrowbanded conditions on the 10th, 12th, and 13th are to some extent unusual for East Coast beaches, being more typical of Pacific swell. This is reflected in the resulting values of B , which for these three days are very close to that obtained for the Santa Barbara beach. On the 11th, a nearby "southeaster" produced the least narrowbanded of the four DELILAH data sets, requiring use of a slightly lower value of B .

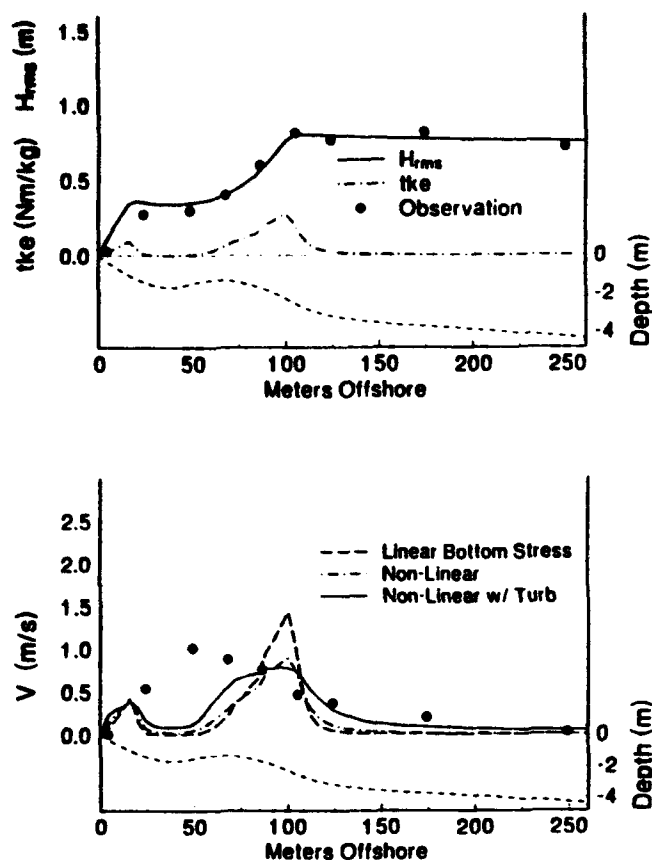


Fig. 8. Model predictions and observations for DELILAH 10 Oct: linear ($C_f=0.008$), non-linear ($C_f=0.006$), and non-linear with addition of breaking wave induced turbulence ($A=2.0$, $C_n=0.0010$).

Calculation of c_n

c_n , which is important away from the breaking-wave induced turbulence, has been determined based upon an assumed balance of surface wind stress and bottom stress at a location well seaward of wave breaking. Mean values for winds and offshore current for the four DELILAH data sets are contained in Table 1 and are plotted in Fig. 12. Winds were measured at the FRF pier, located approximately 500 m south of the cross-shore array and approximately 550 m offshore. Current data were taken 800 m offshore at the along-shore position of the main cross-shore array. The correlation coefficient between W_y and V is 0.991 and that for W_y^2 and V^2 is 0.994, both with y -intercepts near zero. Equation (19) includes the non-linear wave-current interaction in the bottom stress treatment and so the iterative method previously mentioned is used to obtain c_n values for the four data sets of 0.0010, 0.0014, 0.0010, and 0.0008 (mean value of 0.0010). It is interesting to note that neglecting the effects of the wave motion, i.e. treating the flow as unidirectional, yields c_n values roughly twice these, demonstrating the increased

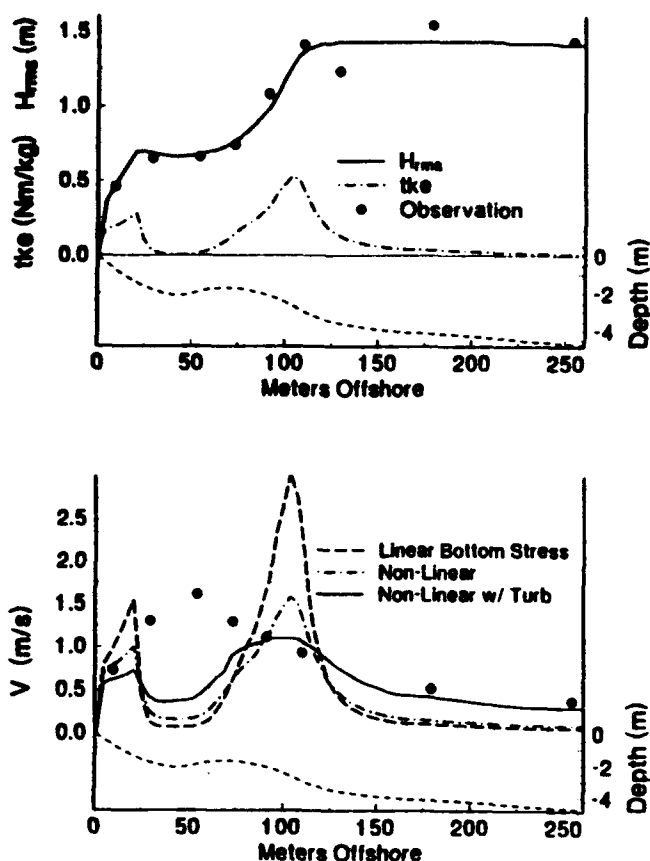


Fig. 9. Model predictions and observations for DELILAH 11 Oct: linear ($C_f=0.008$), non-linear ($C_f=0.006$), and non-linear with addition of breaking wave induced turbulence ($\lambda=3.0$, $C_n=0.0014$).

stress resulting from combined wave-current flow noted by Grant and Madsen (1979).

Longshore current modeling

Fitting of the Santa Barbara velocity profiles (Fig. 7), for the two spatially constant c_f cases, linear and non-linear (without breaking-wave induced turbulence), produces c_f values of 0.008 and 0.006. As expected, the non-linear coefficient is lower. In the absence of offshore wind/current data for Santa Barbara, the mean c_n value obtained from the four DELILAH cases has been assumed. The proposed model with $\lambda=4.0$ and $c_n=0.001$ produces a smoother profile throughout the most intense breaking region (where c_f dominates) with increased velocity on the seaward extreme (where c_n dominates). The overall result is slightly better agreement with observations. It should be remembered that the adjustment of $\tan\beta$ necessitated by the bar has been included strictly for comparison and is not physically necessary. Without this

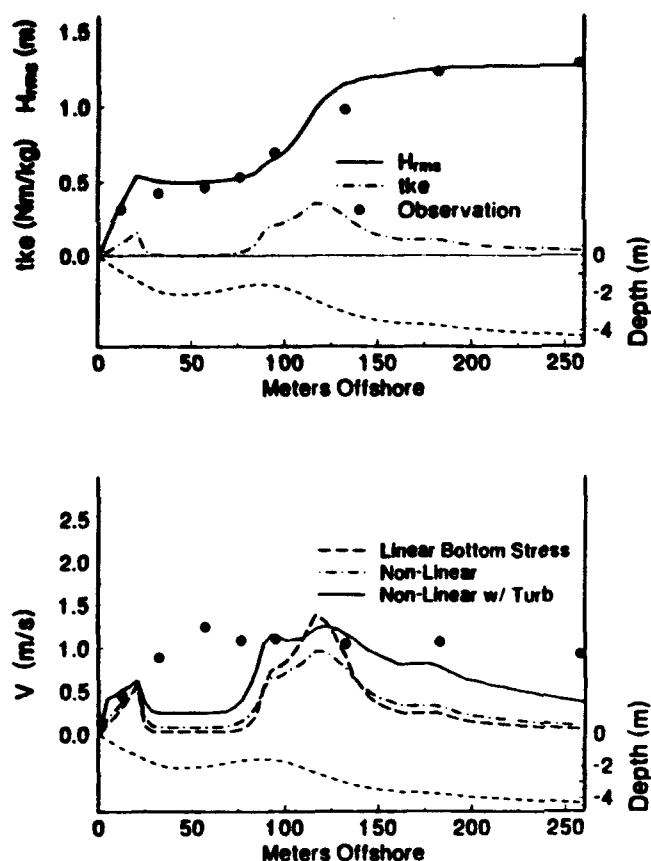


Fig. 10. Model predictions and observations for DELILAH 12 Oct: linear ($C_r=0.008$), non-linear ($C_r=0.006$), and non-linear with addition of breaking wave induced turbulence ($\lambda=1.2$, $C_n=0.0010$).

adjustment a value of $\lambda=7.5$ is found (the resulting velocity profile has been omitted as it is essentially identical to that shown).

In the case of the barred beach studied in DELILAH (Figs. 8–11), long-shore current profiles for the linear and non-linear (without breaking-wave induced turbulence) bottom stress cases show maxima at the seaward face of the bar and at the beach face. The dissimilarity between either of these and the observed profile is such that attempts at fitting are futile and so the values of 0.008 and 0.006 (those found for the Santa Barbara data) have been used for comparison. Again, none of the velocity profiles include horizontal mixing. For the case of the proposed bottom stress form, fitting of the predicted profiles in the high turbulence regions (the vicinity of the bar and beach face), where c_r dominates, yields λ values of 2.0, 3.0, 1.2 and 2.2 for the four days.

In the offshore region, reduced c_r values, controlled primarily by c_n , result in increased velocity predictions and improved agreement with observations. In the cases of the 12th and 13th, while significant velocities are predicted seaward of the bar, these predictions are well below the observations. Average

DELILAH 13 OCT.

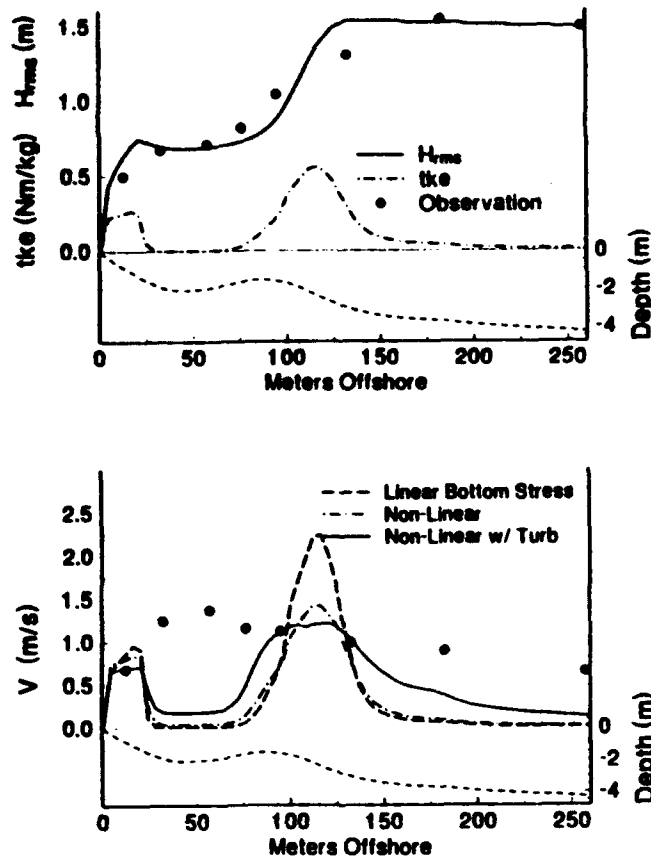


Fig. 11. Model predictions and observations for DELILAH 13 Oct: linear ($C_f=0.008$), non-linear ($C_f=0.006$), and non-linear with addition of breaking wave induced turbulence ($\lambda=2.2$, $C_n=0.0008$).

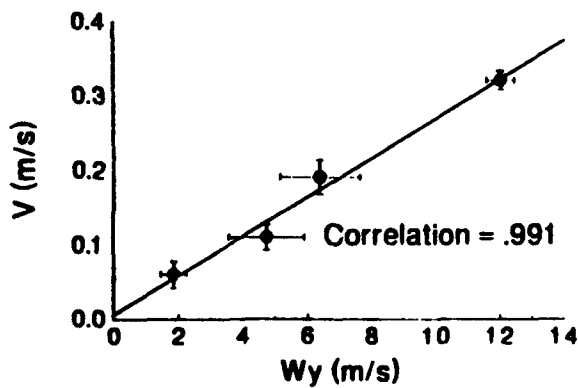


Fig. 12. Linear regression of mean longshore current (measured approximately 800 m offshore) with mean alongshore winds (measured at the seaward end of the FRF pier).

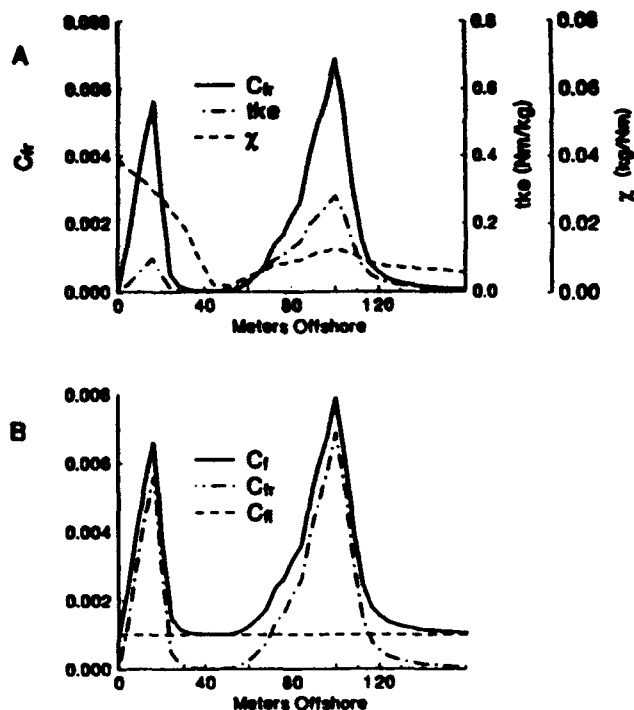


Fig. 13. (a) Cross-shore profile of c_r and its two variable components, χ and tke , for Oct 10; (b) c_r and its two additive components c_n and c_{fr} , also for Oct 10.

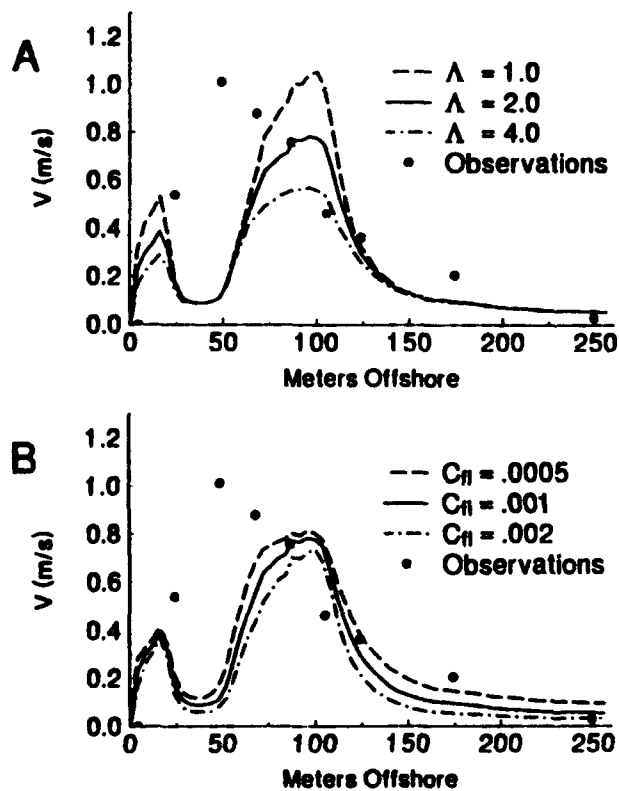


Fig. 14. Sensitivity test on (a) Λ , with c_n held constant at 0.001, and (b) c_n , with Λ held constant at 2.0.

wind magnitude during the period studied on the 12th was 6.8 m/s and 4.7 m/s on the 13th and offshore current velocities measured at the 8 m FRF meter were 0.2 m/s for the 12th and 0.1 m/s for the 13th, indicating that wind forcing was not responsible for the observed strong flows.

In the vicinity of the trough, wind forcing coupled with reduced c_f predicts velocities of 0.1–0.5 m/s. Elsewhere in the surf zone the radiation stress forcing dominates and the wind stress contribution is negligible. As a result the only region within the surf zone where the predicted longshore current profile is significantly altered by inclusion of the wind stress is in the trough region. c_{fr} and its two spatially variable components, χ and τ_{ke} , are shown for Oct 10 in Fig. 13 along with the cross-shore profile of c_n , c_{fr} , and their sum c_f . Sensitivity tests on A and c_n are shown in Fig. 14. The three profiles of V shown represent three values of A (1.0, 2.0, and 4.0) with c_n held constant at 0.001. It can be seen that the profiles are not overly sensitive to A with a doubling of A producing only a 20–25% change in V_{max} . The converse situation is also shown where A is held constant (2.0) and c_n is varied. As expected, the changes are found in the trough and seaward of the bar, regions away from the domination of breaking-wave induced turbulence.

DISCUSSION

Consideration of the effective bottom friction coefficient as the composite of two separate contributions has been shown to improve prediction/observation agreement for the five cases considered. Although the calculated values of c_n : 0.0010, 0.0014, 0.0010, and 0.0008, are significantly lower than c_f values used in previous studies, it should be emphasized that when combined with the remotely generated turbulence effects of c_{fr} , the net values are increased over much of the surf zone. Considering the 160 m closest to the shore, the cross-shore means of $c_f = c_{fr} + c_n$, (0.0025, 0.0042, 0.0020, and 0.0030), are comparable to the spatially constant non-linear c_f values found in the literature; cf. Thornton and Guza (1986): 0.006; Visser (1984): 0.003 and 0.008; Wu et al. (1985): 0.010; Larson and Kraus (1991): 0.0035 and 0.004).

The results of Whitford and Thornton (1993), based upon SUPERDUCK data, support both the idea of a spatially variable c_f and qualitatively the predicted values. Using a mobile instrumented sled, Whitford and Thornton made estimates of the various terms in the momentum equation in order to obtain values of c_f across the surf zone. Their mean results of 0.004 (offshore of the bar), 0.003 (over the bar), and 0.001 (over the trough) are in general agreement with the values of c_f shown in Fig. 13.

The proposed treatment, while differentiating between the dramatically different flow characteristics of breaking and non-breaking regions, assumes the characteristics of all non-breaking flow to be the same. Specifically it is assumed that the c_n value calculated for 800 m offshore is appropriate

throughout the surf zone. In the trough the wave height model does not predict wave forcing and so it could be speculated that the observed currents might be wind driven. To examine this possibility, the modeled wind forcing (observed winds and the WAMDI friction coefficient) was compared with the observed flow, giving a high correlation of 0.92, but a regression y-intercept of 0.97 m/s (Fig. 15). This could be interpreted as indicating that while the current over the trough may be related to wind forcing, there exists a background flow of approximately 1.0 m/s which has not yet been explained.

It may also be argued that the wind friction coefficient may well vary in the cross-shore direction over the surf zone due to differences in surface roughness (primarily due to waves) and the ability of the turbulent crest/trough layer to transfer momentum throughout the water column. In the present study wind forcing has been considered constant over the entire domain. If some mechanism should greatly increase the wind friction coefficient in the region of the trough, this might explain the longshore current maximum. Such issues are not clearly understood at this time, but again the linear regression based on the four data sets studied does not support this idea.

An additional possibility in explaining the current maximum in the trough is the violation of the longshore uniformity assumption, such that a pressure gradient in the alongshore direction could produce accelerations not recognized by the model. Irregularities in the bar could produce differential wave breaking resulting in alongshore variability in set-up/down profiles, thus creating alongshore surface slopes (pressure gradients). However, as pointed out by Holman (personal communication, 1992) this idea is not supported by the high level of correlation between changes in the wave incidence quadrant and direction of the current measured over the trough observed during DELILAH. It should also be noted that such a displacement in the point of maximum set-down creates two surface slopes, one on the seaward side of the

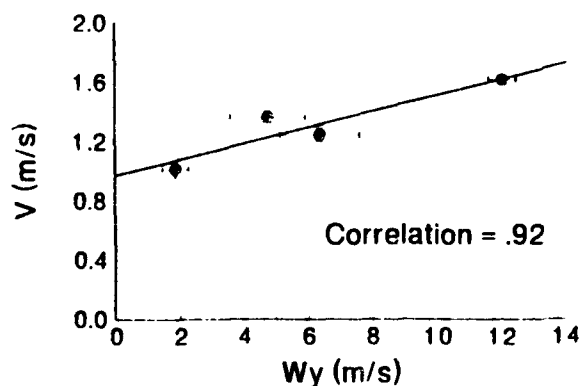


Fig. 15. Linear regression of mean longshore current (measured over the trough) with mean alongshore winds (measured at the seaward end of the FRF pier).

breaker zone, and an oppositely directed one on the shoreward side. Such sharp gradients of longshore current have not been observed.

Inclusion of the turbulent radiation stress has potential for improved modeling. Roelvink and Stive (1989) use tke to predict turbulent radiation stress in a two dimensional (cross-shore directed) study of undertow, which requires describing S'_{xx} and therefore the variances, $\overline{u'u'}$, $\overline{v'v'}$, and $\overline{w'w'}$. After predicting the total level of turbulent kinetic energy in the column and making reasonable assumptions regarding the distribution of this energy between u , v , and w , cross-shore profiles of S'_{xx} may be obtained. The study of longshore currents however, requires specifying the turbulent radiation stress (S'_{yx}) which requires knowledge of the covariance between turbulent velocity components ($\overline{u'v'}$) within the surf zone, a topic with little theoretic background to draw upon. Measurement of such a term in the surf zone has not been done to date, because it is not known how to separate out the much larger wave induced velocity contributions.

Although horizontal momentum mixing has neither been treated explicitly nor parameterized within the proposed model, it is recognized that mixing does occur to some extent in nature and new mechanisms such as mean cross-shore flow and shear instabilities are being explored. Certainly, mixing would be likely to transfer some longshore momentum into the trough region, but generation of the velocity maximum via classical mixing length theory/velocity shear, and thereby the demand for up-gradient momentum transfer, does not appear rational.

CONCLUSIONS

The assumption that the relationship between the free stream longshore current velocity and the bottom stress is constant across the surf zone has been brought into question. Field data from DELILAH have been used to demonstrate that a spatially variable bottom friction coefficient, representing the inclusion of breaking-wave induced turbulence effects, improves model predictions of the longshore current profile without reliance on horizontal mixing. Data from NSTS Santa Barbara are used to demonstrate that the proposed model is similarly applicable to planar beaches. Disparities between predicted and observed velocities over the trough are suggested to be due to a failure to identify a significant alteration of the forcing mechanism in this particular region.

ACKNOWLEDGEMENTS

The authors wish to express their appreciation to all those who participated in the DELILAH experiment and in particular the staff of the Coastal Engineering Research Center's Field Research Facility, under the direction of Mr.

William Birkemeier. Directional wave spectra were provided by C. Long. In addition, special appreciation is expressed to T. Stanton of the Naval Postgraduate School for significant technical assistance, Rob Wyland, Naval Postgraduate School, and Katie Scott, Univ. of Calif. Santa Cruz, for their roles in acquisition of wave and current data, and to Mary Bristow, Naval Postgraduate School, for initial processing of the data. E.B.T. was funded by ONR Coastal Sciences Grant N00014-92-AF-0002 and J.C.C. is an ONR fellow.

REFERENCES

- Battjes, J.A., 1975. Modeling of turbulence in the surf zone. In: Proc. of the Symposium on Modeling Techniques, ASCE, pp. 1050-1061.
- Battjes, J.A., 1983. Surfzone turbulence. In: Proc. IAHR Cong. 20th Semin. Hydrodyn. Coastal Zone, Moscow. Vol. 7, pp. 137-140.
- Battjes, J.A. and Janssen, J.P.F.M., 1978. Energy loss and setup due to breaking of random waves. In: Proc. 16th Coastal Eng. Conf., ASCE, pp. 569-587.
- Bowen, A.J., 1969. The generation of longshore currents on a plane beach. *J. Mar. Res.*, 27: 206-215.
- Christoffersen, J.B. and Jonsson, I.G., 1985. Bed friction and dissipation in a combined current and wave motion. *Ocean Eng.*, 12(5): 387-423.
- Dally, W.R., Dean, R.G. and Dalrymple, R.A., 1985. Wave height variation across beaches of arbitrary profile. *J. Geophys. Res.*, 90(C6): 11,917-11,927.
- Deigaard, R., Fredsøe, J. and Brøker Hedegaard, I., 1986. Suspended sediment in the surf zone. *J. Waterw. Port. Coastal Ocean Div. ASCE*, 112: 115-127.
- Deigaard, R., Justesen, P. and Fredsøe, J., 1991. Modelling of undertow by a one-equation turbulence model. *Coastal Eng.*, 15: 431-458.
- Dodd, N. and Thornton, E.B., 1990. Growth and energetics of shear waves in the nearshore. *J. Geophys. Res.*, 95(C9): 16,075-16,083.
- Goda, Y., 1975. Irregular wave deformation in the surf zone. *Coastal Eng. Jpn.*, 13-26.
- Grant, W.D. and Madsen, O.S., 1979. Combined wave and current interaction with a rough bottom. *J. Geophys. Res.*, 84(C4): 1797-1808.
- Guza, R.T., and Thornton, E.B., 1978. Variability of longshore currents. In: Proc. 16th Coastal Eng. Conf. ASCE, pp. 756-775.
- Jonsson, I.G., 1967. Wave boundary layers and friction factors. In: Proc. 10th Coastal Eng. Conf. ASCE, pp. 127-148.
- Larson, M.L. and Kraus, N.C., 1991. Numerical model of longshore current for bar and trough beaches. *J. Waterw. Port. Coastal Ocean Div. ASCE*, 117: 327-347.
- Launder, B.E. and Spalding, D.B., 1972. *Mathematical Models of Turbulence*. Academic Press, London and New York.
- Longuet-Higgins, M.S., 1970a. Longshore currents generated by obliquely incident sea waves, 1. *J. Geophys. Res.*, 75: 6778-6789.
- Longuet-Higgins, M.S., 1970b. Longshore currents generated by obliquely incident sea waves, 2. *J. Geophys. Res.*, 75: 6790-6801.
- McDougal, W.G. and Hudspeth, R.T., 1986. Influence of lateral mixing on longshore currents. *Ocean Eng.*, 33: 419-433.
- Phillips, O.M., 1966. *The Dynamics of the Upper Ocean*. University Press, Cambridge, pp. 22-70.

- Putrevu, U. and Svendsen, I.A., 1991. Nearshore mixing due to the interactions of the undertow and longshore currents (abstract). *Eos Trans. AGU*, 72: 253.
- Roelvink, J.A. and Stive, M.J.F., 1989. Bar-generating cross-shore flow mechanisms on a beach. *J. Geophys. Res.*, 94(C4): 4785-4800.
- Sleath, J.F.A., 1990. Velocities and bed friction in combined flows. In: *Proc. 22nd Coastal Eng. Conf.*, ASCE, pp. 450-463.
- Sleath, J.F.A., 1991. Velocities and shear in wave-current flows. *J. Geophys. Res.*, 96(C8): 15,237-15,244.
- Svendsen, I.A., 1987. Analysis of surf zone turbulence. *J. Geophysical Res.*, 92(C5): 5115-5124.
- Thornton, E.B., 1970. Variation of longshore current across the surf zone. In: *Proc. 12th Coastal Eng. Conf.*, ASCE, pp. 291-308.
- Thornton, E.B. and Guza, R.T., 1981. Longshore currents and bed shear stress. In: *Proc. 12th Coastal Eng. Conf.*, ASCE, pp. 291-308.
- Thornton, E.B. and Guza, R.T., 1983. Transformation of wave height distribution. *J. Geophys. Res.*, 88(C10): 5925-5938.
- Thornton, E.B. and Guza, R.T., 1986. Surf zone longshore currents and random waves: Field data and models. *J. Phys. Oceanogr.*, 16: 1165-1178.
- Thornton, E.B. and Whitford, D.J., 1993. Longshore currents over a barred beach, II. Model. *J. Phys. Oceanogr.*, submitted.
- Trowbridge, J. and Madsen, O.S., 1984. Turbulent wave boundary layers, I. Model formulation and first-order solution. *J. Geophys. Res.*, 89(C5): 7989-7998.
- Visser, P.J., 1984. Uniform longshore current measurements and calculations. In: *Proc. 19th Coastal Eng. Conf.*, ASCE, pp. 2192-2207.
- Whitford, D.J. and Thornton, E.B., 1993. Longshore currents over a barred beach, I. Field experiment. *J. Phys. Oceanogr.*, submitted.
- Wu, C.S., Thornton, E.B. and Guza, R.T., 1985. Waves and longshore currents: comparison of a numerical model with field data. *J. Geophys. Res.*, 90(C3): 4951-4958.

III. VERTICAL PROFILES OF LONGSHORE CURRENTS: FIELD OBSERVATIONS

(This chapter consists of work submitted to
Coastal Engineering in September 1993)

VERTICAL PROFILES OF LONGSHORE CURRENTS: FIELD OBSERVATIONS

J.C. Church and E.B. Thornton

Department of Oceanography, Naval Postgraduate School, Monterey, CA 93943

R.T. Guza

Scripps Institution of Oceanography, La Jolla, CA 92093

K.A. Scott

Earth Sciences Board, University of California, Santa Cruz, CA 95064

ABSTRACT

Vertical profiles of mean longshore currents are examined using vertically stacked electromagnetic current meters at varying locations across the surf-zone. Field data were collected at a near-planar beach (Scripps Beach, Ca 1987) and a barred beach (Duck, North Carolina 1986). Significant vertical shear is observed in the mean current structure during periods when $\gamma = H_{rms}/h$ is below 0.30 (mean change in V over depth as a percent of the bottom current meter value is 49%). Of the 64 profiles studied, 15 were considered to be statistically indistinguishable from vertical; all 15 occurring during periods when $\gamma \geq 0.3$. Logarithmic profiles are fit to the data and c_f values obtained. For the three stacks of current meters at Scripps Beach (from seaward stack shoreward) mean values are 0.008 (std dev = 0.005), 0.010 (0.004), and 0.006 (0.003), with an overall mean value of 0.008. The mean c_f estimated for the barred beach, based on measurements at various cross-shore positions is 0.014 (std dev = 0.007). The apparent roughness height, z_a , shows a decreasing trend as the ratio of the magnitude of wave velocity to mean longshore current near the bottom goes from zero to 1.3. Given the estimated accuracy of the mean current values (± 3 cm/s), the data may

be explained equally well by either assumed logarithmic or linear profiles, requiring measurements closer to the bottom to distinguish between the two.

INTRODUCTION

Bottom stress is important in the nearshore region not only because of its role in the momentum equation governing the mean longshore current, but also because of its effects on sediment transport. In the simplest form, the longshore current equation is a balance between the breaking waves radiation stress gradient and the bottom stress felt by the mean longshore current. Following the work done in open-channel hydraulics, the bottom stress is typically modeled as proportional to the velocity squared through a bottom friction coefficient, c_f :

$$\overline{\tau^b} = c_f \rho |\overline{U}| \overline{U} \quad (1)$$

where ρ is water density and U is the instantaneous near bottom velocity. In the alongshore (y) direction this may be rewritten as

$$\overline{\tau^b}_y = c_f \rho |\overline{U}| (\overline{V} + \overline{v}) \quad (2)$$

in which V is the mean longshore current and \bar{v} represents the alongshore oscillatory wave component. The non-linear form is frequently linearized using assumptions regarding either the ratio of the mean current to the wave velocity or the angle of incidence, (for example Longuet-Higgins (1970), Liu and Dalrymple (1978)). In the present study the full non-linear form will be employed using the velocities measured at the lowest meter within each stack.

It is recognized that the bottom friction experienced by combined wave/current flow is greater than that experienced by currents in the absence of waves. Bijker (1967) carried

out an early investigation of this phenomenon, followed by a number of investigators principally focusing on the case of co-linear waves and current. Recently the general case of arbitrary wave-current angle and that of perpendicular wave-current interaction have been considered (for example Grant and Madsen (1979), Fredsøe (1984), Christoffersen and Jonsson (1985), and Sleath (1991)). Close to the bed, wave boundary layer turbulence (mixing) restricts the gradient in mean current (Fig. 1). As height above the bed increases, this wave boundary layer turbulence decreases and the mean current profile becomes logarithmic. If the profile above the region of wave boundary layer turbulence is examined in semi-log form, the zero-intercept is at z_0 , commonly referred to as the "apparent" bottom roughness.

As mentioned above, it is generally assumed that the undisturbed vertical profile of the mean current is logarithmic. For the specific case of waves perpendicular to the current, that most closely approximating the surf-zone, laboratory experiments are difficult owing to the problems of generating both orbital motion and a mean current which are not co-linear. Visser (1984) utilized a large wave basin in which breaking waves generated a longshore current. Measuring three points in the vertical using dye displacement, and averaging over the alongshore direction, the profiles appeared to be more linear than exponential. Visser (1986) examined combined non-breaking waves and currents generated using a mechanically driven circulation in the same wave basin, with velocities measured using both micro-propeller and laser doppler anemometers and bottom stress inferred from surface slope; the resulting profiles appeared generally logarithmic. Sleath (1990) used a steady-flow recirculating flume with the wave orbital motion simulated by oscillating the bed perpendicular to the steady flow. Velocities were measured using a laser doppler anemometer and the bottom stress inferred

from the observed vertical shear in the velocity profiles, which again were logarithmic. Simons *et al.* (1992) presented results from an extensive wave basin study in which bottom stress was measured directly using a shear plate, while velocities in the wave boundary layer were measured using a small fiber-optic laser anemometer and higher in the column using an ultrasonic flow meter. The vertical velocity profiles again tended to be logarithmic.

DATA ACQUISITION

SUPERDUCK Experiment

Data from a barred beach were obtained during SUPERDUCK, conducted in 1986 at the US Army Corps of Engineers Field Research Facility (FRF) located at Duck, North Carolina. The data were obtained using an instrumented mobile sled equipped with three Marsh-McBirney electromagnetic current meters mounted 0.7, 1.0, and 1.5m above the sea bed. (Martens and Thornton (1987) provide specific information on the design of the sled and calibration of its instrumentation.) This sled was towed seaward beyond the surf-zone by the FRF's CRAB (for Coastal Research Amphibious Buggy) and then pulled shoreward along a predetermined transect, stopping to acquire data at multiple cross-shore positions. Each data collection station was maintained for approximately 37 minutes, with data sampled at 8 Hz. Conditions during the 11 runs studied are provided in Table 1. Runs were centered temporally on tidal maxima in an effort to minimize tidal contamination within the current signal. Orientation of the sled during the collection periods was done to within ± 0.5 degrees using laser surveying of two prisms mounted atop the sled. Any angle recorded between the sled and the local bathymetry was then numerically corrected for in the data processing phase. The meters were at all times positioned on the "up-current" side of the sled

to minimize the effects of any flow distortion created by the sled's structure. Pre- and post-calibration of the current meters agreed within ± 3 percent in gain and 1-4cm/s in offset. Collection periods during which one or more of the currents meters became exposed above the water surface were noted and are not included within this study. The runs from the four most energetic days of the experiment, Oct. 15-18, constitute the 11 barred-beach velocity profiles studied. Whitford and Thornton (1993) provide further description of the sled's deployment in the investigation of longshore current mechanics.

UTOAD Experiment

Data from the near-planar beach at the Scripps Institution of Oceanography, La Jolla, California were acquired during the 1987 *UTOAD* experiment to examine cross-shore circulation. Three stacks of instruments were deployed within the surf-zone, each containing three Marsh-McBirney current meters, two open-frame electromagnetic current meters designed by Scripps, and two pressure sensors. Guza *et al.* (1988) intercompared the two designs of current meters and found good agreement. Based on their analysis, measurement error estimates of ± 3 cm/s are applied to all *UTOAD* velocity observations. The instruments were mounted on vertical bars at elevations ranging from 28 to 205cm above the bottom (see Table 2). These vertical bars were attached to a horizontal bar, being separated in the alongshore direction by approximately 1 m. The horizontal mounting bars were installed parallel with the bathymetry and caused varying degrees of scour, ranging in depth between 0-15cm below the surrounding bottom level. The horizontal extent of the scour was up to approximately 30cm in the cross-shore direction and spanned the length of the mounting bar in the alongshore direction. It is assumed that these features had negligible effect upon the

flow field and all subsequent meter elevations will be relative to the general bottom level and will not include these depressions. Unfortunately, the strength of this assumption cannot be adequately tested by the data obtained.

Data were sampled at 2 Hz and divided into 1.1 hour segments (8192 points). Over the nine days of the experiment, more than 120 hours of data were acquired for each of the three stacks deployed. In addition to providing mean depth and wave information, the pressure sensor time-series was used to identify periods during which meters located in the upper part of the water column might emerge above the surface. Further, periods were identified when the Marsh-McBirney current meters were less than 5cm below the surface, and the open-frame current meters less than 15cm, in order to avoid degraded electromagnetic signals due to proximity to the surface. The velocity signals were set to zero during these conditions and the percentage of the segment so effected was noted.

Initial calibration was performed at the Scripps Institution of Oceanography facility, providing the gain corrections applied to the data. *In situ* bias corrections were determined by identifying times of "no-flow" conditions (vertically averaged $V = 0$). Four such segments were found for stack A, three for stack B, and six for stack C. Of the 15 current meters, 13 had bias correction of 2.0cm/s or less, the remaining two current meters, OA2 and OB6, required corrections of 7 and 10cm/s, respectively. These two current meters were considered unreliable and therefore excluded.

Data quality requirements restricted the number of segments examined. These requirements were that a minimum of three current meters must be submerged over the entire period (current meters exposed at any time during the segment were excluded from the final data set); and, the mean current must exceed 10cm/s at some point within the vertical

profile. The first requirement provides a minimal bases for exponential and linear curve fitting, and the latter sets a minimum signal-to-noise ratio criterion. Based upon these two restrictions 45 profiles were examined, 22 from stack A (located 76m offshore), 19 from stack B (105m), and 4 from stack C (148m). The limited number of profiles from stack C prompted consideration of relaxing the restriction on zero time out of the water. It was decided that meters out of the water $\pm 5\%$ of the time would be included within the stack C data set only, relying on the assumption that the calculated mean velocities were also representative of the additional 1-5% during which the current meters were out of the water. This resulted in the addition of 8 more profiles, bringing the total to 53. Conditions during these 53 segments are contained in Tables 3-5.

PROFILE MODELING

As stated previously, the vertical profile of the mean longshore current has generally been assumed logarithmic, but was observed by Visser (1984), and theoretically suggested by Svendsen and Lorenz (1989) and Putrevu and Svendsen (1992), to be more linear. Both logarithmic and linear models are applied to the data and assessed in a simple least-squares manner.

Starting with Prandtl's mixing length hypothesis,

$$\tau^b = \rho l^2 \left\{ \frac{\partial V(z)}{\partial z} \right\}^2 \quad (3)$$

where V is the alongshore current and the mixing length, l , is κz , with κ , the von Karman constant taken as 0.4. Assuming a constant stress within the boundary layer and that U and V flow fields may be treated independently, yields

$$v(z) = \frac{v_*}{\kappa} \ln \left(\frac{z}{z_0} \right) \quad (4)$$

where v_* represents the friction or shear stress velocity and is related to the bottom stress through:

$$\tau_b = \rho v_*^2 \quad (5)$$

It should be noted that the roughness height, z_0 , has been replaced above by the apparent roughness height, z_o , which includes the effect of waves upon the bottom stress experienced by the current. z_o is typically found in laboratory studies by plotting the vertical current profile (without waves) in semi-log form and finding the vertical intercept, thus it is the height at which the logarithmic profile goes to zero. The mean longshore current is strongly linked to wave forcing in the field situations studied herein and so no opportunity exists to observe the current in the absence of waves. A wide variety of empirical formulae exist relating z_o to various parameters such as mean grain size (approximately 0.2mm) and ripple structure. Detailed measurement of such parameters was outside the objectives of the experiment and given the range in z_o values predicted through the various formulae, speculation does not seem to benefit the work; therefore no values of z_o have been calculated.

An estimate of v_* may be obtained from the slope of a least-squares fit to the data in semi-log form. Combining Eqs.(2) and (5)

$$c_f = v_*^2 \{ [U](V+\bar{v}) \}^{-1} \quad (6)$$

from which c_f may be found using the calculated v_* and measured near-bottom velocities. It is noted, that in semi-log form, measurements in the upper region of the column are

compressed and so the fitting process benefits greatly from points nearer the bottom.

Two conditions were imposed upon the fitting process. In consideration of the $\pm 3\text{cm/s}$ measurement error bars placed on the mean current values, profiles with less than 3cm/s vertical variation were considered indistinguishable from vertical and have not been included in the logarithmic fitting process. This effected 15 of the 64 total profiles studied. Of the remaining 49 profiles, 4 had one or more data points which fell more than 3cm/s from the fitted logarithmic profile and were therefore deemed to be weak fits. These weak fits are included in tables 6 through 9, but have not been included in the statistical summaries of the data sets. Finally, 2 c_f outliers (2.5 and 3.5 standard deviations from the mean) have been excluded from the summaries.

RESULTS

Tables 6 through 9 summarize the results obtained for the entire data set. Two objectives of this study are to examine the amount of vertical shear present in the mean longshore current and to determine whether this shear could best be modeled by logarithmic or linear models. Significant vertical shear is observed in the mean current during periods when $\gamma = H_{rms}/h$ is below 0.30 (mean change in V over depth as a percent of the bottom current meter value is 49%). Of the 64 profiles studied, 15 were considered to be statistically indistinguishable from vertical; all 15 occurring during periods when $\gamma \geq 0.30$. This phenomenon may be expressed through both the percent change in V from bottom current meter to top (Fig. 2), and the slope of the linear best fit line measured relative to vertical (Fig. 3). The principle difference between the two being that the percentage form includes the magnitude of the near-bottom current, while the slope form does not. It can be seen that the percentage increase in V decreases rapidly as γ increases. Four data points from stack C are

the exception. It is interesting to note that these four values and the neighboring value from stack B all occurred while the mean current was flowing to the south, with the flow toward the north during the remainder of the experiment. As previously mentioned, vertical shear was much less evident for γ values greater than 0.30. Measured in terms of the linear best fit slope relative to vertical this can be seen as a steady ramping up of the linear slope value followed by a more rapid falling off for γ values above 0.30. Again the four data points from stack C and one from stack B in the vicinity of γ are somewhat anomalous for the UTOAD data. The falling off is also seen in the SUPERDUCK data, although the slope values themselves are much higher.

Logarithmic profiles were fitted to the 49 segments which were distinguishable from vertical and c_f values obtained. Of the Scripps Beach data only 2 (5%) of the segments could not be fitted within the ± 3 cm/s measurement error estimates. For the three stacks of current meters (seaward stack shoreward) mean values are 0.008 (std dev = 0.005), 0.010 (0.004), and 0.006 (0.003), with an overall mean value of 0.008. The mean c_f estimated for the barred beach, based on measurements at various cross-shore positions is 0.014 (std dev = 0.007). Histograms of c_f values are shown in Fig. 4. Among the measured parameters, the strongest relationship to c_f is the ratio of near-bottom wave velocity magnitude to mean longshore current velocity, u_m/V (Fig 5). While the data presented reflects a trend for decreasing c_f with increasing u_m/V . The strongest relationship for z_a is also with u_m/V , (Fig 6), again showing a decreasing trend as u_m/V increases. It must be noted that more observations at values of u_m/V above 1 are needed to establish whether c_f and z_a increase after a minima in the region of equal wave velocity magnitude and mean current velocity.

DISCUSSION

Possible effects of breaking wave induced turbulence on the vertical profile of mean longshore currents were noted by Deigaard *et al.* (1986) and by Church and Thornton (1993). In the first case, the contribution of a mean shear stress near the surface from the roller modifies the vertical distribution of shear stresses and results in an imbalance over the vertical. For the case considered, a reduction in the depth-averaged mean longshore current of 20% is seen from the same bottom stress without breaking waves. Church and Thornton (1993) suggested that vertical momentum mixing produced from turbulence due to the breaking waves would similarly produce a more vertical velocity profile for a given shear stress. Typically the mean current boundary layer turbulence exists in equilibrium with the current, maintaining the amount of shear which the resulting mixing will permit. If the shear should increase, more mixing takes place until the shear is reduced. Such a balance does not exist for the "top-down" mixing proposed to be caused by breaking waves. This second source of turbulence is independent of the mean flow properties and instead related to the breaking wave characteristics.

Such effects of breaking waves pose a potential explanation for the vertical nature of the profiles for γ (which may be taken as proportional to the percentage of waves breaking) greater than 0.30. It cannot be said at what point these 15 profiles fall off to zero (assuming a no-slip condition does exist), or specifically whether they do so logarithmically, and theory predicting the vertical extent of breaking-wave effects is not fully developed. It is noted though, that many of the profiles (22% of the UTOAD set) indicate significant shear over the lowest two or three current meters with a vertically uniform region above (Stack B Segment 1001 is shown in Fig. 7). Such profiles might also be explained by breaking wave

effects, but resolution of such relatively subtle modifications requires greater accuracy than available in the experiments studied. It is again noted that Visser (1984) observed that wave basin experiments using breaking waves produced more vertical uniformity of the alongshore averaged profiles, "due to the large turbulent velocities". Visser (1986) found logarithmic profiles for the case of non-breaking waves.

Svendsen and Lorenz (1989) proposed a combined undertow and longshore current theory which assumed an oscillatory bottom boundary layer of negligible thickness. This treatment permitted non-zero bottom velocities of the mean currents (cross-shore or alongshore). The profiles of mean longshore current predicted were very nearly vertically uniform, slightly increasing bottom to top. While Svendsen and Lorenz (1989) neglected the influence of cross-shore and alongshore currents upon one another, Putrevu and Svendsen (1992) included such interaction for the simplified case of vertically uniform cross-shore flow. Cross-shore transport of longshore momentum (mixing) predicted by their theory, depends critically on the vertical variation of the longshore current, vanishing when the mean longshore current is vertically uniform. In their treatment the current magnitude increases with elevation above the bed from the shore seaward until a the ratio of depth to depth-of-breaking exceeds 0.7 (for the conditions studied), at which point the trend reverses and the current's magnitude decreases with elevation above the bed. Such trends may be seen in the Visser (1984) data, but are not clearly seen in this study. There are only three instances when the mean longshore current is greater at depth than at the surface, and only one of these cases has vertical variation greater than 3cm/s. All three cases occur at stack A, the stack closest to shore, during periods of γ values above 0.30, indicating that the stack was within the surf-zone. Conversely, at stack C, during the 4 segments with γ values below 0.30

(indicating they were outside the surf-zone), the vertical profiles increase with elevation above the bed. The SUPERDUCK data contain four segments representing conditions outside of the surf-zone, with γ values of 0.33, 0.29, 0.19, and 0.25, and in each case the currents increase with elevation above the bed. Certainly the contrast with the results of Visser (1984) point out the need for further field study with increased accuracy and sampling resolution.

Mention is warranted of the differences which may exist between measured mean longshore currents and their treatment within numerical models, most often involving vertical integration. Typically, data is acquired using individual meters at various cross-shore locations, and which are placed at some elevation above the bed which is expected to leave the meter unaffected by any anticipated morphological changes (specifically, bar movement). The velocity values obtained are assumed to represent the entire water column, regardless of the form of bottom stress used. For the data examined in this study, when γ is below 0.3 the mean increase in V over the range measured was 49%. Whether the current's vertical profile is believed to be logarithmic or linear, such an effect on the vertically integrated value is noteworthy.

CONCLUSIONS

It is painfully clear that in order to satisfactorily resolve the vertical structure of mean longshore currents one must have both current meters located very near the seabed, as well as extreme accuracy. The assessment of 3cm/s measurement error bars on the mean values in this work reflects the results of Guza *et al.* (1988) in which meters were extensively intercompared using data from within and near the surf-zone. For experimental planning purposes it may be desirable to quantify the maximum meter elevation allowable for

placement of current meters to resolve the difference between logarithmic and linear profiles. To examine this, through hindsight, mean values of v_* and z_a are calculated for both experiments and current meter elevations as existed (stack B has been arbitrarily chosen for the UTOAD example) are used. For the Scripps Beach data (max V typically 20-40cm/s), mean values are $v_* = 1.9\text{cm/s}$ (std dev = 0.5) and $z_a = 3.4\text{cm}$ (std dev = 2.5). For the SUPERDUCK data (max V typically 75-100cm/s) mean $v_* = 7.0\text{cm/s}$ (std dev = 1.0) and $z_a = 5.3$ (std dev = 4.8). Treating these values as given, and using the meter elevations as existed, one may produce an assumed logarithmic profile which defines the synthetic data points at the elevations applicable (Fig. 8). Separately, a best-fit linear profile may be found for these synthetic data. If the least-squares error of the linear profile is small, then addition, or relocation of another current meter is required. Examining the difference between the two profiles, the elevation may be identified where the difference between the velocities is greater than the assumed measurement error. For the case of the UTOAD data, this height would be 13cm, and 50cm for SUPERDUCK (Fig. 9). These calculations rely on provided values for v_* and z_a and are affected by the assumed current meter distribution, and so do not answer the question universally. It is apparent though that preplanning is critical to adequately resolving the subtleties of the current structure.

As stated previously, the UTOAD data set, which is most heavily relied upon in this work, was acquired as part of an undertow study and so was specifically designed to include measurement of the shoreward transport above trough level. As such, the experimental design was not maximized for the below trough measurements applicable to longshore current study. Still, the data examined provides information not previously available from field observations. Significant vertical shear does exist in the mean longshore current, but is absent

during times of substantial wave breaking. Resolution of the logarithmic/linear question requires further study.

ACKNOWLEDGEMENTS

The authors wish to express their appreciation to all those who participated in the UTOAD and SUPERDUCK experiments and in particular CDR Denny Whitford of the Naval Oceanographic Office, and to Mary Bristow, Naval Postgraduate School, for initial processing of the SUPERDUCK data. E.B.T. was funded by ONR Coastal Science Grant N0014-92-AF-0002 , R.T.G. was funded by ONR Coastal Science Grant, K.A.S. was funded by ONR Coastal Science Grant and J.C.C. is an ONR fellow.

REFERENCES

- Bijker, E.W., 1967. Some considerations about scales for coastal models with movable bed. Delft Hydraulics Laboratory, Pub. no. 50, 142pp.
- Christoffersen, J.B. and I.G. Jonsson, 1985. Bed friction and dissipation in a combined current and wave motion. *Ocean Engng.*, 12(5), 387-423.
- Church, J.C. and E.B. Thornton, 1993. Effects of breaking wave induced turbulence within a longshore current model. *Coastal Eng.* 20: 1-28.
- Deigaard, R., Fredsøe, J., and Hedegaard, I.B., 1986. Mathematical model for littoral drift. *J. Watrw. Port. Coastal Ocean Div., ASCE*, 112: 351-369.
- Fredsøe, J., 1984. Turbulent boundary layer in wave-current motion. *H. Hydraul. Eng.*, 110(8): 1103-1120.
- Grant, W.D., and O.S. Madsen, 1979. Combined wave and current interaction with a rough bottom. *J. Geophys. Res.*, 84(C4), 1797-1808.
- Guza, R.T., Clifton, M.C. and Rezvani, F., 1988. Field intercomparisons of electromagnetic current meters. *J. Geophys. Res.*, 93(C8), 9302-9314.
- Jonsson, I.G., 1967. Wave boundary layers and friction factors. *Proc. 10th Coastal Engr. Conf.*

ASCE, 127-148.

Liu, P.L-F. and R.A. Dalrymple, 1977. Bottom frictional stress and longshore currents due to waves with large angles of incidence, J. Marine Res. 36: 357-475.

Longuet-Higgins, M.S., 1970. Longshore currents generated by obliquely incident sea waves, 1. J. Geophysical Res., 75 6778-6789.

Martens, D.E., and E.B. Thornton, 1987. Nearshore zone monitoring system. Proc. Coastal Hydrodynamics Conf., ASCE, 579-588.

Putrevu, U. and I.A. Svendsen, 1992. A mixing mechanism in the nearshore region. Proc. 23rd Coastal Eng. Conf., ASCE, 2758-2771.

Simons, R.R., Grass, T.J., and Mansour-Tehrani, M., 1992. Bottom shear stresses in the boundary layers under waves and currents crossing at right angles. Proc. 23rd Coastal Engr. Conf., ASCE, 604-617.

Sleath, J.F.A., 1990. Velocities and bed friction in combined flows. Proc. 22nd Coastal Engr. Conf., ASCE, 450-463.

Sleath, J.F.A., 1991. Velocities and shear in wave-current flows. J. Geophys. Res., 96(C8) 15,237-15,244.

Svendsen, I.A., and R.S. Lorenz, 1989. Velocities in combined undertow and longshore currents. Coastal Eng. 13, 55-79.

Visser, P.J., 1984. A mathematical model of uniform longshore currents and the comparison with laboratory data, Communication on Hydraulics. Report 84-2, Dept. of Civil Eng., Delft University of Technology, 151pp.

Whitford, D.J. and E.B. Thornton, 1993. Longshore currents over a barred beach, I. Field Experiment, J. Phys. Oceanogr., submitted.

Visser, P.J., 1986. Wave basin experiments on bottom friction due to current and waves, Proc. 20th Coastal Eng. Conf. ASCE, 807-821.

Segment #	1501	1502	1503	1504	1602	1603	1606	1701	1702	1801	1802
depth (cm)	279	178	167	230	333	189	191	385	259	380	238
Hrms (cm)	92	76	57	59	98	80	49	72	69	93	84
peak freq (Hz)	.156	.156	.156	.203	.188	.188	.188	.172	.172	.203	.125
incident wave angle (°)	9.1	5.2	2.5	5.0	14.7	12.1	5.4	6.3	5.7	11.8	8.6
cross-shore posit. (m)	244	216	192	147	269	219	155	265	230	276	227
bottom slope	.029	.029	.029	.053	.012	.034	.005	.017	.034	.007	.032

TABLE 1. Conditions during SUPERDUCK experiment.

Stack A Cross-shore Position: $x = 76$ m bottom slope = .0178					
Meter ID	MA5	OA2	OA4	MA1	MA3
Height above bed (cm)	30	40	50	65	84
Stack B Cross-shore Position: $x = 105$ m bottom slope = .0125					
Meter ID	MB3	OB6	OB2	MB5	MB1
Height above bed (cm)	28	44	78	102	138
Stack C Cross-shore Position: $x = 148$ m bottom slope = .0284					
Meter ID	MC1	OC6	OC2	MC5	MC3
Height above bed (cm)	28	73	115	161	205

TABLE 2 Meter deployment during UTOAD experiment.

Segment #	601	901	902	903	904	1001	1002	1102	1103	1104	1203
depth (cm)	157	125	146	141	109	112	115	139	153	142	105
Hrms (cm)	36	25	24	25	22	23	24	26	28	26	23
peak freq (Hz)	.078	.070	.078	.078	.082	.082	.082	.082	.074	.074	.078
Segment #	1302	1303	1304	1703	1704	1705	1706	1707	1903	1906	1909
depth (cm)	126	147	145	121	135	139	129	108	112	135	90
Hrms (cm)	28	31	31	34	40	41	38	31	35	42	27
peak freq (Hz)	.066	.086	.066	.063	.063	.066	.063	.066	.066	.070	.078

Table 3. Scripps Beach, Ca data, Stack A, crossshore position=76m, beach slope=.018

Segment #	801	802	803	901	1001	1002	1102	1103	1104	1202	1203
depth (cm)	174	174	151	167	153	157	180	193	182	141	146
Hrms (cm)	31	35	33	25	25	25	25	26	24	26	27
peak freq (Hz)	.086	.082	.078	.070	.082	.082	.082	.074	.074	.078	.078
Segment #	1302	1303	1304	1703	1704	1705	1706	1906			
depth (cm)	168	188	186	157	171	174	164	170			
Hrms (cm)	30	30	33	48	55	54	54	62			
peak freq (Hz)	.066	.086	.066	.063	.063	.066	.063	.070			

Table 4. Scripps Beach, Ca data, Stack B, crossshore position=105m, beach slope=.013

Segment #	803	804	1204	1205	1603	1604	1605	1606	1803	1804	1805	1902
depth (cm)	223	182	206	184	179	172	165	163	179	182	183	200
Hrms (cm)	33	33	28	27	48	49	46	45	69	71	72	76
peak freq (Hz)	.078	.070	.086	.063	.063	.063	.063	.063	.063	.066	.063	.066

TABLE 5. Scripps Beach, Ca data, Stack C, crossshore position=148, beach slope=.028

Seg #	meters	u_{m}/V (near bottom)	γ	%V increase bottom meter to top	max ΔV	Z_0	U_*	Cf	line slope	least square error (log)	least square error (log)
601	4	.26	.26	34	3.2	5.3	1.43	.0104	.047	1.95	2.00
901	4	.53	.22	44	4.9	4.8	2.23	.0118	.093	1.92	2.50
902	4	.38	.18	68	4.7	11.19	2.50	.0273@	.091	3.08	2.06
903	4	.52	.19	36	3.5	2.3	1.45	.0063	.067	0.29	0.26
904	4	.82	.22	26	3.9	1.9	2.12	.0076	.108	1.02	0.46
1001	4	.65	.23	28	3.4	0.8	1.33	.0034	.062	0.09	0.39
1002	3	.51	.22	43	4.5	4.1	2.00	.0101	.085	1.19	1.90
1102	4	.57	.22	44	4.8	2.9	1.82	.0076	.084	0.53	0.40
1103	4	.49	.22	39	3.8	2.4	1.52	.0059	.064	0.86	1.04
1104	4	.94	.21	27	4.8	0.6	1.82	.0049	.085	0.31	0.42
1203	4	2.01	.24	07	5.0	.15	2.87	.0034	.074	13.38	7.87
1302	4	1.06	.23	20	4.5	0.3	1.92	.0035	.087	0.43	1.12
1303	4	.99	.22	23	5.0	0.4	2.00	.0041	.092	0.18	0.98
1304	4	1.23	.23	20	5.7	0.2	2.30	.0039	.108	0.28	0.52
1703	3	.89	.31	00	1.7	*	*	*	.037	*	0.81
1704	4	.51	.33	15	2.8	*	*	*	.051	*	1.35
1705	4	.41	.32	17	2.2	*	*	*	.044	*	0.49
1706	3	.60	.33	12	2.1	*	*	*	.058	*	0.42
1707	3	.58	.31	19	2.9	*	*	*	.082	*	0.33
1903	3	.48	.34	06 ‡	2.1	*	*	*	.030	*	1.67
1906	3	.38	.34	10 ‡	2.9	*	*	*	.040	*	3.54
1909	3	.80	.32	17 ‡	3.5	ud	ud	ud	.097	ud	0.22

TABLE 6. Profile fitting results for stack A, UTOAD, @ denotes c_f outlier, ‡ denotes profile increasing with depth, * denotes profile not log fitted due to lack of ΔV .

Seg #	meters	u_m/V (near bottom)	γ	%V increase bottom meter to top	max ΔV	Za	U_0	Cf	line slope	least square error (log)	least square error (linear)
801	4	.47	.20	87	8.5	4.6	2.19	.0114	.078	0.31	3.92
802	4	.53	.22	90	11.0	4.9	2.82	.0142	.101	0.25	5.51
803	4	.42	.23	86	8.5	6.1	2.57	.0142	.116	0.16	0.14
901	4	.41	.17	90	6.6	6.0	1.85	.0113	.060	1.88	5.86
1001	4	.49	.18	65	5.7	3.6	1.69	.0079	.052	2.50	6.09
1002	4	.32	.17	53	3.5	3.7	1.04	.0043	.026	2.11	3.15
1102	4	.37	.17	139	8.4	9.5	2.08	.0160	.073	2.61	2.60
1103	4	.49	.16	74	5.9	3.7	1.56	.0068	.051	1.53	3.60
1104	4	.52	.16	88	7.2	5.0	1.88	.0111	.063	2.05	4.71
1202	3	.96	.21	41	8.1	1.9	2.74	.0087	.111	3.01	5.91
1203	3	1.35	.21	33	8.9	0.8	3.01	.0064	.123	1.70	4.63
1302	3	.60	.18	36	6.4	3.4	2.20	.0095	.070	6.51	7.45
1303	4	.37	.16	57	4.7	5.1	1.48	.0069	.033	6.61	6.32
1304	4	.60	.19	53	6.9	2.2	1.99	.0070	.059	4.81	8.30
1703	3	.51	.35	03	2.2	*	*	*	.013	*	2.19
1704	3	.34	.36	03	1.9	*	*	*	.010	*	1.77
1705	3	.33	.35	03	2.4	*	*	*	.003	*	3.27
1706	3	.41	.36	07	2.1	*	*	*	.019	*	1.26
1906	3	.26	.39	20	2.9	*	*	*	.022	*	3.36

TABLE 7. Profile fitting results for stack B, UTOAD, * denotes profile not log fitted due to lack of ΔV .

Seg #	meters	u_m/V (near bottom)	γ	%V increase bottom meter to top	max ΔV	Za	U_*	Cf	line slope	least square error (log)	least square error (linear)
803	4	.23	.16	116	5.2	6.2	1.24	.0098	.036	0.87	2.97
804	3	.34	.19	62	5.5	6.5	1.85	.0125	.051	5.32	6.93
1204	4	.61	.15	68	7.2	3.6	2.04	.0125	.049	7.33	14.14
1205	4	.96	.16	50	8.4	1.4	2.28	.0089	.057	8.06	16.49
1603	3	.21	.30	06	1.6	*	*	*	.007	*	1.11
1604	3	.19	.32	20	3.2	0.06	1.03	.0021	.037	0.48	1.22
1605	3	.20	.32	01	0.7	*	*	*	.001	*	0.28
1606	3	.09	.32	11	1.3	*	*	*	.015	*	0.02
1803	3	.33	.42	51	10.0	16.7	4.35	.0371 †	.056	72.90	38.18
1804	3	.48	.42	44	3.9	3.6	1.44	.0043	.045	4.40	1.54
1805	3	.33	.42	35	3.3	0.6	0.94	.0017	.038	0.36	0.03
1902	3	.38	.41	124	5.1	9.8	1.45	.0117	.059	0.61	0.01

TABLE 8. Profile fitting results for stack C, UTOAD, † denotes weak fit, * denotes profile not log fitted due to lack of ΔV .

Seg #	meters	u_m/V (near bottom)	γ	%V increase bottom meter to top	max ΔV	Za	U_*	Cf	line slope	least square error (log)	least square error (linear)
1501	3	.67	.33	17	7.9	4.7	5.50	.0106 †	.095	17.35	8.12
1502	3	.78	.43	02	3.7	0.2	5.15	.0029 †	.023	40.38	5.21
1503	3	.73	.34	17	12.6	1.0	6.94	.0061	.160	4.73	1.15
1504	3	.13	.26	22	15.1	2.8	8.19	.0112	.190	5.08	.88
1602	3	.16	.29	21	9.2	4.4	5.93	.0113	.121	11.34	5.31
1603	3	.30	.42	09	10.4	0.4	7.23	.0042 †	.126	29.3	13.7
1606	3	.30	.26	24	14.6	4.2	8.26	.0139	.187	9.43	3.09
1701	3	.26	.19	58	11.0	22.0	6.11	.0469 @	.140	4.16	1.15
1702	3	.64	.27	40	10.2	14.9	6.02	.0264	.132	7.28	2.95
1801	3	.07	.25	34	12.1	7.8	6.40	.0182	.152	1.62	0.04
1802	3	1.18	.35	21	13.6	2.0	7.31	.0084	.172	3.36	0.42

TABLE 9. Profile fitting results for SUPERDUCK, † denotes weak fit, @ denotes c_f outlier.

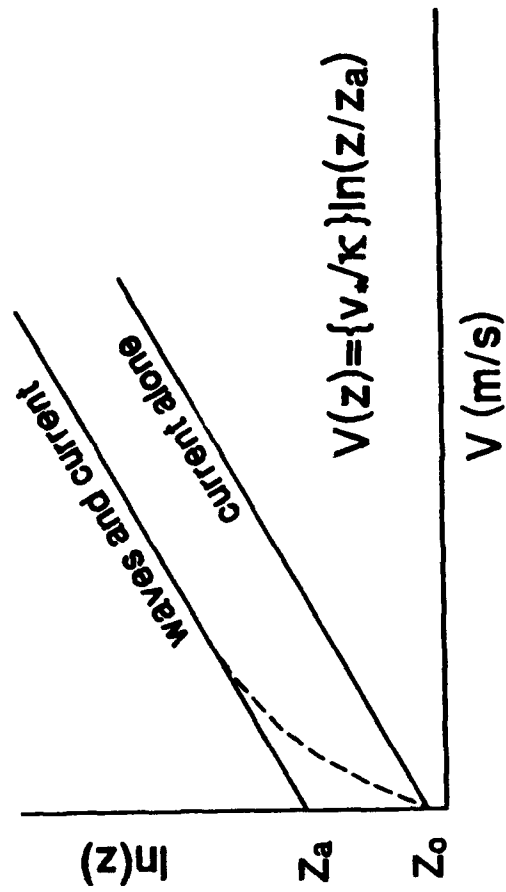


Fig. 1 Depiction of apparent roughness height produced by superimposing waves over mean current.

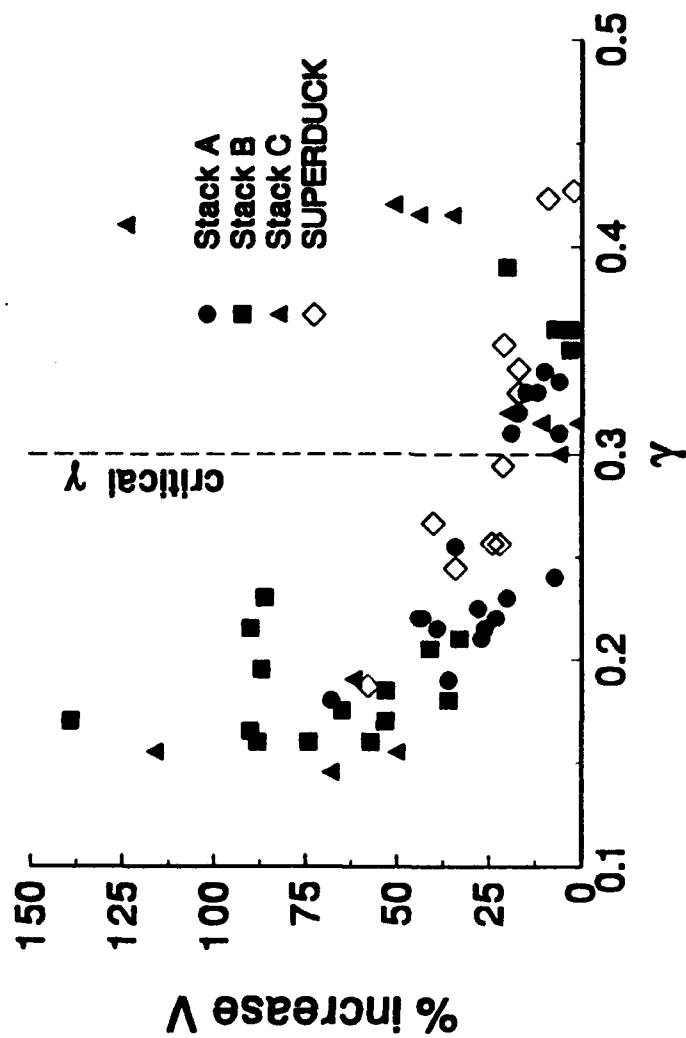


Fig. 2 Percentage increase in mean longshore current from lowest meter to highest as a function of $\gamma = H_{rms}/h$.

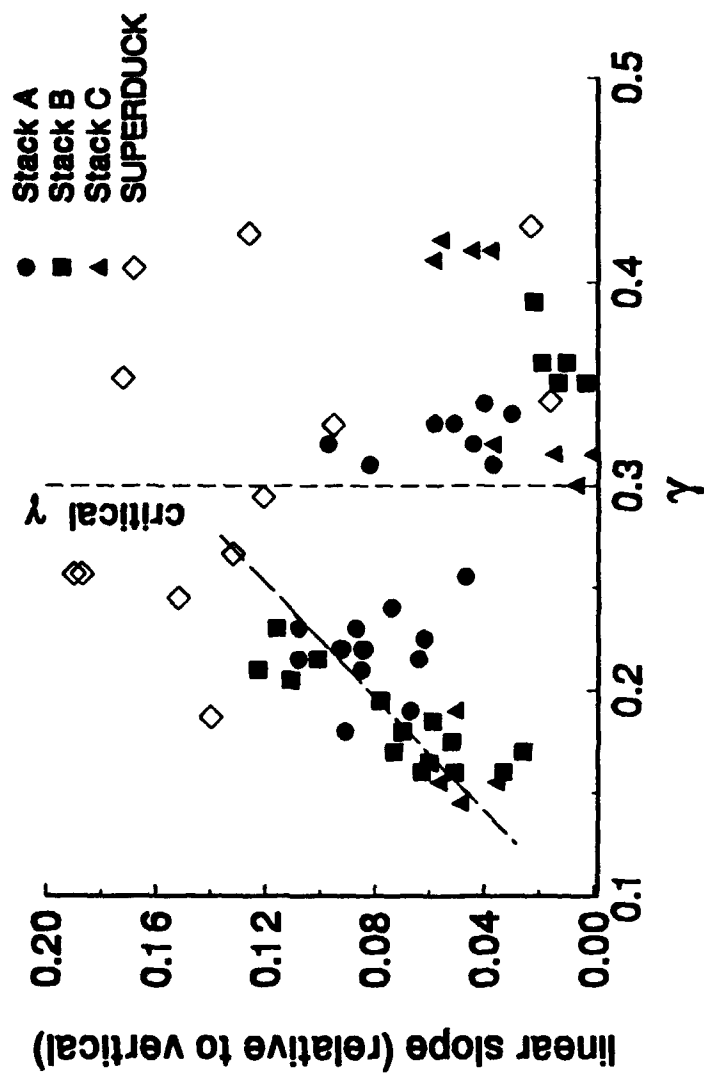


Fig. 3 Slope of linear best-fit to mean current profiles (measured relative to vertical) versus $\gamma = H_{rms}/h$.

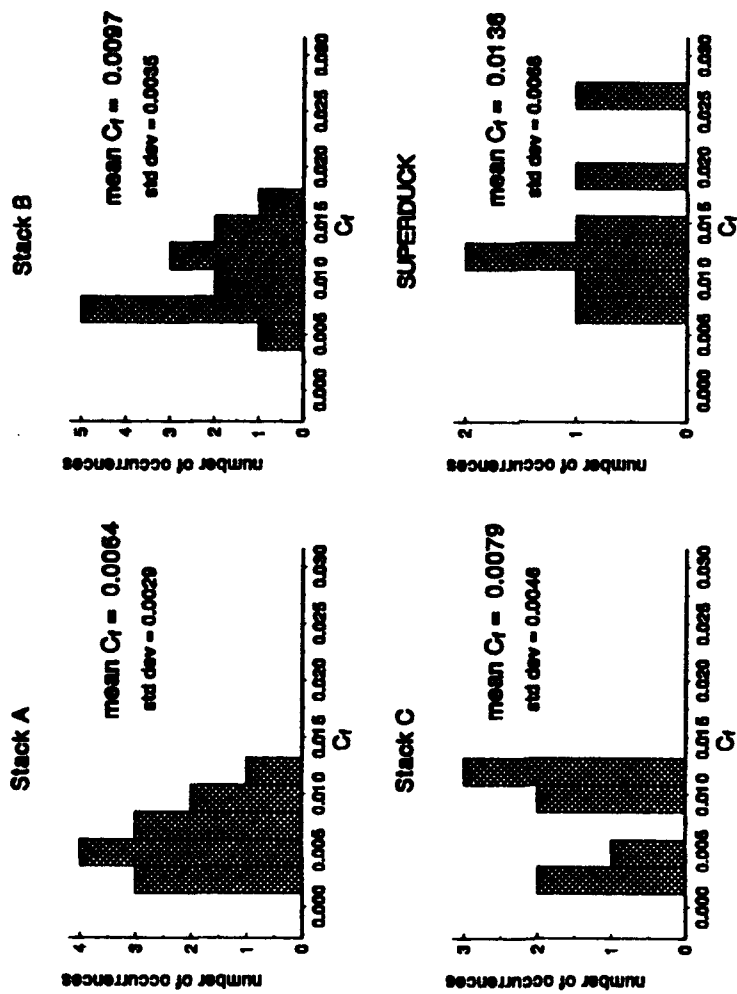


Fig. 4 Drag coefficient, c_f

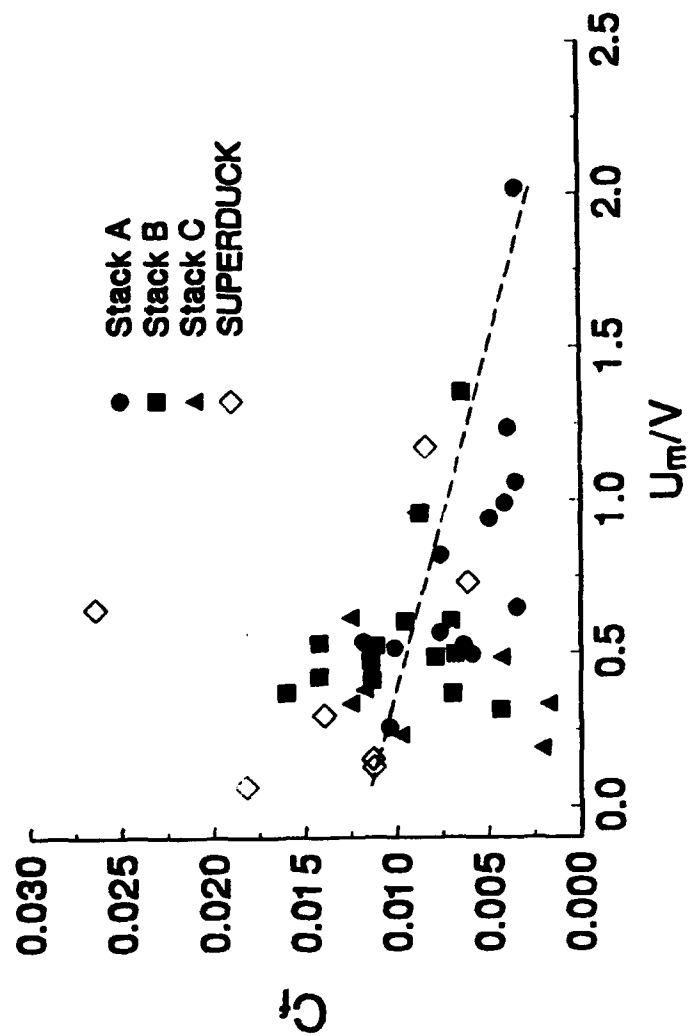


Fig. 5 Drag coefficient as a function of the ratio of near-bottom wave velocity magnitude to mean current measured at lowest current meter.

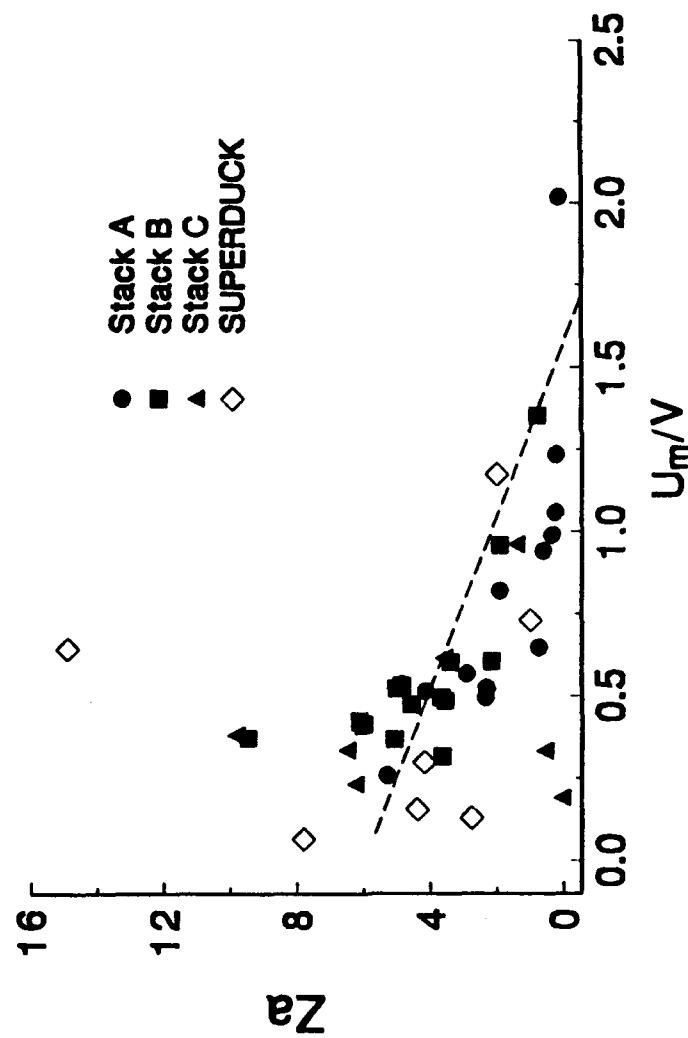


Fig. 6 Apparent roughness height as a function of the ratio of near-bottom wave velocity magnitude to mean current measured at lowest current meter.

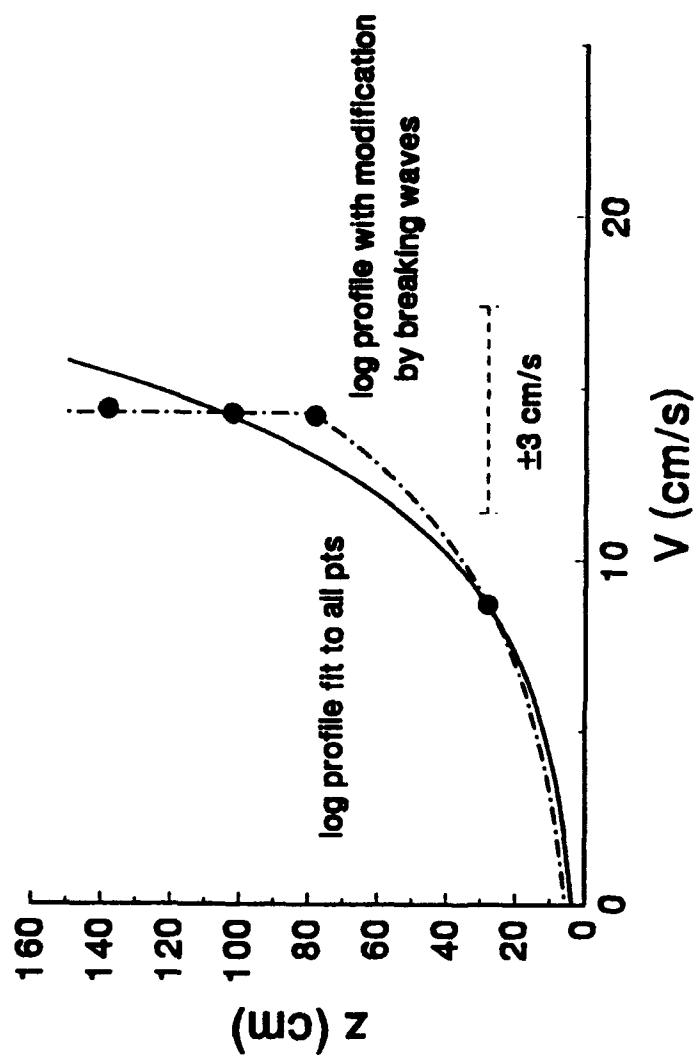


Fig. 7 Depiction of suggested effects of breaking-wave induced turbulence with measurement error bar.

UTOAD

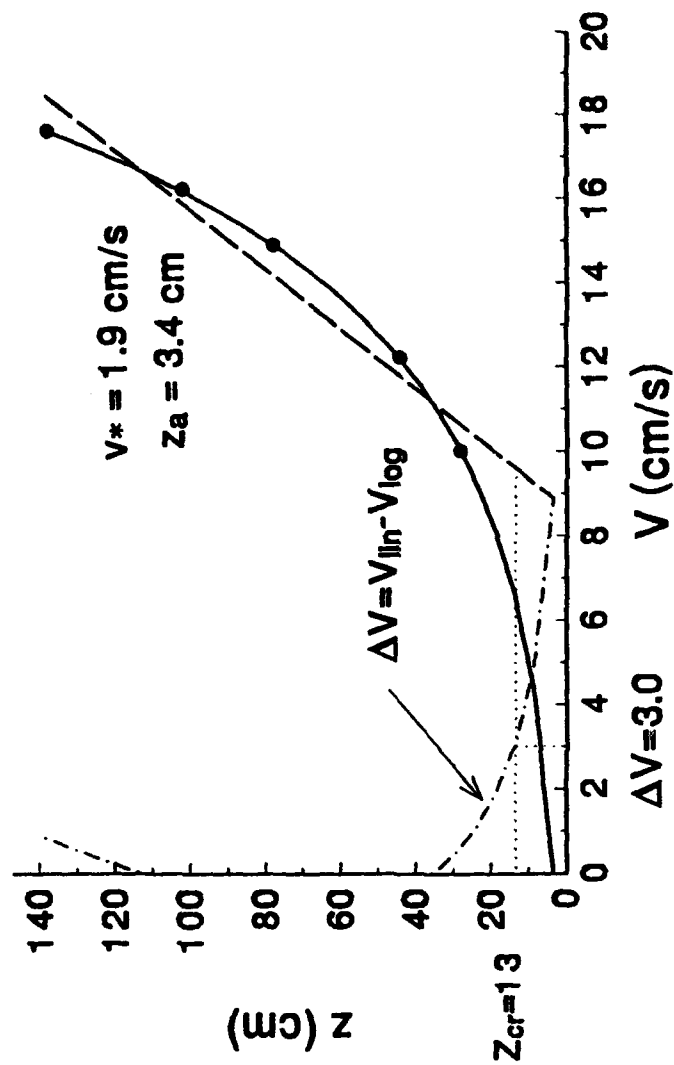


Fig. 8 Estimation of critical height below which measurement is required to resolve between logarithmic and linear profiles, in case of UTOAD conditions, and using measurement error value of 3cm/s.

SUPERDUCK

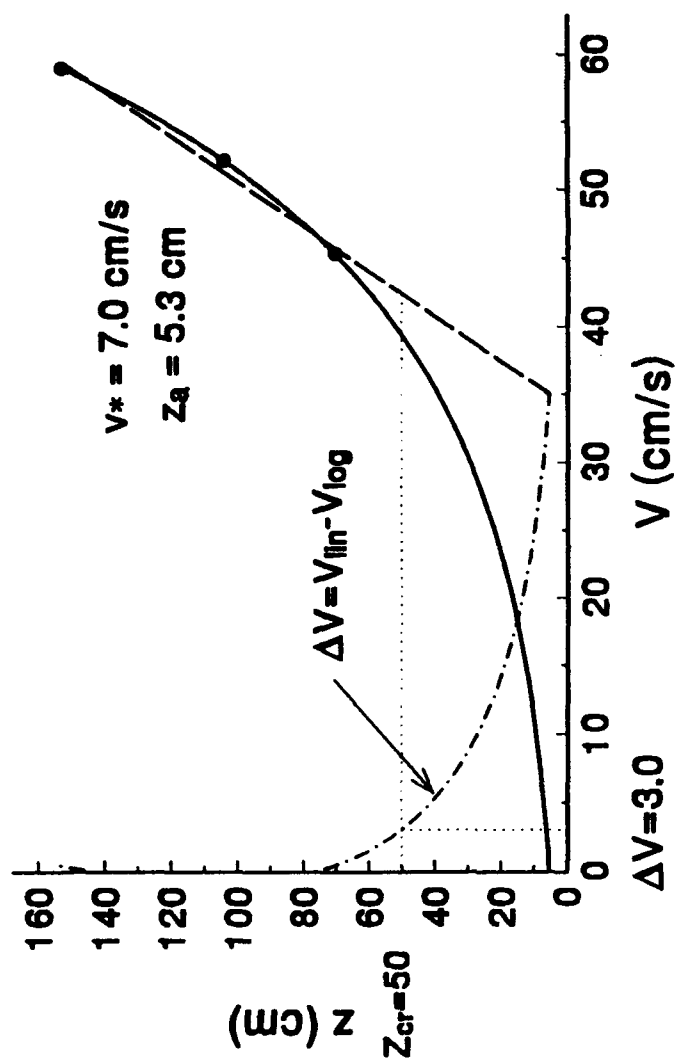


Fig 9. Estimation of critical height below which measurement is required to resolve between logarithmic and linear profiles, in case of SUPERDUCK conditions, and using measurement error of 3 cm/s.

IV. MIXING BY SHEAR INSTABILITIES OF THE LONGSHORE CURRENT

(This chapter consists of work submitted to the
Journal of Geophysical Research in July 1993)

MIXING BY SHEAR INSTABILITIES OF THE LONGSHORE CURRENT

J.C. Church and E.B. Thornton

Department of Oceanography, Naval Postgraduate School, Monterey, CA 93943

J. Oltman-Shay

Northwest Research Associates,

300 120th Ave NE, Bldg 7, Suite 220, Bellevue WA 98005.

ABSTRACT

Shear instabilities of the longshore current (nominally frequencies < 0.01 Hz) are examined as a possible source of horizontal turbulent momentum mixing (i.e. cross-shore gradients of $\rho \overline{u'v'}$ with x positive offshore) within the surfzone. Such mixing is of potential importance in the surfzone of a barred beach where existing models of longshore current produce poor agreement with observations. $\overline{u'v'}(x)$ profiles are calculated using model generated stream functions whose amplitudes are calibrated via observed energy density spectra. Data from the DELILAH experiment, conducted over the barred beach at Duck, North Carolina are examined. The predicted and observed wavenumber/frequency range of shear instabilities are found to be in good agreement. The modeled profiles of $\frac{1}{2}(\overline{u'^2} + \overline{v'^2})$ and $\overline{u'v'}$ are in reasonable agreement with observations, although slightly compressed shoreward. The modeled $\overline{u'v'}$ profiles, calibrated with the data, indicate that shear instabilities may be a strong source of mixing within the surf zone with a maximum predicted value for $\overline{u'v'}$ of $0.07 \text{ m}^2\text{s}^{-2}$. The mixing predicted due to shear instabilities is found to be in qualitative agreement with that required for modeled longshore current profiles to agree with observed profiles for the barred beach studied.

1. INTRODUCTION

During the 1986 nearshore experiment SUPERDUCK, Oltman-Shay *et al.* (1989) observed low frequency oscillations (<0.01 Hz), with wavelengths less than 300m. Free surface gravity waves below 0.05 Hz consist of two classes of waves: edge waves which are trapped by refraction along the beach face and occur at discrete modes, and "leaky" waves, composed of a continuum of reflected waves escaping seaward; these waves have been observed in great detail and are collectively termed "infragravity" waves because of their low frequencies relative to the sea-swell band. The uniqueness of the oscillations observed by Oltman-Shay *et al.* (1989) at SUPERDUCK lies in the fact that the wavelengths measured were an order of magnitude shorter than the shortest infragravity wave under applicable conditions (a function of frequency and beach slope). These oscillations were considered to be kinematically distinct based upon their frequency / wavenumber range.

Energy density distributions represented by gray shading in wavenumber-frequency space for 10 October 1982, during the DELILAH experiment, are shown in Fig. 1. The theoretical dispersion curves for trapped edge waves, modes 0, 1, and 2 are shown for the appropriate beach slope. Significant energy is seen outside of these edge wave curves; this energy is linear in f - K space (where f is frequency in Hz and K , cyclic alongshore wavenumber, is equal to $k(\text{wavenumber})/2\pi$), indicating that these oscillations, considered to be alongshore progressive waves, are non-dispersive. Oltman-Shay *et al.* (1989) linked the phase speed of these oscillations (given by the wavenumber-frequency slope) to the magnitude of the mean longshore current shear, indicating that the longshore current, and its associated kinetic energy, were the driving force behind these oscillations.

Bowan and Holman (1989) in a companion paper to Oltman-Shay *et al.* (1989) explained these observations as shear instabilities using a conservation of potential vorticity equation as a theoretical framework in which the vorticity of the longshore current shear

functioned as the restoring force. They also related a phase shift in the stream functions produced by the instabilities to non-zero $\overline{u'v'}$ values (u being cross-shore velocity and v alongshore) which were suggested as possible sources of mixing in the nearshore. Putrevu and Svendsen (1992) carried out a numerical study of shear instabilities over various topography and using an order of magnitude analysis, concluded that even a weak shear in the longshore current might be capable of producing significant mixing.

Existing models of longshore current generation (for example Church and Thornton 1993, Larson and Kraus 1991, and Whitford and Thornton 1993) typically predict two principle regions of forcing over a barred beach; the first where the waves break over the bar, and the second at the beach face. Observations during DELILAH routinely indicate a longshore current maximum over the region of the bar trough, where model predicted forcing is near zero. Horizontal momentum mixing, in the typical form of an eddy viscosity/mixing length term, offers little hope in explaining this situation as the generation of a single maximum between two previous maxima would require unlikely up-gradient momentum transfer. To avoid such problems of parameterization, possible sources of non-zero $\overline{u'v'}$ values must be examined directly. Shear instabilities offer one such opportunity.

There are three principle approaches to the estimation of the stream function amplitudes of shear instabilities. Dodd and Thornton (1992) apply weakly non-linear theory to the simplified case of an analytical longshore current profile over a planar beach. Such mathematically rigorous non-linear models contain the stream function amplitudes explicitly. Linear models (which are better suited to observed current profiles over measured bathymetry) utilize stream functions which are of arbitrary amplitude; thus the magnitudes of the predicted velocities, which are based on the gradients of the stream functions, are likewise arbitrary. A second method was employed in Dodd *et al.* (1992), assuming that the growth rates predicted by the model may be taken as an indication of the ultimate distribution of

energy across the wavenumber spectrum. For example, should wavenumber k_1 have a predicted growth rate twice that of wavenumber k_2 , it would be assumed that the steady state energy of k_1 will be twice as great also. Linear theory is then used to relate energy to amplitude squared. This relative method allows for the inter-comparison of different wavenumbers, but lacks an absolute reference. A third method is to measure the shear instability kinetic energy density, S_{ske} , (the sum of the u and v energy densities associated with shear instabilities where the vertical velocity is assumed zero through the rigid lid approximation) over the frequency range of interest and then scale the model-produced stream function amplitudes such that the predicted and observed energy densities match. This approach produces an absolute reference and is used in the current work. S_{ske} is used for calibration, instead of the cross-spectra, S_{uv} , as S_{ske} is invariant with current meter alignment errors (studied further in appendix A). Once the stream function amplitudes are calibrated, one may obtain a model predicted alongshore averaged profile of $\overline{u'v'}(f,x)$ for each wavenumber/frequency for which growth is predicted. The cross-shore gradient of $\overline{u'v'}(x)$ (integrated over frequency) produces a profile which represents the net mixing associated with the shear instabilities. Data obtained during the 1990 DELILAH experiment are used to evaluate the magnitude and structure of this term across a barred beach. The effects of this term on the longshore current profile are discussed.

2. SHEAR INSTABILITY THEORY

Linear wave theory is utilized, with the x-axis positive seaward. Mean and perturbation current velocities are vertically integrated and the mean current is assumed steady state. The longshore current and bathymetry are assumed uniform in the alongshore direction.

Bowen and Holman (1989) developed a theoretical basis for shear instabilities. Using conservation of potential vorticity as the restoring force, they were able to relate the mean

longshore current shear to observed oscillations. The momentum and mass continuity equations, with the velocity consisting of perturbations (u' , v') and a mean longshore current (V) are:

$$\frac{\partial u'}{\partial t} + V \frac{\partial u'}{\partial y} = -g \frac{\partial \eta}{\partial x} \quad (1)$$

$$\frac{\partial v'}{\partial t} + u' \frac{\partial V}{\partial x} + V \frac{\partial v'}{\partial y} = -g \frac{\partial \eta}{\partial y} \quad (2)$$

$$\frac{\partial \eta}{\partial t} + \frac{\partial (hu')}{\partial x} + \frac{\partial (hv')}{\partial y} = 0 \quad (3)$$

where η is surface elevation. These equations are linearized and the non-divergent (rigid lid) approximation is applied allowing the use of stream functions to represent the transport, such that:

$$u' = -\frac{1}{h} \frac{\partial \Psi}{\partial y} \quad v' = \frac{1}{h} \frac{\partial \Psi}{\partial x} \quad (4)$$

Cross differentiating to combine equations and eliminate η , gives:

$$\left(\frac{\partial}{\partial t} + V \frac{\partial}{\partial y} \right) \left(\frac{\Psi_{yy}}{h} + \left(\frac{\Psi_x}{h} \right)_x \right) = \Psi_y \left(\frac{V_x}{h} \right)_x \quad (5)$$

where the subscripts denote differentiation. Term 1 represents the local rate of change. Term 2 is the advection by the mean longshore current. Term 3 is the relative potential vorticity of the perturbations. Term 4 represents the advection of the background vorticity of the mean longshore current (V_x/h), by the perturbations. This potential vorticity equation is comparable to the barotropic Rossby equation used for planetary scale flow with the

exception that the background vorticity of the current shear is used in place of the Coriolis parameter.

A solution is then assumed of the form:

$$\Psi = \text{Re}\{\phi(x) e^{i(ky - \omega t)}\} \quad (6)$$

where ϕ is a cross-shore structure function. The alongshore wavenumber, k , is taken to be real, but ω , the angular frequency ($\omega = f/2\pi$), and ϕ may be complex. The form of the solution which allows growth with time is then:

$$\Psi = \exp(\omega_{im} t) \text{Re}\{\phi(x) \exp[i(ky - \omega_{re} t)]\} \quad (7)$$

Inserting this solution in (5) yields:

$$(V - c) \left(\phi_{xx} - k^2 \phi - \frac{\phi_x h_x}{h} \right) - h \phi \left(\frac{V_x}{h} \right)_x = 0 \quad (8)$$

where $\text{Re}\{c\}$ is the phase speed of the shear wave, equal to ω/k .

Dodd *et al.* (1992) included the dissipative effects of bottom friction through a parameterization, $\mu = 2c_f U_o/\pi$, where c_f is a friction coefficient and U_o is the magnitude of the incident swell orbital velocity. The resulting modification of the basic equation produces:

$$\left(V - \frac{i\mu}{kh} - c \right) \left(\phi_{xx} - k^2 \phi - \frac{\phi_x h_x}{h} \right) - h \phi \left(\frac{V_x}{h} \right)_x + \frac{i\mu}{kh} \left(\frac{\phi_x h_x}{h} \right) = 0 \quad (9)$$

The principle result of the inclusion of dissipation is a dampening effect on instabilities as indicated through the model by the reduced range over which growth is predicted. Model sensitivity to the value chosen for c_f will be examined.

After inserting known topography and an *a priori* longshore current profile, this equation takes the form of a quadratic equation in ω . This may be written in matrix form as $[A] \{\phi\} = c [B] \{\phi\}$

which produces the eigenvalues, c , for each wavenumber. Using $c = \omega/k$ the real and imaginary parts (should ω be complex) may be found. It is the cases when ω_{im} is positive that growth is predicted for an instability of that particular wavenumber.

For any instability to grow, (i.e. to have a positive ω_{im}) there must be some source of energy, be it either potential (baroclinic instability) or kinetic (barotropic instability). A mechanism must then exist to transfer this energy from its source, here the longshore current, to the growing perturbation. Dodd and Thornton (1990) derive a set of energy equations to further study this transfer, yielding:

$$\frac{\partial}{\partial t} (ke) = - \int_0^{\infty} \overline{u'v'} v_x dx - g \int_0^{\infty} \frac{h_x}{h} \overline{u'\eta} dx \quad (10)$$

where ke denotes the specific kinetic energy density of the perturbations and the averaging has been done over the y direction (all further references to kinetic energy will implicitly mean specific kinetic energy density, or $\frac{1}{2} (\overline{u'^2} + \overline{v'^2})$). The first term on the right hand side represents the role of the Reynold's stresses ($\overline{u'v'}$) in transferring energy and the second term the work done by the surface pressure gradients. This second term is generally negligible as a result of the ratio of the depth, h , to the bottom slope in the x direction. Thus simplified, the required condition for a growing instability is that there must be a negative correlation between $\overline{u'v'}$ and the shear of the longshore current.

3. EXPERIMENT

The 1990 DELILAH experiment was conducted at the U.S. Army Corps of Engineers Field Research Facility at Duck, North Carolina, (the same site as SUPERDUCK), with one of the specific goals being to measure shear instabilities. Two alongshore arrays composed of 5 and 6 current meters were used to identify shear instabilities. One array was located in the trough, in approximately 1.5 meters of water, and the other was located on the seaward

face of the bar in approximately 3 meters of water. Phase lagged analysis was conducted on three-hour data blocks centered on the period of interest. f-K spectra were produced for the arrays using an Iterative Maximum Likelihood Estimator (Pawka 1982). Frequency resolution for the f-K processing was 0.001 and cyclic alongshore wavenumber resolution 0.00098. Daily bathymetric measurements were surveyed using an autonomous Coastal Research Amphibious Buggy (CRAB), described in detail by Birkemeier and Mason (1984). The longshore current was measured using a cross-shore array of 9 current meters and wave sensors extending across the surf zone. These three principle arrays, shown in Fig. 2, were used to acquire near-continuous data for three weeks at a sampling rate of 8 Hz. A wide variety of wave conditions occurred during the experiment, including a northeaster which drove broad-banded waves, and two distant hurricanes which generated narrow banded swell incident at large angles to the beach. These events resulted in strong longshore currents and concomitant shear instabilities. Three two-hour periods were selected for analysis based on range of longshore current strength (maximum values of 1.1, 0.7, and 1.6 m/s) and high tide conditions which were observed to correspond with periods of improved signal-to-noise ratios in the alongshore array analysis.

4. MODEL CALIBRATION

Model verification is addressed in three sections. First, the wavenumber/frequency ranges predicted by the shear instability model are compared with the estimated f-K spectra obtained using the two alongshore arrays. Second, a method is described to remove infragravity contamination from the energy density spectra measured at the individual current meters using coherence between horizontal velocities and surface elevation; the results are compared with the energy partitioning provided by f-K spectra estimated for each of the two alongshore arrays (i.e. where infragravity energy is identified via the dispersion curves). Finally, the stream functions are calibrated, and $\overline{u'v'}$ profiles are compared with values

measured at each of the nine current meters in the cross-shore array.

The cross-shore profile of the longshore current is required as input to the shear instability model and in the present work is obtained through application of a cubic spline to the two-hour mean observations at the nine locations. Dodd *et al.* 1992 noted the sensitivity of their shear instability model to the "smoothness" of the longshore current profile and opted to use a model predicted current profile as input in order to minimize any discontinuous derivatives. In the present study, using a spline with subjectively chosen weighting assigned to individual points produces a smooth profile in sufficient agreement with the observations. Three splined profiles are shown in Fig. 3 together with the measured bathymetry and the calculated background vorticity. The background vorticities exhibit relative minima, corresponding to an elimination of the restoring force, just shoreward of the bar crest in all three of the cases studied herein.

Two examples of model predicted stream functions (cyclic alongshore wavenumbers 0.00125, 0.005) are shown for 9 Oct, in Fig. 4. The splined longshore current profile is overlaid on Fig. 4 and demonstrates the opposing tilt of the stream function lines relative to the current profile. This condition is mathematically described by Eq. (10) as that required for the transfer of energy from the mean current to the instability. Stream functions with the same tilt as the current profile (e.g. $\int_0^{\pi} \overline{u'v'} v_x dx > 0$), transfer energy to the mean current and unless supported by some other source of energy, such as baroclinic instability, will decay over time.

The role of this "tilt" in the transfer of energy may be demonstrated schematically using a linear segment of longshore current profile (Fig 5) where the positive x-direction is taken as eastward and the positive y-direction is taken as northward. When the instability is aligned parallel to the current profile, (panel A), the westward component of the instability transfers low velocity-mean momentum westward into a region of higher mean velocity while

contributing its own positive northward velocity. Conversely, the eastward component of the instability brings high velocity mean momentum into a region of lower mean velocity while contributing its southward, or retarding, velocity. The result is that the northward and southward contributions from the instability are so positioned as to oppose any mixing resulting from the east/west transfer of the mean momentum. Thus the mean current structure is supported at the expense of the instability. This agrees mathematically with Eq. (10) in as much as $\overline{u'v'}v_x > 0$, and so the energy transfer is negative (i.e. away from the instability). The counterclockwise oriented flow of the instability has been arbitrarily chosen and the argument above is unchanged should the direction of the circulation be reversed ($\overline{u'v'}$ remains negative).

When the instability's tilt is opposing the mean current profile (panel B), the westward component moves low velocity mean momentum toward a region of higher velocity, while contributing its southward velocity, and thereby further increasing the negative momentum transport. The eastward component, moves high velocity mean momentum into a region of lower velocity with the additional positive contribution of the instability's northward component. So oriented, the northward and southward momentum contributions enhance the momentum transport resulting from the westward and eastward components. In this case, $\overline{u'v'}v_x < 0$ and the instability receives energy at the expense of the energy of the mean current.

Differences in the frequency range over which shear instability energy was observed were routinely noted during DELILAH between the trough array and the array located seaward of the bar (Fig. 1 a & b) with the trough array consistently detecting energy over a frequency range extending beyond that of the more seaward array. Noting the cross-shore positions of these two arrays (Fig. 4), these differences seem to be explained by the decreased cross-shore span of the higher frequency instabilities.

Model predicted growth rate, ω_{im} , and frequency, $f = \omega_{re}/2\pi$, versus cyclic alongshore wavenumber are shown in Fig. 6 for two choices of the bottom friction coefficient, ($c_f = 0.002$ and 0.004). The lack of predicted growth in the lowest wavenumber bins for the $c_f = 0.004$ case does not agree well with the observations and therefore $c_f = 0.002$ has been used throughout the present work. The parameterization of bottom friction within the surfzone is a topic of ongoing research and the form used here, following Dodd *et al.* (1992) is considered an order of magnitude estimate. As a result it is not appropriate to attempt to draw conclusions concerning the generality of the chosen value of c_f . The predicted dispersion relations may be compared with the observed f-K spectra, shown in Fig. 7, wherein measured spectral values of u have been shown as solid dots and those of v as empty dots. The solid line indicates the range over which the model predicts growth. Note that although some energy may be seen away from the predicted range, the primary concentration of energy lies close to the prediction in all three cases.

Contamination of shear instabilities by infragravity energy

Estimates of the shear instability energy density spectra (S_{ske}), from each of the nine cross-shore current meters (Fig. 2), are required to calibrate the amplitudes of the model-produced stream functions (e.g. Fig 4). The two-hour record length was broken up into 8 sub-records, with 50% overlap, based on the required record length necessary to produce the desired frequency resolution of 0.0005. The resulting degrees of freedom (16) produce large confidence intervals. Conversely, a record length long enough to produce significantly more degrees of freedom strains the steady-state assumption. While the shape of the estimated spectra is used within the calibration process, the final comparisons between model and data use variances obtained by integrating over frequency.

It is assumed that the measured spectra, S_{ke} , includes both shear instability energy, S_{ske} , as well as infragravity wave contamination, S_{ike} . To remove the infragravity wave

contamination, the coherence between the velocity components and the surface elevation signature is calculated. Bowen and Holman (1989) demonstrated that the rigid lid assumption was reasonable in the case of shear instabilities and so the cross-spectral coherence between η and the horizontal velocity components is assumed to be zero. Conversely, the coherence for infragravity waves is assumed to be unity. Following Thornton (1979) in which the coherence between surface elevation and velocity, i.e.

$$\gamma_{\eta u}^2(f) = \frac{|S_{\eta u}(f)|^2}{S_{\eta}(f) S_u(f)} \quad (11)$$

was suggested as a means to separate the wave energy from alongshore component of the horizontal turbulence, the velocity spectrum in the frequency range of interest is now considered composed of an infragravity component, u_i , and a shear instability component, u_s , where it is assumed the shear instabilities and infragravity waves are statistically independent. The cross-spectra of u and η is written as $S_{\eta u}(f) = S_{\eta u_i}(f) + S_{\eta u_s}(f)$. Again it is expected that the cross-spectra between η and u is zero for shear instabilities, and the last term is neglected. Substituting, the coherence may be written:

$$\gamma_{\eta u}^2(f) = \frac{|S_{\eta u_i}(f)|^2}{S_{\eta}(f) S_{u_i}(f)} \left[1 + \frac{S_{u_s}(f)}{S_{u_i}(f)} \right]^{-1} \quad (12)$$

The first term on the right hand side is the coherence between η and u_i which is assumed equal to one. Finally, the ratio of S_{u_i} to S_u is obtained

$$\gamma_{\eta u}^2(f) = \left[1 + \frac{S_{u_s}(f)}{S_{u_i}(f)} \right]^{-1} = \left[\frac{S_{u_i}(f) + S_{u_s}(f)}{S_{u_i}(f)} \right]^{-1} = \frac{S_{u_i}(f)}{S_u(f)} \quad (13)$$

The same process is carried out for v , ultimately yielding

$$S_{ike}(f) = \gamma_{\eta u}^2(f) S_u(f) + \gamma_{\eta v}^2(f) S_v(f) \quad (14)$$

It should be noted that the assumptions made lump any turbulent energy at the same frequencies into the category of shear instability energy.

Sensitivity of this method to the assumed zero surface elevation / velocity coherence for shear instabilities may be tested in the following manner. Returning to Eq. (11), we may write

$$\gamma_{\eta u}^2(f) = \frac{|S_{\eta u}(f)|^2 + |S_{\eta us}(f)|^2}{S_{\eta}(f)[S_u(f) + S_{us}(f)]} \quad (15)$$

which, following the previous derivation, may be written as

$$\gamma_{\eta u}^2(f) = \gamma_{\eta ui}^2(f) \left(\frac{S_u(f)}{S_u(f)} \right) + \gamma_{\eta us}^2(f) \left(\frac{S_{us}(f)}{S_u(f)} \right) \quad (16)$$

Again combining both u and v components, with $\gamma_{\eta vi}^2 = \gamma_{\eta ui}^2$ and $\gamma_{\eta vs}^2 = \gamma_{\eta us}^2$, the ratio of S_{ike} to S_{ke} is given by

$$\frac{S_{ike}}{S_{ke}} = \frac{S_u(\gamma_{\eta u}^2 - \gamma_{\eta us}^2) + S_v(\gamma_{\eta v}^2 - \gamma_{\eta vs}^2)}{(S_u + S_v)[\gamma_{\eta ui}^2 - \gamma_{\eta us}^2]} \quad (17)$$

This quantity is plotted for 9 OCT 2213 for $\gamma_{\eta us}^2 = 0.0$ and 0.1, (Fig. 8) and shows at most roughly a 10% difference.

The shear instability spectrum, S_{ske} , is calculated by subtracting the magnitude of the infragravity contamination, S_{ike} , from the measured S_{ke} . The method of calculating the shear instability spectrum using a single meter location is checked at the two alongshore arrays where the estimated f-K spectra may be used to partition energy by both frequency and alongshore wavenumber, where energy with K within the zero mode dispersion curves is

assumed associated with infragravity waves. S_{ske} spectra calculated using these two methods are compared in Fig. 9.

Stream function calibration

Calibration of the model predicted stream functions is performed by assuming that the growth term in Eq.(7), (e.g. $\exp(\omega_{im}t)$) can be represented in a steady-state form by an amplitude variable, $A(f)$. $A(f)$ is then solved for by fitting the modeled kinetic energy density surface to the measured data in f - K space. The modeled $\overline{u'^2}(f,x)$ and $\overline{v'^2}(f,x)$, averaged over one wavelength in the alongshore direction are re-written:

$$\overline{u'^2}(f,x) = \frac{A(f)^2 k(f)^2}{2h(x)^2} (\phi_r(f,x)^2 + \phi_i(f,x)^2) \quad (18)$$

$$\overline{v'^2}(f,x) = \frac{A(f)^2}{2h(x)^2} \left[\left(\frac{\partial \phi_r(f,x)}{\partial x} \right)^2 + \left(\frac{\partial \phi_i(f,x)}{\partial x} \right)^2 \right] \quad (19)$$

The model predicted $\frac{1}{2}(\overline{u'^2} + \overline{v'^2})(f,x)$ is the sum of Eq. (18) & (19) and is represented spectrally as S_{mske} . Using 10 OCT 2254 as an example, the 9 current meters produce 9 lines of $S_{ske}(f)$, one at each of the cross-shore positions of the meters. This surface is splined over the x direction such that the grid density is increased to match that of the model output (Fig. 10). For the model output, there are 22 frequencies which have growth predicted, and so there are 22 profiles of $S_{mske}(x)$ distributed over frequency. Each of these 22 profiles of $S_{mske}(x)$ is scaled independently to the corresponding profile from S_{ske} such that one $A(f)$ value is obtained for each frequency for which the model predicts growth. Above the maximum frequency for which growth is predicted $A(f)$ is set to zero. Observed energy above this cut-off is treated as noise and no fitting between S_{mske} and S_{ske} is attempted. Scaling is done at each frequency for which growth is predicted in a best fit manner based upon equal areas under the curves over the cross-shore region between the second and

seventh meters. This range was chosen based on the diminished model/data agreement at the shoreward-most meter (presumably related to the minimal water depth of typically less than 1m) and the relative lack of signal seaward of the seventh meter. These profiles taken collectively produce calibrated S_{mske} surfaces (Fig. 10).

Comparison of the net effect of shear instabilities is done by integrating S_{ske} and S_{mske} across frequency producing observed and predicted $\frac{1}{2}(\overline{u'^2} + \overline{v'^2}) (x)$ variance profiles (Fig. 11). Both surfaces are integrated over the entire frequency range considered (0.0005 - 0.015) and therefore the observed profile contains energy which has been regarded as noise because of being at frequencies for which the model predicts zero energy. The largest noise contribution occurs for 9 OCT 2213 due to the narrowness of the frequency range for which the model predicted growth.

The model predicted $\overline{u'v'}_m(f,x)$ profile is obtained using the previously calibrated stream functions:

$$\overline{u'v'}_m(f,x) = -\frac{A(f)^2 k}{2h(x)^2} (\phi_r(f,x) \frac{\partial \phi_i(f,x)}{\partial x} - \phi_i(f,x) \frac{\partial \phi_r(f,x)}{\partial x}) \quad (20)$$

where m again denotes model predicted. This is represented in spectral density as $S_{muv}(f,x)$. Inserting the $A(f)$ values obtained through the calibration of S_{ske} produces a calibrated $S_{muv}(f,x)$ (Fig. 12). The observed $S_{uv}(f,x)$ surface is again based on spectra obtained at the 9 current meter cross-shore positions and is also splined over the x direction to increase the grid density to match that of the model output (Fig. 12). It is emphasized that splining of S_{uv} is for comparison of the surfaces only as the calibration process is only carried out for S_{mske} and not S_{muv} . Finally, these surfaces are integrated across frequency producing observed and predicted $\overline{u'v'}(x)$ covariance profiles representing the net effect of shear instabilities (Fig.

13). Once again the observed profile contains "noise" from frequencies above the band over which the model predicts growth.

5. SHEAR INSTABILITY MODEL/DATA COMPARISON

The method used to evaluate shear instabilities as a possible source of non-zero $\overline{u'v'}$ observed within the surf zone relies on both satisfactory results from the model in predicting frequencies, growth rates, and spatial structure, as well as the appropriate scaling of the resulting stream functions. The method of scaling in turn relies to some degree on the ability to remove infragravity contamination from the observed spectra.

The infragravity (S_{ike}) / shear instability (S_{ske}) energy density partitioning based on the surface coherence method is compared with the partitioning of energy done through the estimated f-K spectra obtained at the two alongshore arrays (Fig. 9) and lends confidence to the rigid lid assumption. Examination of this variance partitioning using the coherence method, over the entire cross shore array of nine meters (Figs. 14-16) reveals that the estimates of infragravity energy (S_{ike}) at current meter 40 are consistently higher than other meters and have a spectral shape very similar to the shear instability energy (S_{ske}), while the infragravity contribution (S_{ike}) estimated at the other meters typically have spectral shapes which differ. It is suspected that the cross-shore location of this meter (located over the bar, see Fig. 3) corresponds with the region wherein the rigid lid approximation is weakest. Any vertical motion occurring would produce a surface signature which the decontamination method would attribute to infragravity energy. Although current meter density is insufficient to test the validity of the rigid lid approximation in the field, it may be examined within the model by comparison of the magnitudes of the surface displacement term in the mass continuity equation (Eq.(3)) and the horizontal convergence term, the former being solved for as a residual. Modeled stream functions for 9 OCT 2213 ($f=0.001\text{Hz}$ / $K=0.00125$ and $f=0.005\text{Hz}$ / $K=0.005$, shown in Fig. 4), together with the splined velocity profile, and

measured bathymetry are used. The ratio for $f=0.001\text{Hz}$ (Fig 17) exhibits a 12 meter (cross-shore) broad peak centered over the position of meter 40 (in the vicinity of the bar). The profile for $f=0.004\text{Hz}$ is more singular, again at the location of meter 40. The ratio values of .10 - .15 indicate that the rigid lid approximation is strained within the model at this location, at least for the lower frequencies, but the ratios elsewhere across the surfzone are sufficiently small to consider the model internally consistent.

The performance of the shear instability model in predicting the range of wavenumbers which will experience growth and their corresponding frequencies may be assessed by examining the distribution of energy density measured by the two alongshore arrays in f - K space (Fig. 7). In general, good agreement is observed with only relatively small levels of energy being observed beyond the predicted range. The observed energy densities shown reflect the removal of infragravity wave energy, as identified by the theoretical infragravity dispersion curves. The vertical scale of the seaward array (panel B) has been exaggerated by a factor of five to more clearly show structure. As noted previously, this seaward array consistently observed energy over a decreased range of frequencies and at decreased magnitudes for the entire frequency range. Both of these conditions may be explained by noting the cross-shore structure of the stream functions as discussed earlier (Fig. 4).

Two methods of evaluating the calibration of the stream function magnitude are the comparison of the observed and modeled S_{ske} and S_{uv} spectral shapes (in f - K space) and the integrated $\frac{1}{2}(\overline{u'^2} + \overline{v'^2})$ and $\overline{u'v'}$ profiles. Comparison of the observed S_{ske} and modeled S_{mske} surfaces (Fig. 10) indicates at least qualitative agreement for all three cases. A shared result is the apparent "compression" of the model's cross-shore structure; this is most obvious in the 9 OCT 2213 case and to a lesser degree the 10 OCT 2254 case. The calibration term, $A(f)$, does not vary in the cross-shore direction and so this spatial compression cannot be

remedied through calibration. At this time it cannot be determined if this is an indication of some deficiency within the physics of the model. This compression is perhaps more easily seen in the integrated $\frac{1}{2}(\overline{u'^2} + \overline{v'^2})$ profiles (Fig. 11), which have been annotated with arrows marking the cross-shore location of the bar. The possibility that the vicinity of the bar might be a region in which the rigid lid approximation may be violated has been previously discussed. It is unclear at present whether the apparent compression of the model profile compared with the observations is a result of overprediction by the model in the vicinity of the bar or whether some unrecognized mechanism is reducing the instabilities effect there. Although the rigid lid approximation within the model appears sufficiently maintained, the previously suggested breakdown near the bar (based upon the analysis of the surface coherence partitioning of the spectra (Figs. 14-16)), would be expected to yield observed $\frac{1}{2}(\overline{u'^2} + \overline{v'^2})$ and $\overline{u'v'}$ profiles differing from those modeled.

The model's under-prediction of energy close to the shoreline is also quite evident in Fig. 11, particularly in the cases of 1022 and 2254 on 10 OCT. It is noteworthy that in all three cases the measured energy at the current meter closest to shore gave no indication of the rapid falling off to zero as indicated by the model. In each of the three cases, the relative minima predicted near current meter 30 (located 50-60 m offshore) seems to be in agreement with observations.

Examining the observed/predicted S_{uv} surfaces (Fig. 12) and $\overline{u'v'}$ profiles (Fig. 13) reveals similar behavior. It is emphasized that $\frac{1}{2}(\overline{u'^2} + \overline{v'^2})$ profiles were used to calibrate the stream functions and therefore good agreement of these profiles should be expected. Comparison of S_{uv} surfaces and $\overline{u'v'}$ profiles test the modeled relationship between $\frac{1}{2}(\overline{u'^2} + \overline{v'^2})$ and $\overline{u'v'}$ via the stream function shape. Qualitative agreement is seen, but again the predicted profiles appear "compressed" toward the shoreline. The fact that the

predictions are of the same general magnitude and sign is taken as an encouraging indication of the feasibility of the overall method.

A disappointing result was the inability to compare the modeled and observed phase structure of u and v . It was pointed out by Bowen and Holman (1989) that the unique cross-shore structure of the u/v phase angle, (in phase within the current shear region and out of phase elsewhere) was a potential means of recognizing shear instabilities and evaluating the current structure associated with them. Processing of the time series used in this work suggested that even slight current meter alignment error, in the presence of a strong, but slowly varying, longshore current could severely degrade any information on the u/v phase angle.

One of the key points in this work is use of the observed energy density spectra (Figs. 14-16) to calibrate the predicted stream functions (as opposed to using the relative scaling of the predicted growth rates, shown in Fig. 6). For 9 OCT 2213 and 10 OCT 1022, the predicted "maximum growth-rate" frequencies of ~ 0.0025 and 0.0027 (Fig. 6) both appear slightly higher in frequency than the observations. 10 OCT 2254 exhibits a non-monotonic predicted growth-rate structure and an observed spectrum with the peak frequency (~ 0.005) significantly higher than the other two cases. It should be remembered that the two principle benefits of the use of observed energy densities in calibrating the stream functions is that it need not be assumed that the steady state (observed) spectral distribution of energy is given by the distribution of growth-rates and that this method provides an absolute reference frame and thereby dimensional $\frac{1}{2}(\overline{u'^2} + \overline{v'^2})$ and $\overline{u'v'}$ predictions.

6. APPLICATIONS TO LONGSHORE CURRENT MODELING

Simple longshore current models (based on an alongshore balance between the radiation stress gradient and bottom shear stress) applied to barred topography predict two current maxima in the form of "jets", the first over the bar, and the second at the shore face.

Conversely, observations during DELILAH show a single longshore current maximum, found in the vicinity of the trough. Typically, longshore current models employ some sort of horizontal mixing term to try to eliminate this disparity. This mixing term is a parameterization of the turbulent radiation stress gradient and is usually described in terms of eddy viscosity. Turbulence is present in the surf zone over a wide range of frequency and spatial scales. In this section the turbulent radiation stress associated with shear instabilities is examined.

The time averaged, depth integrated momentum equation in the alongshore direction (neglecting molecular viscosity and surface wind stress), is a balance between the gradient of the total radiation stress and bottom stress, e.g. Phillips (1966):

$$\frac{\partial S_{yx}}{\partial x} = \frac{\partial \tilde{S}_{yx}}{\partial x} + \frac{\partial}{\partial x} \int_{-h}^0 \rho \overline{u'v'} dz = \overline{\tau_y^b} \quad (21)$$

where the radiation stress is separated into two terms, one associated with the wave motion (-) and the other due to turbulence ('). The turbulent radiation stress is equivalent to the Reynold's stress, $\rho \overline{u'v'}$, integrated over depth, and is obtained using the calibrated shear instability model.

A "base state" longshore current profile is modeled by balancing the wave induced radiation stress gradient and linearized bottom shear stress (neglecting mixing), using the Thornton & Guza (1986) model. Wave height transformation, required as input, is provided through the Thornton and Guza (1983) model in which randomness in wave height is modeled by the Rayleigh distribution for both broken and unbroken waves inside and unbroken waves outside the surf zone. H_{rms} is used as a representative statistic of the ensemble wave height transformation. After applying Snell's law for wave refraction based on the assumption of straight and parallel contours, the gradient of the alongshore wave-

induced momentum flux given by linear wave theory may be written:

$$\frac{\partial \bar{s}_{yx}}{\partial x} = \rho \frac{\partial}{\partial x} \int_{-h}^0 \bar{u} \bar{v} dz = \frac{\sin \alpha_0}{c_0} \frac{\partial}{\partial x} (E C_g \cos \alpha) \quad (22)$$

in which the ensemble averaged wave energy, $E = \frac{1}{2} \rho g H_{ms}^2$, α is the wave incidence angle from shore normal, c is the wave phase speed (the subscript 0 denotes initial conditions), and C_g is the wave group velocity. The linearized bottom stress is written

$$\bar{\tau}_y^b = c_f \rho u_m V \quad (23)$$

with u_m as the maximum near-bottom wave induced orbital velocity. The H_{ms} -wave height transformation and base state longshore current profile for 10 October 1022 are plotted in Fig. 18, together with bathymetry and H_{ms} and V observations.

With the turbulent radiation stress term omitted from Eq. (21) (i.e. no mixing) the predicted longshore current "base state" profile obtained shows poor agreement with observations. To address the question of how much improvement results from inclusion of the shear instability turbulent radiation stress, an important point must first be clarified. The shear instability solutions studied are all based on splined profiles of the *observed* data, as is appropriate since it is the observed energy density spectra that have been used to calibrate the stream functions. As demonstrated by Fig. 18, the profile predicted by the longshore current model does not represent the observed profile and if used as input into the shear instability model, produces significantly differing results. Specifically, use of the "base state" current profile as input results in three growing modes being predicted, with frequency/growth rates as shown in Fig. 19. The "crossing-over" between fastest, second fastest, and third fastest growing modes is rather visually confusing, but is simply an indication that one mode may have the higher growth rate within one wavenumber band but not in some other.

(Putrevu and Svendsen (1992) provide an excellent discussion of such situations in their numerical study). By modifying various sections of the "base-state" input current profile and noting the effects upon the output, the three regions responsible for the modes are identified. The point most relevant to this study is that in having three dispersion curves there no longer exists a clear way to associate the observed energy density spectra $\frac{1}{2} (\overline{u'^2} + \overline{v'^2}) (f)$ with distinct wavenumber components. This prohibits the use of data in calibrating the stream function amplitudes.

Proper treatment would require an assumed base state current profile with mixing due to its related shear instabilities, leading to some slightly modified current profile and again slightly different shear instabilities. This would be carried out in increments until a "final state" is obtained which might then be compared with the observed current/shear instability information. Again, the present means of amplitude calibration cannot be employed and any such effort is beyond the scope of the present study. In summary, two principle problems prevent use of the base state as input into the shear instability model. First, the only observations with which to perform the calibration are presumably related to the drastically different steady-state current profile. Secondly, the existence of three distinct shear instability dispersion curves prohibits the association of measured energy spectra, $\frac{1}{2} (\overline{u'^2} + \overline{v'^2}) (f)$, with a unique wavenumber.

Inclusion of the turbulent radiation stress term (based upon the shear instability modeled $\overline{u'v'}$ profile (Fig. 16)) into Eq. (21) with the base state wave forcing yields an obviously non-physical longshore current profile (Fig. 20). It is be pointed out that a reversal in the sign of the total radiation stress (wave + turbulence) gradient occurs, resulting from the turbulent radiation stress contribution producing regions with oppositely flowing longshore currents. Such a reversal in the sign of the radiation stress gradient never occurs in the wave term, (i.e. wave energy flux does not increases shoreward), and so the physical feasibility of

an increase in radiation stress must be considered. If one assumes that sufficiently far offshore $\overline{u'v'}$ associated with the shear instabilities is zero, and that somewhere near the beach face returns to zero, then $\frac{\partial}{\partial x} \int_{-h}^0 \rho \overline{u'v'} dz$ will have both positive and negative regions. If the assumption is made that the longshore current maxima is observed over the trough because the net forcing is greater there than over the bar, and it is assumed that the wave radiation stress is reasonably well modeled, then some turbulent radiation stress gradient, roughly equal and opposite to that of the wave term, is required to offset the wave forcing in the bar region. The unrealistic longshore current profile obtained is a result of the shear instability's radiation stress gradient being superimposed upon a region which is modeled as void of forcing (i.e. over the trough). Instead of negating the wave's forcing, the turbulent radiation stress gradient forces its own flow in the opposite direction. Inserting the shear instability term into a region lacking any supporting current structure is also conceptually inappropriate as the shear instability is dependent upon the longshore current structure for its generation / maintenance.

A second approach is to ask what $\overline{u'v'}$ profile would be required to balance the difference between the wave generated radiation stress and the bottom shear stress. The turbulent radiation stress profile required to balance Eq. (21) is calculated by assuming that the wave-induced radiation stress term is reasonably modeled and inserting the observed (splined) longshore current profile into the bottom stress term. This method offers the additional benefit that the wave forcing, the shear instabilities, and the longshore current profile are all steady state, avoiding issues of incremental transformation from "base state" to observed. The "required" profiles for the three cases studied (Fig. 21) are compared with the profiles predicted previously by the shear instability model. Qualitative agreement can be seen with respect to both magnitude and structure, with the same "compression" toward the shoreline previously discussed.

6. SUMMARY AND CONCLUSIONS

The magnitude and cross-shore structure of the $\overline{u'v'}$ associated with shear instabilities of the longshore current have been examined. A "smoothing" spline has been used to obtain the longshore current profile required as model input. Shear instability frequencies and growth rates are predicted. Using measured energy density spectra to calibrate the model-generated stream function amplitudes, an absolute reference is used to obtain dimensional values of $\overline{u'^2}$, $\overline{v'^2}$ and $\overline{u'v'}$. Agreement is found between both modeled and observed $\frac{1}{2}(\overline{u'^2} + \overline{v'^2})$ and $\overline{u'v'}$, although the model's consistent shoreward compression of the stream function structure is not presently understood. $\overline{u'v'}(x)$ associated with shear instabilities appears to be a significant source of mixing in the nearshore. Based upon the three cases studied the modeled mixing produced by the shear instabilities appears to be in qualitative agreement with that required to reconcile the disparity between model predicted longshore current profiles and observations.

ACKNOWLEDGEMENTS

The authors wish to express their appreciation to all those who participated in the DELILAH experiment and in particular the staff of the Coastal Engineering Research Center's Field Research Facility, under the direction of William Birkemeier. Nick Dodd of the Institute for Marine and Atmospheric Research, Utrecht University, is thanked for his initial development of the shear instability model code while formerly associated with the Naval Postgraduate School. In addition, special appreciation is expressed to Rob Wyland and Tim Stanton, Naval Postgraduate School, and Katie Scott, University of California, Santa Cruz, for their roles in acquisition of wave and current data, and to Mary Bristow, Naval Postgraduate School, for initial processing of the data. EBT was funded by Office of Naval Research Coastal Sciences Grant N00014-92-AF-0002, JOS was funded by ONR Coastal Sciences Grant N00014-92-C-0014, and JCC is an ONR fellow.

REFERENCES

- Birkemeier, W.A., and C. Mason, The CRAB: a unique nearshore surveying vehicle. *J. Surv. Eng. ASCE*, vol. 110, no. 1, pp. 1-7, 1984.
- Bowen, A.J., and R.A. Holman, Shear instabilities of the longshore current. *J. Geophys. Res.* **94**, 18,023-18,030, 1989.
- Church, J.C., and E.B. Thornton, Effects of breaking wave induced turbulence within a longshore current model. *Coastal Engng.* (in press), 1993.
- Dodd, N., and E.B. Thornton, Growth and energetics of shear waves in the nearshore. *J. Geophys. Res.* **95** (C9), 16,075-16,083, 1990.
- Dodd, N., J. Oltman-Shay, and E.B. Thornton, Shear instabilities in the longshore current: A comparison of observation and theory. *J. Phys. Oceanogr.* **22**, 62-82, 1992.
- Dodd, N., and E.B. Thornton, Longshore current instabilities: growth to finite amplitude., *Proc. 23rd Coastal Engr. Conf., ASCE*, 1992.
- Larson, M.L., and N.C. Kraus, Numerical model of longshore current for bar and trough beaches, *J. Waterw. Port. Coastal Ocean Div. ASCE* **117**, 327-347, 1991.
- Oltman-Shay, J., P.A. Howd, and W. A. Birkemeier, Shear instabilities of the mean longshore current, 2, Field Observations. *J. Geophys. Res.* **94** (C12), 18,031-18,042, 1989.

Pawka, S.S., Wave directional characteristics on a partially sheltered coast. Ph.D. dissertation, Scripps Inst. of Oceanography, UCSD, 1982.

Putrevu U., and I.A. Svendsen, Shear instabilities of longshore currents: a numerical study. *J. Geophys. Res.* **97** (C5), 7283-7303, 1992.

Thornton, E.B., Energetics of breaking waves within the surfzone, *J. Geophys. Res.* **84** (C8), 4931-4938, 1979.

Thornton, E.B., and R.T. Guza, Transformation of wave height distribution, *J. Geophys. Res.* **88**, 5925-5938, 1983.

Thornton, E.B., and R.T. Guza, Surf zone longshore currents and random waves: Field data and models. *J. Phys. Oceanogr.*, **16**, 1165-1178, 1986.

Whitford, D.J., and E.B. Thornton, Longshore currents over a barred beach, II, model. (Submitted to *J Phys. Oceanogr*), 1993.

APPENDIX A

As noted previously, current meter orientation error does not effect $u'^2 + v'^2$, but does effect $\overline{u'v'}$ measurement. A sensitivity test was performed imitating possible meter miss-alignment by numerically rotating the low passed current components. The calculations indicate that at shear instability scales, $\overline{u'v'}$ is relatively insensitive to rotation (Fig. A1). Assuming that the directional resolution, current meter orientation, and alongshore alignment combine to produce an error of less than 5-10 degrees, the results indicate that the measured shear instability $\overline{u'v'}$ error should be less than 20%.

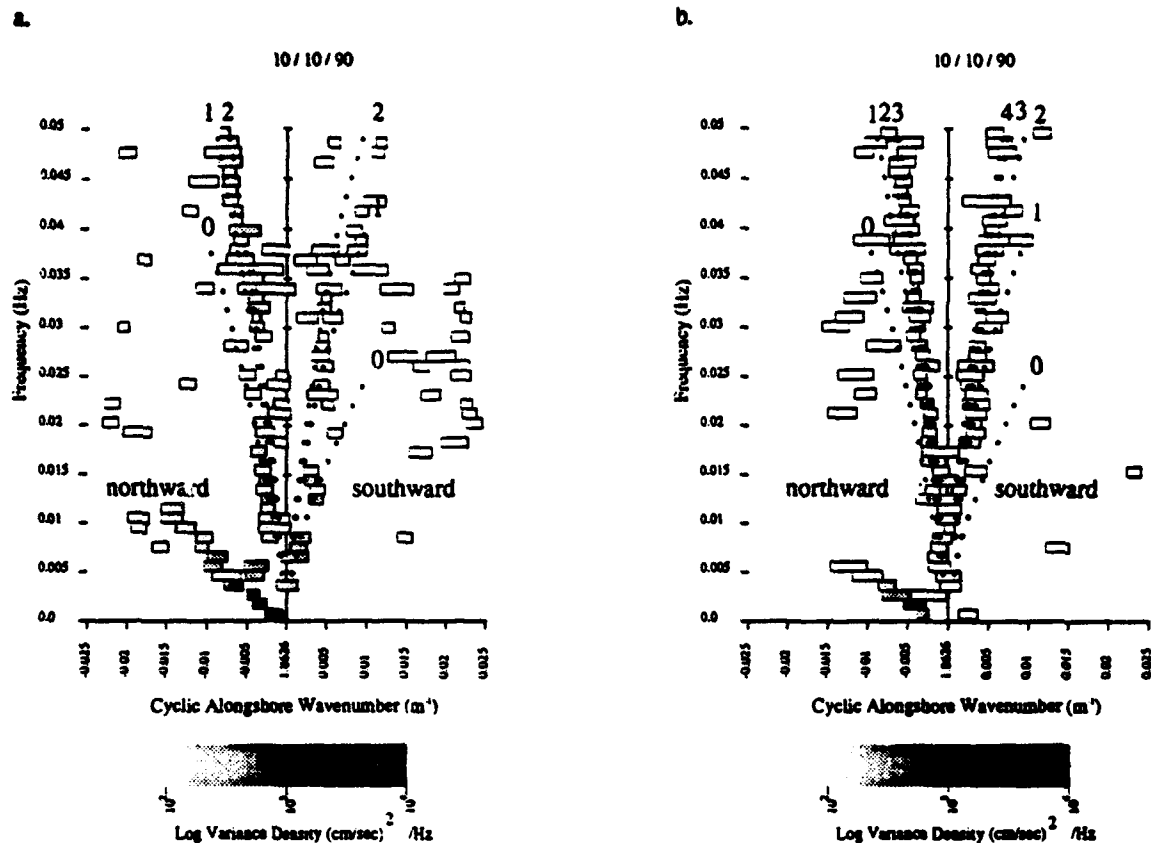


Fig 1 10 OCT 1022: IMLE estimated frequency-alongshore cyclic wavenumber spectra from the a) inner alongshore array located on the trough side of the bar, coincident with current meter 30, and b) outer alongshore array located on the seaward side of the bar, coincident with current meter 70. The rectangular boxes mark the location of variance peaks, the wavenumber width defines the half-power bandwidth. Shading indicates log variance density contained within the half-power bandwidth of the box. The asterisk identify dispersion curves of infragravity edge wave modes, determined from the numerical solutions for depth and current profiles on this day. $\Delta f = 0.00195$ Hz, $\Delta K = 0.0005 \text{ m}^{-1}$, d.o.f. = 38.

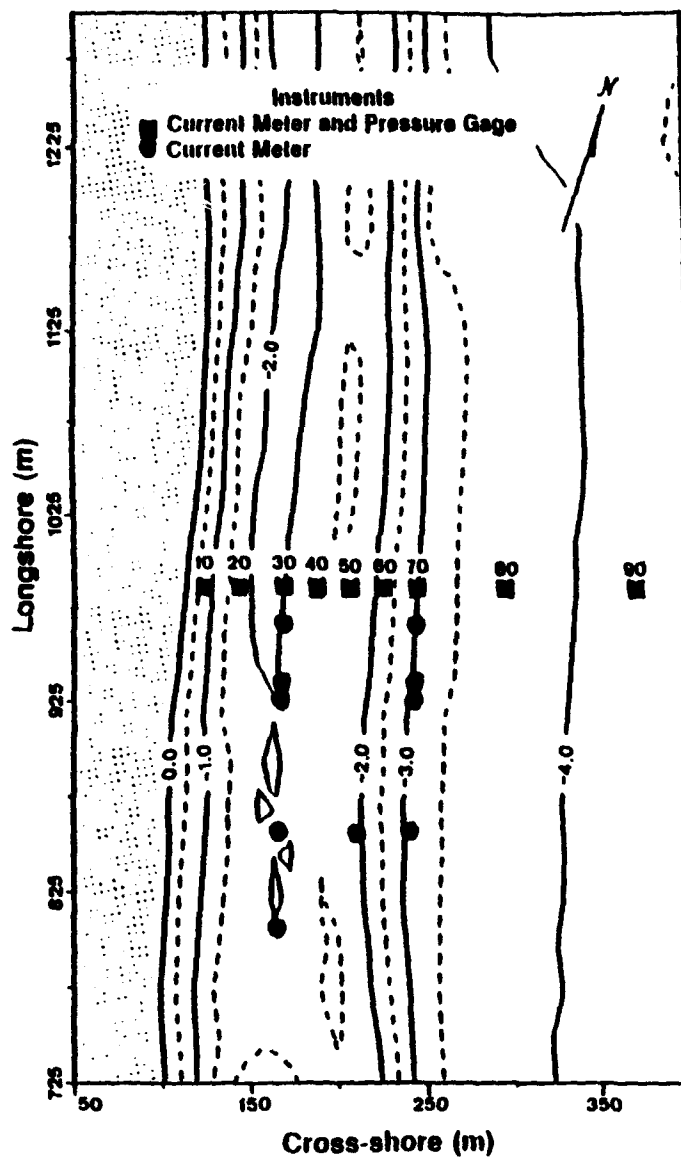


Fig 2 Current meter and pressure gage locations overlaying bathymetry for 12 OCT 90.

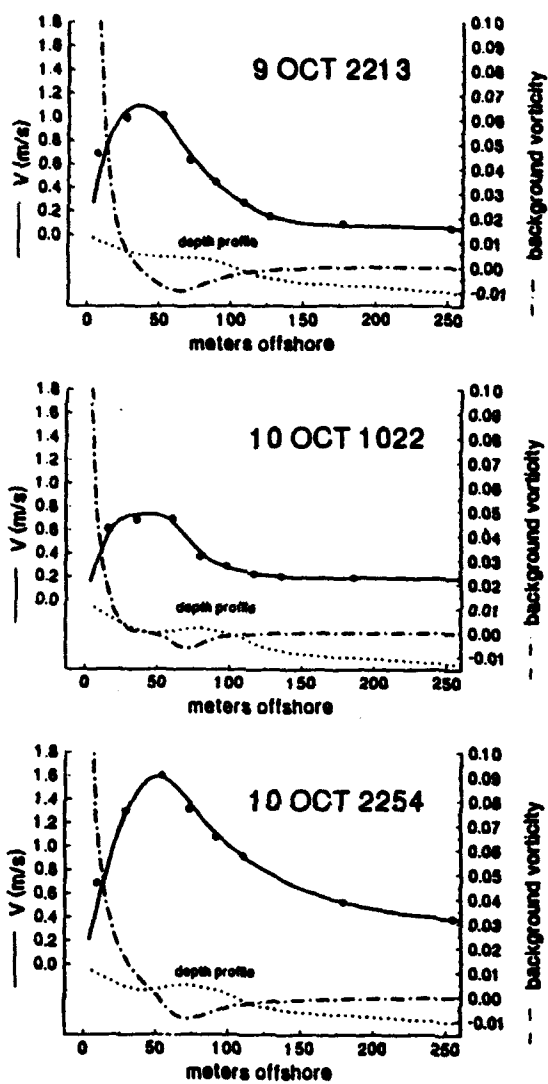


Fig 3 Mean longshore current observations and splined profile with calculated background vorticity profile and measured bathymetry.

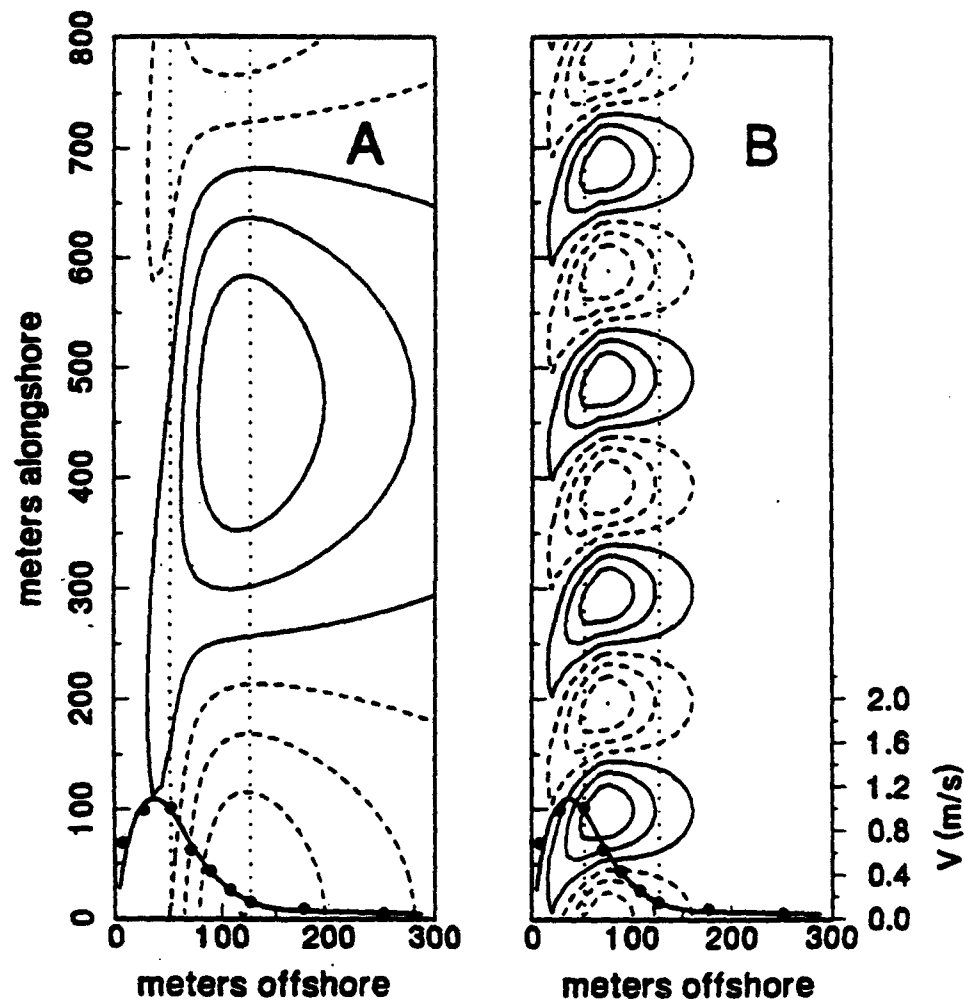


Fig 4 Examples of model generated stream functions for 9 OCT 2213: a) $f=.001\text{Hz} / K=.00125$ b) $f=.004\text{Hz} / K=.005$ (aspect ratios 1:1). Mean longshore current observations and splined profiles superimposed at bottom with direction of flow as depicted. Vertical dotted lines indicate cross-shore position of the two alongshore arrays.

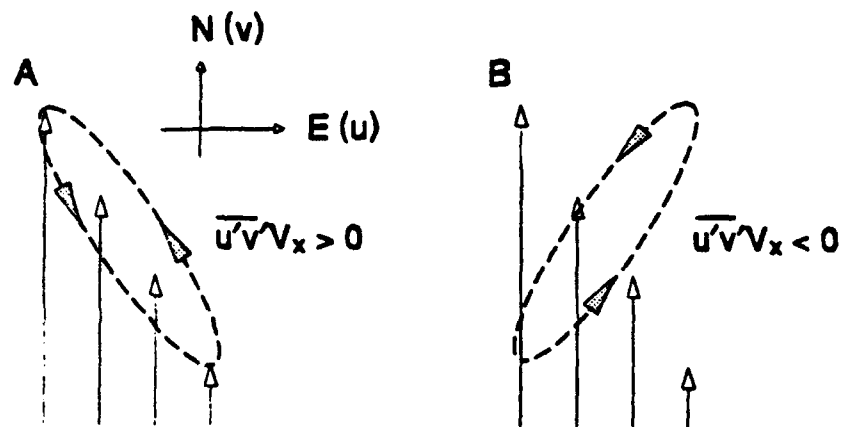


Fig 5 Schematic depicting energy transfer conditions related to the instabilities "tilt" relative to the mean current shear. Panel A): energy transfer from instability to mean current, panel B): from mean current to instability.

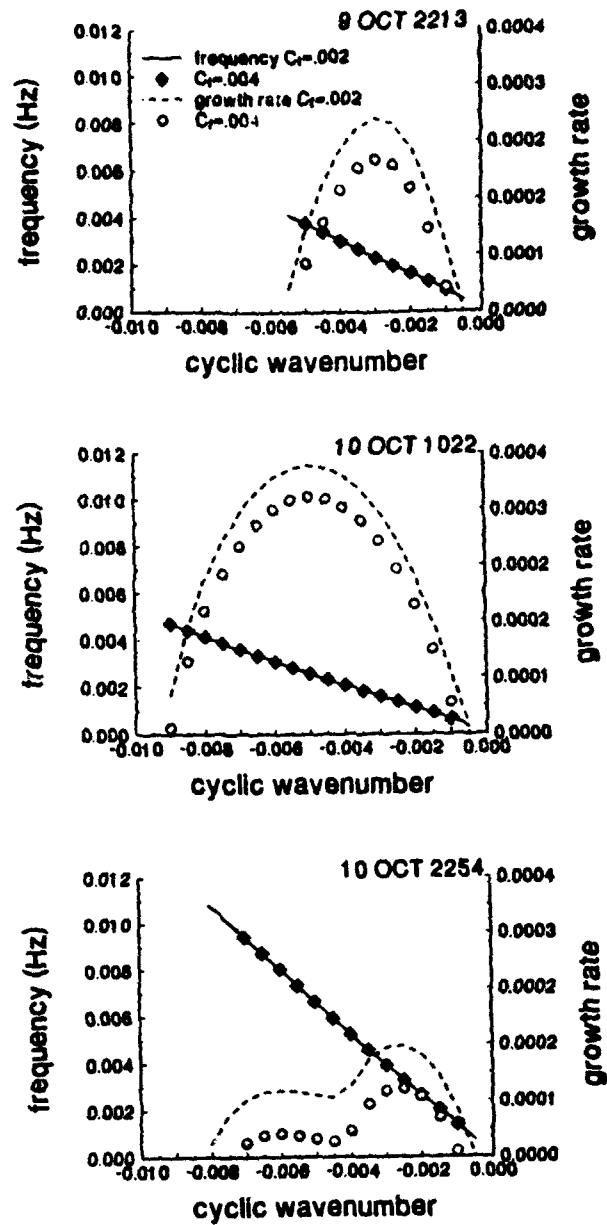


Fig 6 Cyclic alongshore wavenumber versus both frequency and growth rate predicted by the shear instability model for bottom friction coefficient values of 0.002 and 0.004.

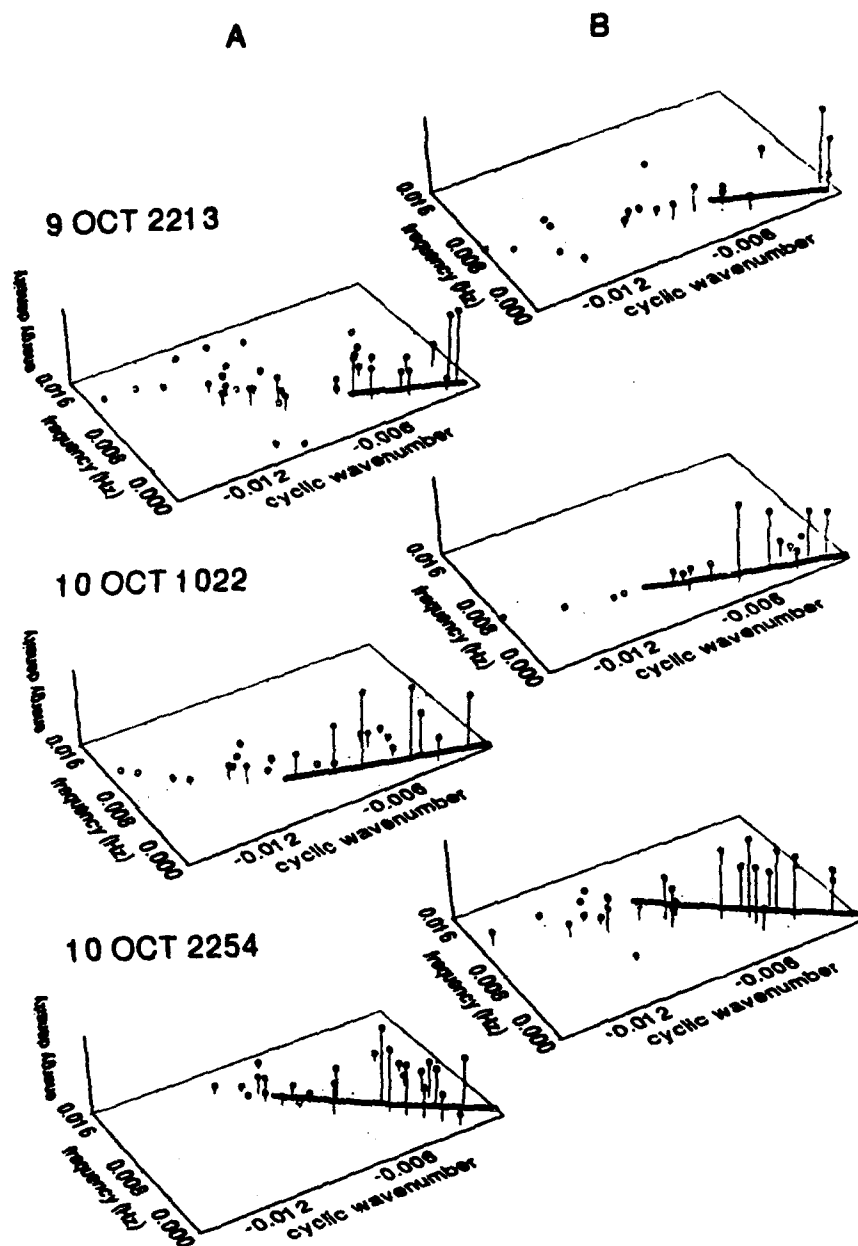


Fig 7 Energy density plots for a) trough alongshore array and b) seaward array. Solid dots represent u component and empty dots v . Vertical height scaled arbitrarily to emphasize structure. Model predicted dispersion curve for wavenumbers with positive growth-rates shown as solid line.

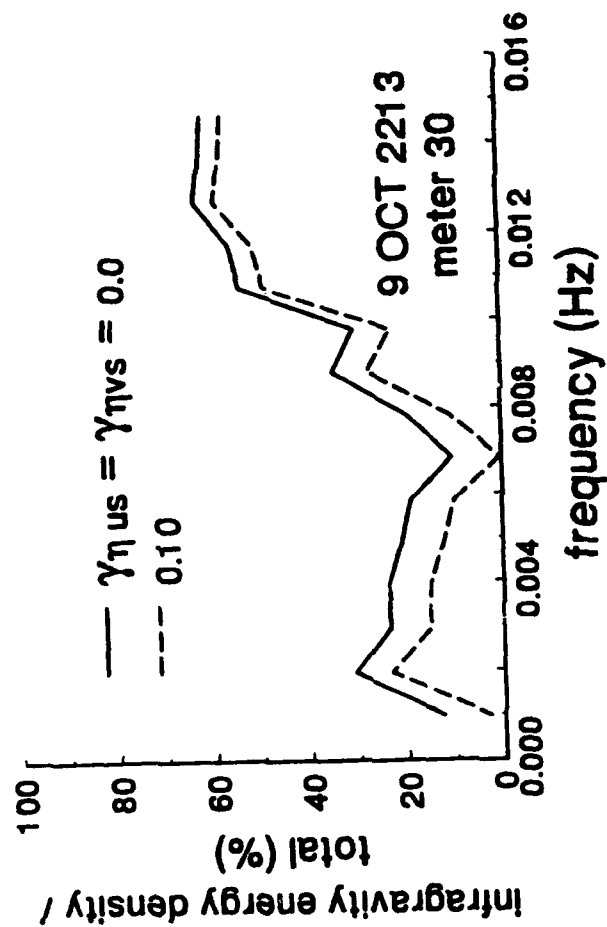


Fig 8 Sensitivity test for surface elevation-horizontal velocity coherence method of energy density partitioning.

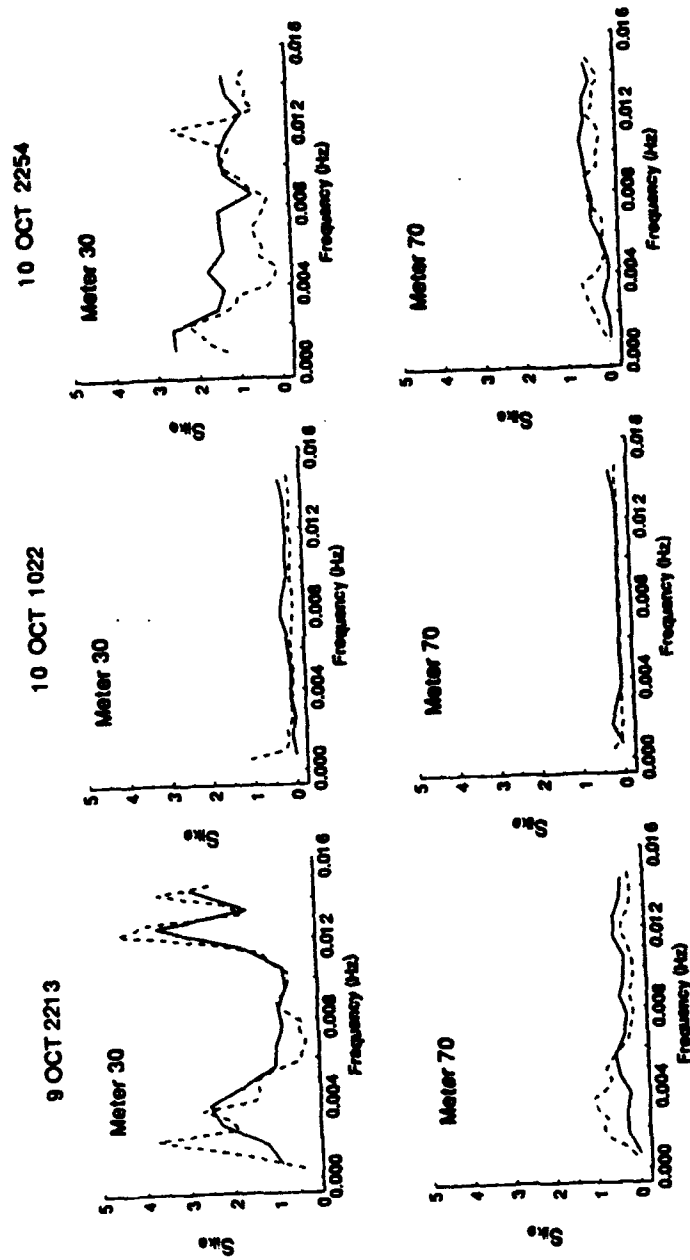


Fig 9 Infragravity energy density calculated using surface elevation-horizontal velocity coherence method (dashed) and f-K spectra estimated for the alongshore arrays (solid).

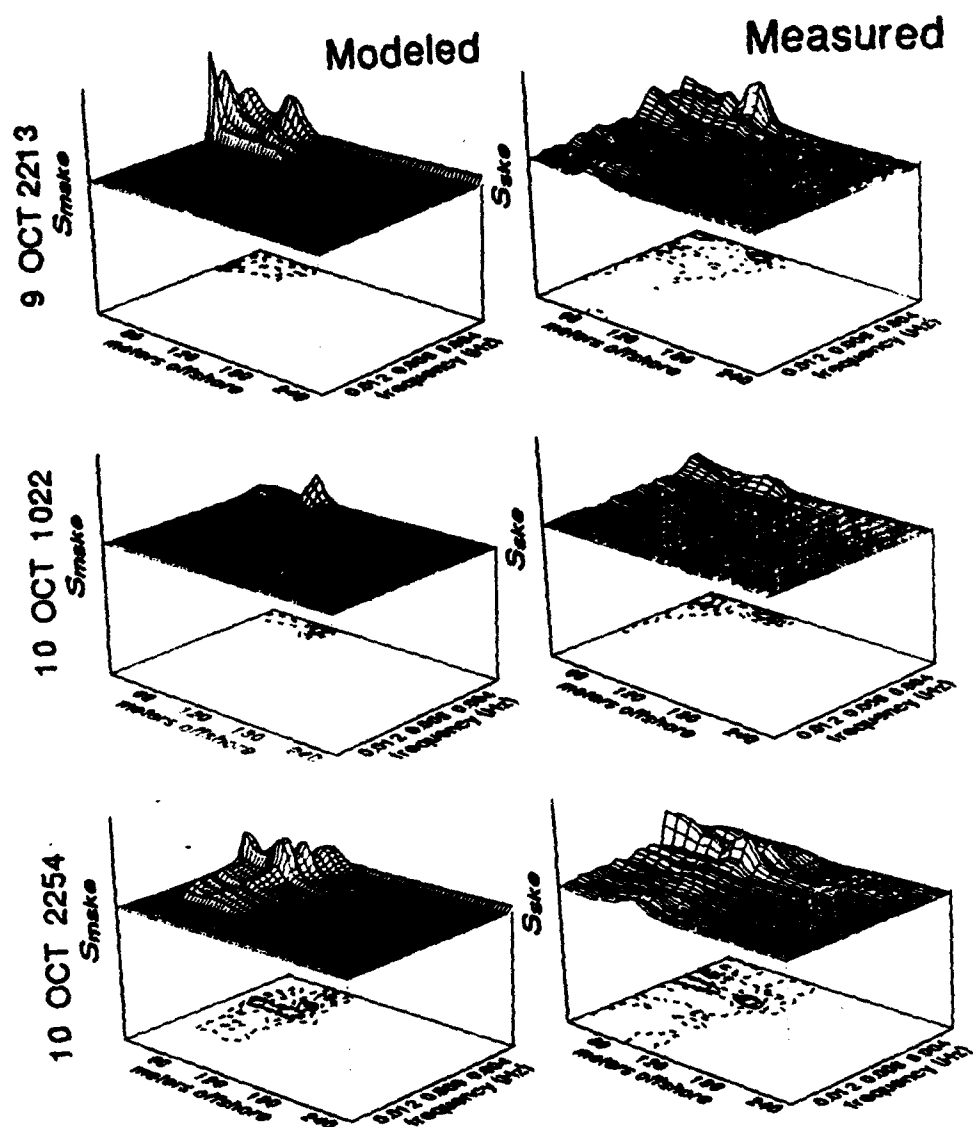


Fig 10 Kinetic energy density f-K surfaces, modeled (S_{model}) and measured (S_{meas} , splined after removal of infragravity contamination).

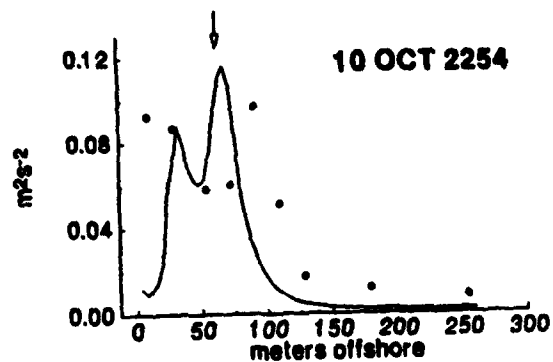
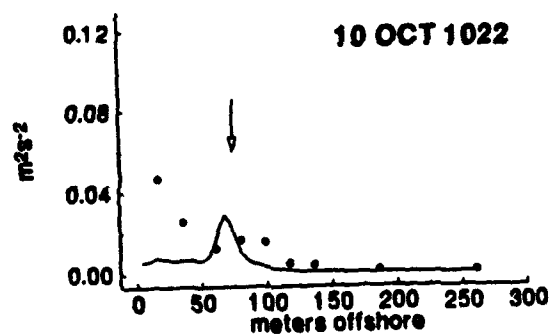
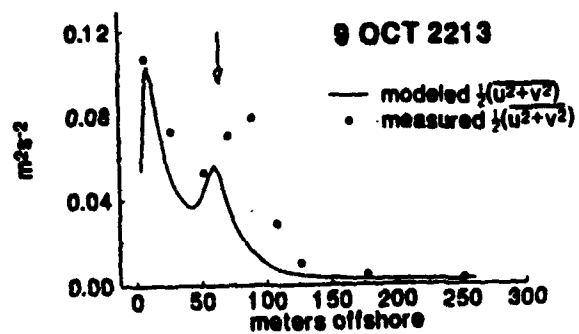


Fig 11 Frequency integrated $\frac{1}{2}(u^2+v^2)$ profiles (modeled) and observations; arrows indicate cross-shore position of bar.

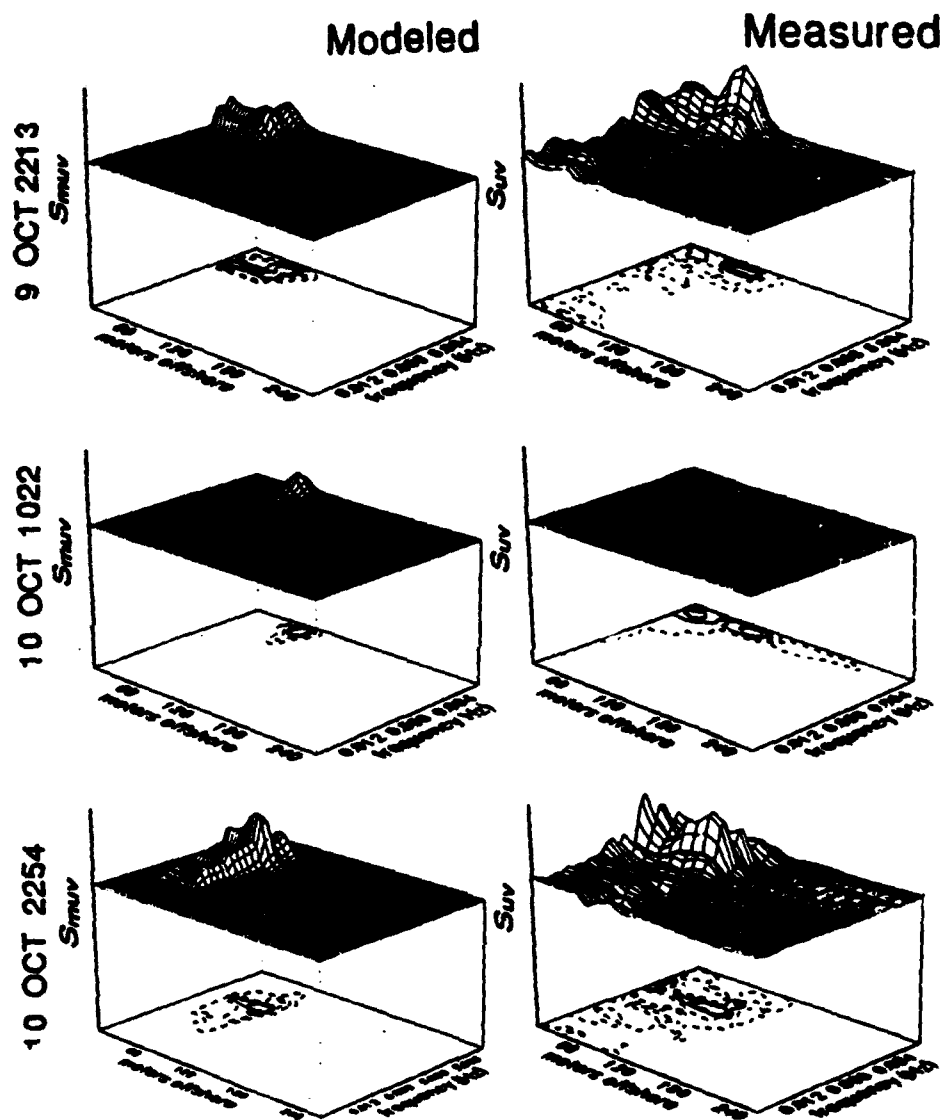


Fig 12 Covariance energy density (S_{uv}) f-K surfaces, modeled and measured.

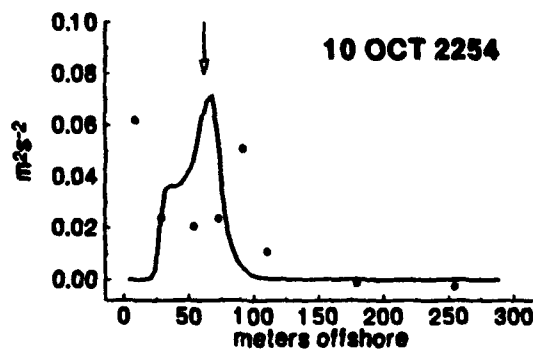
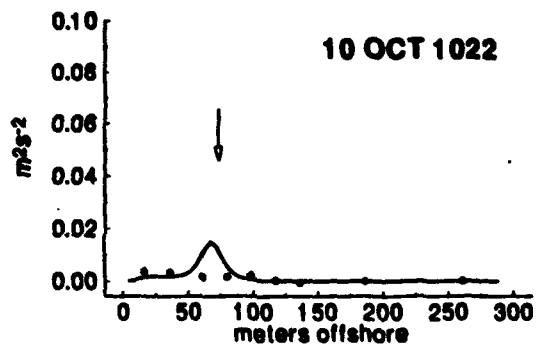
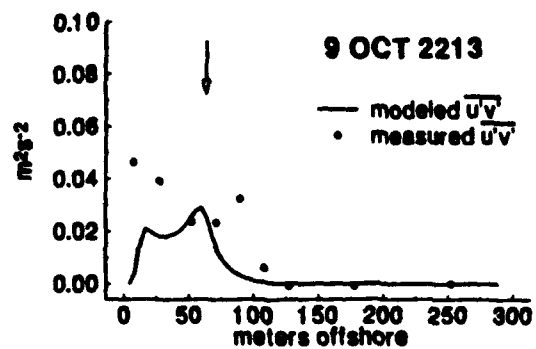
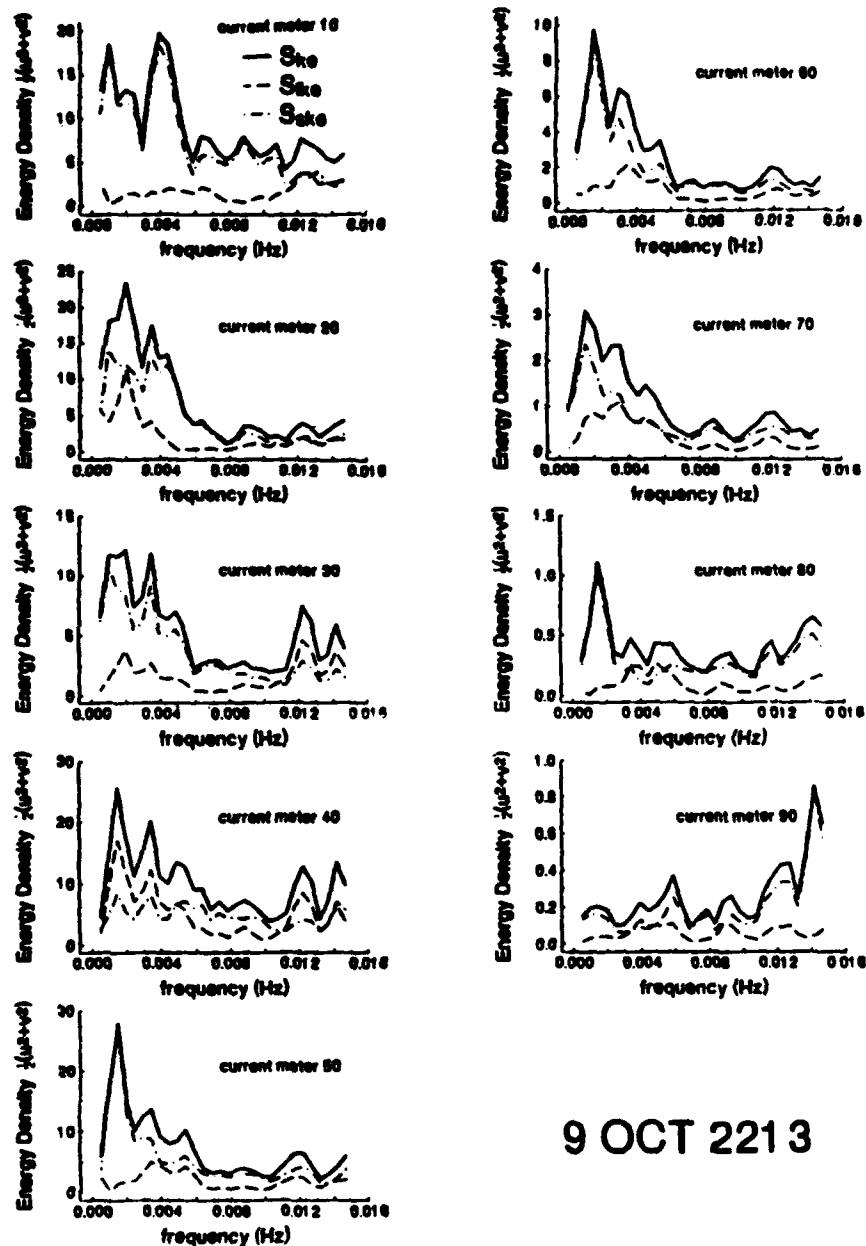
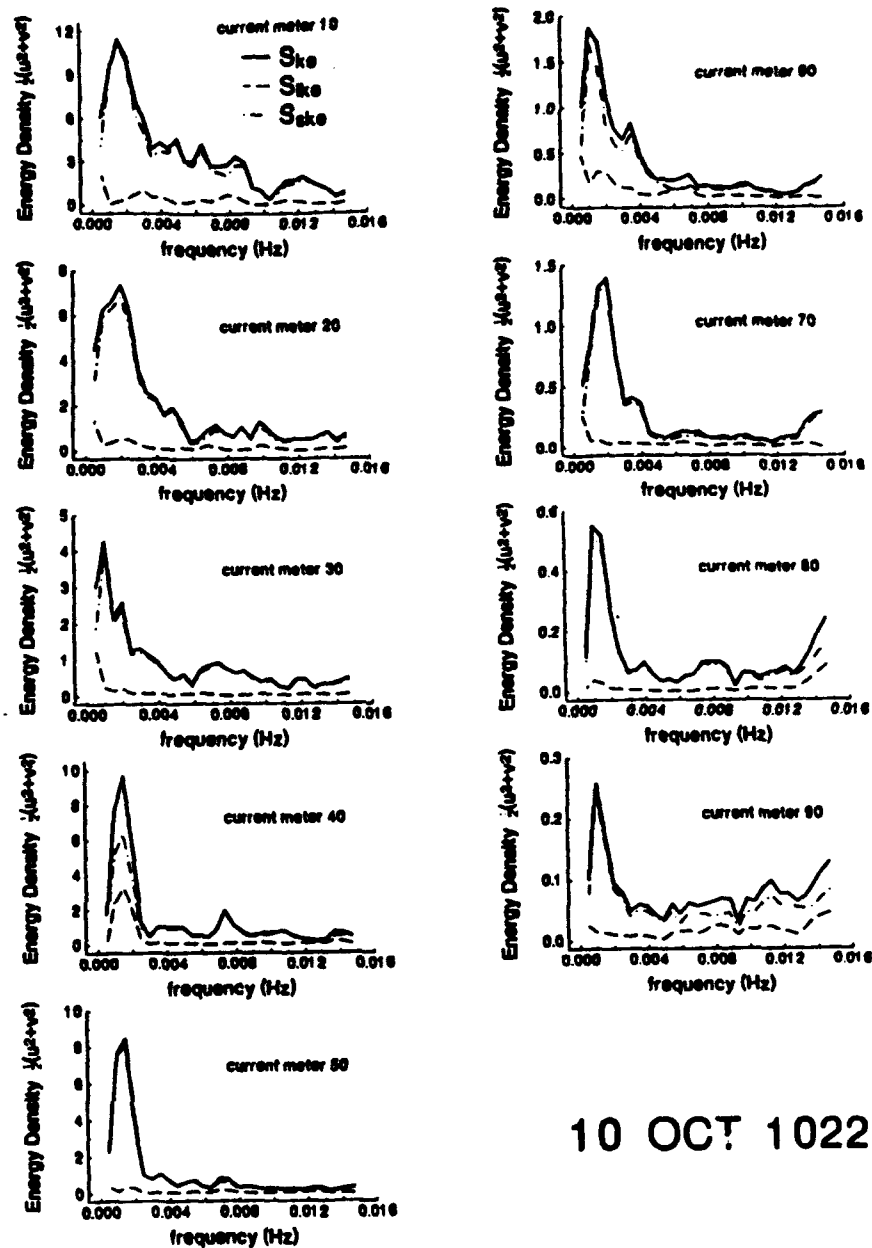


Fig 13 Frequency integrated $\overline{u'v'}$ profiles (modeled) and observations; arrows indicate cross-shore position of bar.



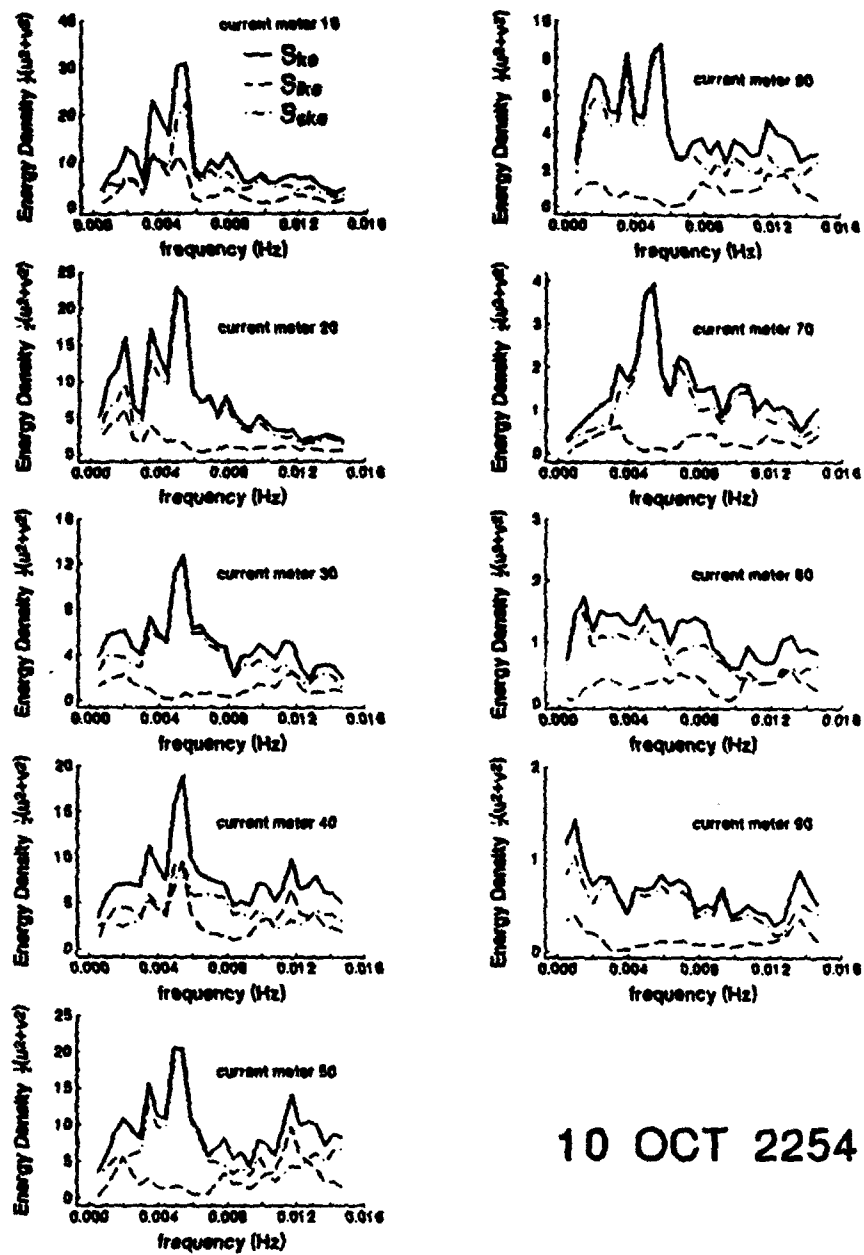
9 OCT 2213

Fig 14 Measured kinetic energy density spectra (S_k), with infragravity (S_{ki}) /shear instability (S_{ksi}), partitioning done through surface elevation-horizontal velocity coherence method.



10 OCT 1022

Fig 15 Measured kinetic energy density spectra (S_{k0}), with infragravity (S_{k1}) / shear instability (S_{k2}), partitioning done through surface elevation-horizontal velocity coherence method.



10 OCT 2254

Fig 16 Measured kinetic energy density spectra (S_{kk}), with infragravity (S_{kk}^i) / shear instability (S_{kk}^s), partitioning done through surface elevation-horizontal velocity coherence method.

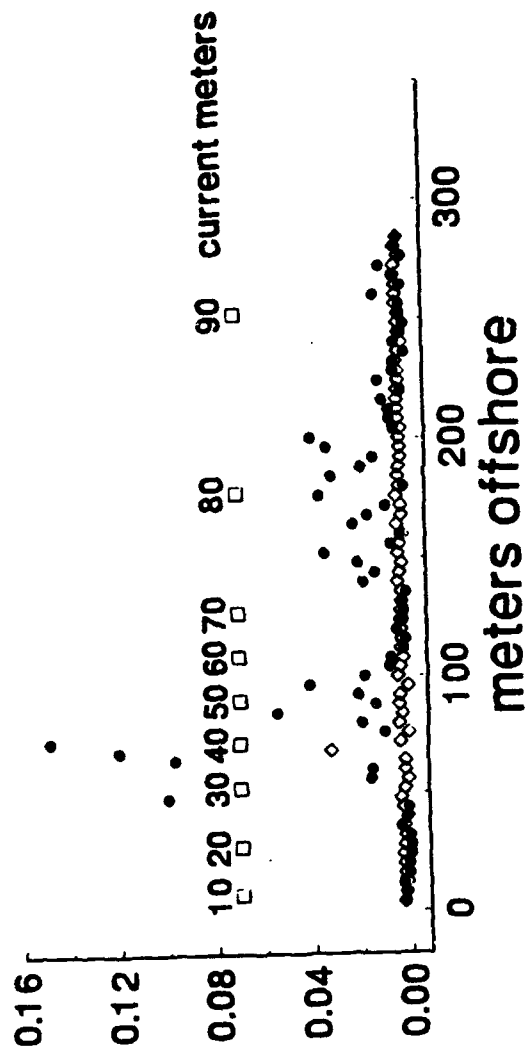


Fig 17 Ratio of model predicted vertical and horizontal terms in the full continuity equation used here as a measure of the validity of the rigid lid assumption. Calculations are based on measured current structure and bathymetry for 9 OCT 2213 and modeled stream functions ($f = .001 \text{ Hz} / K = .00125$ shown as filled circles and $f = .004 \text{ Hz} / K = .005$ shown as open diamonds). Cross-shore positions of current meters marked by boxes.

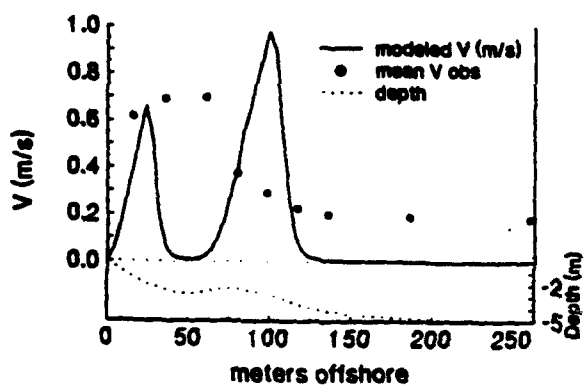
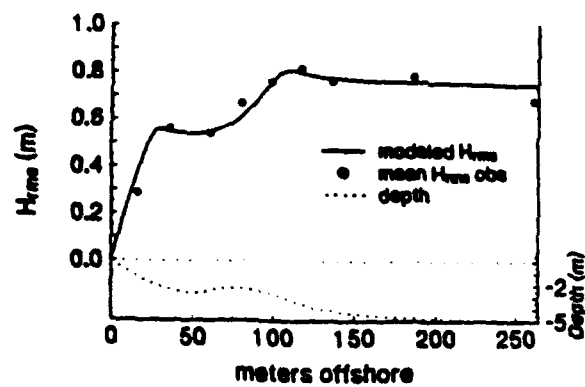


Fig 18 H_{rms} and "base state" longshore current (V) model output (without mixing), observations, and measured bathymetry for 10 OCT 1022.

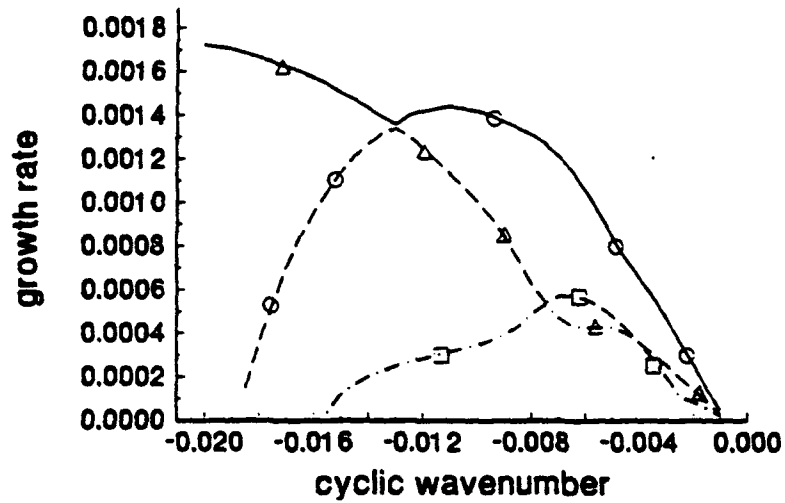
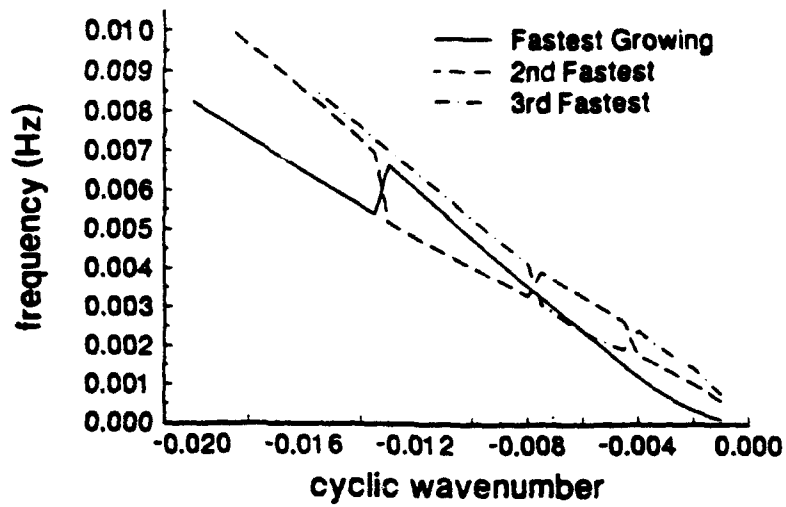


Fig 19 Shear instability model frequency-growth rate output using "base state" longshore current profile (Fig 18) as input with bottom friction coefficient .002 . Triangles identify mode associated with beach face region, circles - seaward side of bar, and boxes - region of trough.

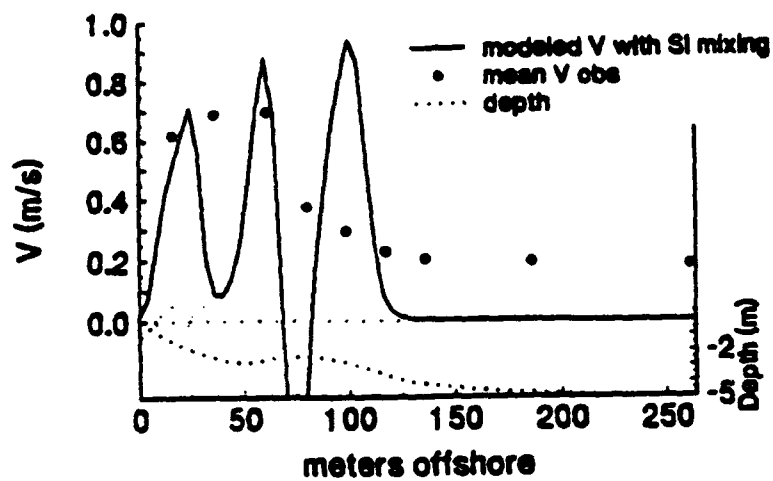


Fig 20 Longshore current model for 10 OCT 1022 as in Fig 18 but with inclusion of mixing by integrated $\overline{u'v'}$ covariance profile given through shear instability analysis (shown in Fig 13).

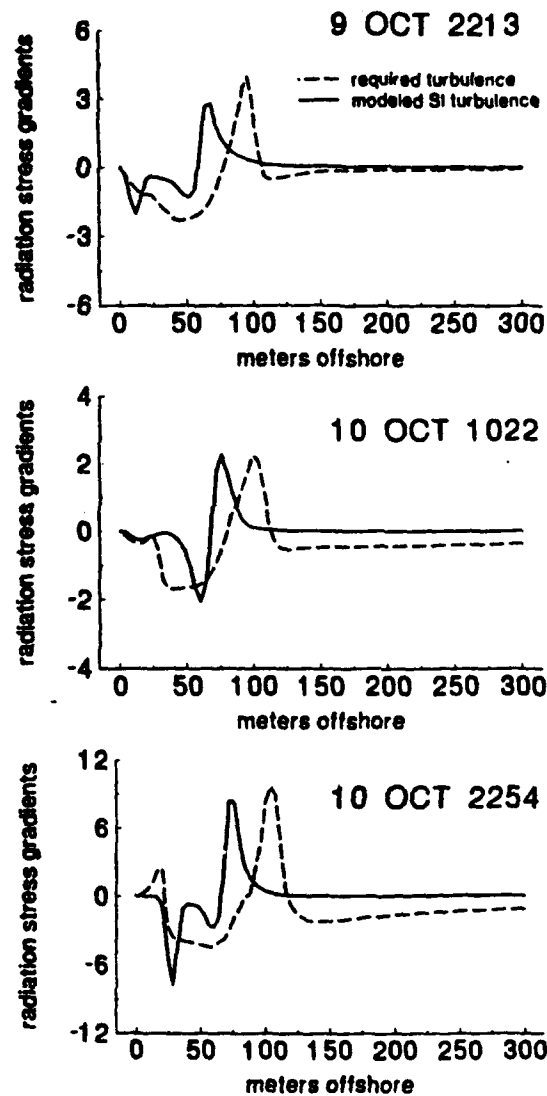


Fig 21 Turbulent radiation stress gradient required to justify wave forcing and observed longshore current profile (dashed) and turbulent radiation stress gradient associated with integrated shear instability $\overline{u'v'}$ profile (solid).

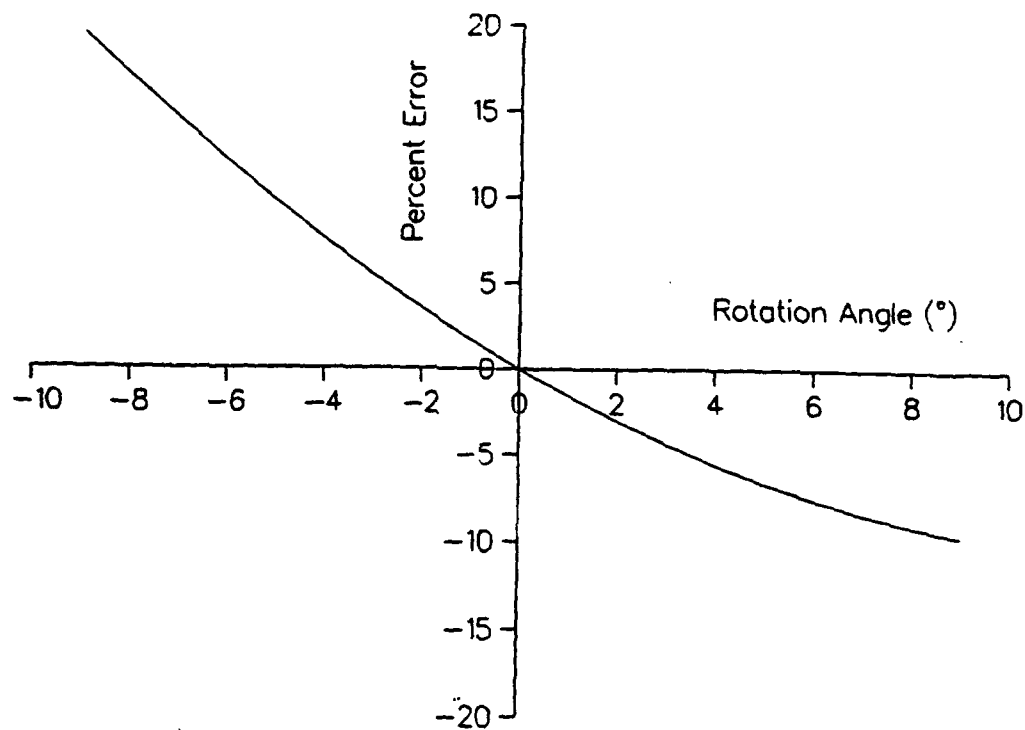


Fig A1 Percent error of \overline{uv} covariance as function of current meter rotation angle.

V. SUMMARY AND CONCLUSIONS

The steady state alongshore momentum equation governing mean longshore currents on straight beaches is a balance between the changes in the momentum flux due to obliquely incident waves with the gradient of the turbulent momentum flux (mixing), bottom stress, and wind stress. Of these four terms, the wave forcing appears to be well specified, and the wind forcing generally negligible. This work has focused on examination of the momentum flux of shear instabilities of the longshore current as a mechanism to describe the turbulent mixing term, and a modified bottom stress treatment which includes proposed effects of breaking wave induced turbulence.

Consideration of the effective bottom friction coefficient as the composite of two separate contributions is shown to improve prediction/ observation agreement except in the vicinity of the trough for the four barred beach cases considered. Good agreement is found with observations in the vicinity of the bar and seaward, a region which has been typically underpredicted by previous models. Although the calculated values of $c_{\bar{f}}$: .0010, .0014, .0010, and .0008, are significantly lower than c_f values used in previous studies, it should be emphasized that when combined with the remotely generated turbulence effects of c_{fr} , the net values are increased over much of the surf zone. Considering the 160m closest to the shore, the cross-shore means of $c_f = c_{fr} + c_{\bar{f}}$, (.0025, .0042, .0020, and .0030), are comparable to the spatially constant non-linear c_f values found in the literature (cf. Thornton and Guza (1986) .006; Visser (1984) .003 and .008; Wu *et al.* (1985) .010; Larson and Kraus (1991) .0035 and .004).

Vertical profiles of mean longshore currents were studied with the specific objective of testing the hypothesis that these profiles are logarithmic. It has been found that for the two experiments examined, lack of current meters sufficiently close to the bed prevents

discrimination between logarithmic and linear current profiles. Significant vertical shear is observed in the mean current structure during periods when $\gamma = H_{rms}/h$ is below 0.30 (mean change in V over depth as a percent of the bottom current meter value is 49%). On the otherhand, of the 64 profiles studied, 15 were considered to be statistically indistinguishable from vertical; all 15 occurring during periods when $\gamma \geq 0.3$, i.e. in a location where most waves are breaking. These results point to the need for increased sensor accuracy together with placement in close proximity to the bed.

It was hypothesized that shear instabilities of the longshore current can describe the turbulent momentum flux term (mixing). Using measured kinetic energy density spectra to calibrate the model-generated stream function amplitudes, an absolute reference is used to obtain dimensional values of $\overline{u'^2}$, $\overline{v'^2}$ and $\overline{u'v'}$. Agreement is found between both modeled and observed magnitudes and shapes of the cross-shore distributions of $\frac{1}{2}(\overline{u'^2} + \overline{v'^2})$ and $\overline{u'v'}$, although the model's consistent shoreward compression of the stream function structure is not presently understood. $\overline{u'v'}(x)$ associated with shear instabilities appears to be a significant source of mixing in the nearshore. Based upon the three cases studied, the modeled mixing produced by the shear instabilities appears in qualitative agreement with that required to reconcile the disparity between model predicted longshore current profiles and observations. Although an explanation for the shoreward shift of the model profiles has not been obtained, the strong similarities between the modeled $\overline{u'v'}(x)$ gradients and those required to produce the observed longshore current horizontal profiles suggests further examination.

Additional possibilities for explaining the current maximum in the trough is the violation of the longshore uniformity assumption, such that a pressure gradient in the alongshore direction could produce accelerations not included in the model, and turbulent mixing at other space/time scales. Irregularities in the bar could produce differential wave

breaking resulting in alongshore variability in set-up/down profiles, thus creating alongshore surface slopes (pressure gradients). However, as pointed out by Holman (personal communication 1992) this idea is not supported by the high level of correlation between changes in the wave incidence quadrant and direction and magnitude of the current measured at five location alongshore in the trough during DELILAH. It is also noted that such alongshore pressure gradients would necessarily result in eventual convergence of flow and concurrent rip currents. Rip currents were not observed during the times of the experiments described herein.

Turbulent mixing at the space/time scales of wave breaking (order height and period of the incident waves) and mean flow have potential for improved modeling. Roelvink and Stive (1986) use the turbulent kinetic energy equation (tke) to predict turbulent radiation stress in a two dimensional (cross-shore directed) study of undertow, which requires describing S'_{xx} and therefore the variances, $\overline{u'u'}$, $\overline{v'v'}$, and $\overline{w'w'}$. After predicting the total level of turbulent kinetic energy in the column and making reasonable assumptions regarding the distribution (magnitudes) of this energy between u, v, and w, cross-shore profiles of S'_{xx} may be obtained. The study of longshore currents however, requires specifying the turbulent radiation stress (S'_{yy}) which requires knowledge of the covariance between turbulent velocity components ($\overline{u'v'}$) within the surf zone, a topic with little theoretical and no experimental background to draw upon. Measurement of such a term in the surf zone has not been done to date, because it is not known how to separate out the much larger wave induced velocity contributions.

Putrevu and Svendsen (1991) suggest mixing can be due to the interaction of vertical shears in the mean longshore and cross-shore currents resulting in $\overline{u'v'} > 0$. Verification of this hypothesis would require resolving the vertical structure of the mean currents better than has been previously accomplished.

Planning of future experiments will require prioritization between improved horizontal resolution (i.e. assessment of the alongshore homogeneity assumptions) and increased vertical resolution. In most field work reported on thus far, the bottom stress term has been inferred through fitting the horizontal velocity profiles by adjusting the drag coefficient. Increasing interest in sediment transport processes argues for direct measurement of bottom stress. It has been shown in this work that adequate resolution of the longshore current profile is likely to require upwards of four or five current meters, placed at appropriate elevations. Theories are developing which require greatly enhanced knowledge of turbulence distributions in the surf zone. Field data to assess such theories will require advances in current technology, but pose perhaps the greatest hope of significantly improving modeling of the longshore current. Finally, re-examination of the wave forcing term, with enhancements to reduce dependence upon narrow-bandedness assumptions in frequency and direction, and links through linear theory, are desirable.

INITIAL DISTRIBUTION LIST

		Number of Copies
1.	Defense Technical Information Center Cameron Station Alexandria, VA 22304-6145	2
2.	Librarian Code 52 Naval Postgraduate School 411 Dyer Rd Rm 104 Monterey, CA 93943-5101	2
3.	Oceanography Department Code OC/Co Naval Postgraduate School 833 Dyer Rd Rm 331 Monterey, CA 93943-5122	1
4.	Prof. E.B. Thornton Oceanography Department Code OC/Tm Naval Postgraduate School 833 Dyer Rd Rm 331 Monterey, CA 93943-5122	1
5.	LCDR J.C. Church Naval Research Laboratory Marine Geosciences Div (Code 7405) Stennis Space Center, MS 39529-5000	6
6.	Commander Naval Oceanography Command Stennis Space Center, MS 39529-5000	1
7.	Commanding Officer Naval Oceanographic Office Stennis Space Center, MS 39529-5001	1
8.	Superintendent Naval Research Laboratory Marine Geosciences Div Code 7400 Stennis Space Center, MS 39529-5000	4

- | | | |
|-----|---|---|
| 9. | Chief of Naval Research
800 N. Quincy Street
Arlington, VA 22217 | 1 |
| 10. | Office of Naval Research
Ocean Sciences Directorate (Code 242)
Attn: Robert Peloquin
800 N. Quincy Street
Arlington, VA 22217 | 1 |
| 11. | Office of Naval Research
Ocean Sciences Directorate (Code 1121 CS)
Attn: Thomas Kinder
800 N. Quincy Street
Arlington, VA 22217 | 1 |
| 12. | Library
Scripps Institution of Oceanography
La Jolla, CA 92037 | 1 |
| 13. | Chairman
Oceanography Department
U.S. Naval Academy
Annapolis, MD 21402 | 1 |
| 14. | Director
U.S. Army Coastal Engineering Research Center
Kingman Building
Ft. Belvoir, VA 22060 | 1 |
| 15. | Director
Waterways Experiment Station
Corps of Engineers
3909 Halls Ferry Rd
Vicksburg, MS 39180-6199 | 1 |
| 16. | Mr. William Birkemeier
Field Research Facility
SR Box 271
Kitty Hawk, NC 27949 | 1 |
| 17. | Commander
Naval Coastal Systems Center
Panama City, FL 3240 | 1 |